Article

Immunity

Tissue resident iNKT17 cells facilitate cancer cell extravasation in liver metastasis via interleukin-22

Graphical abstract

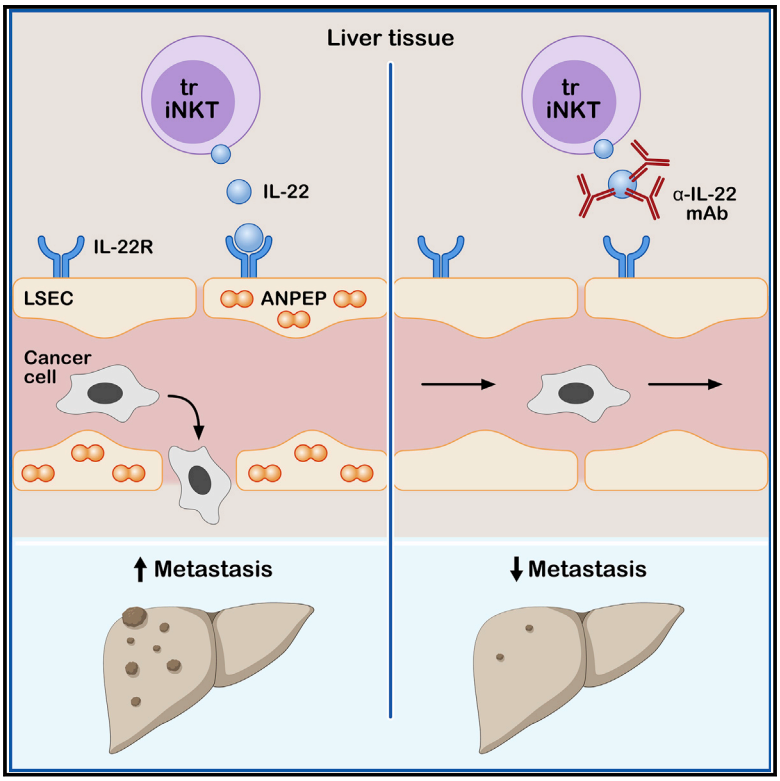

Authors

Anastasios D. Giannou, Jan Kempski, Ahmad Mustafa Shiri, ..., Richard A. Flavell, Nicola Gagliani, Samuel Huber

Correspondence

a.giannou@uke.de (A.D.G.), shuber@uke.de (S.H.)

In brief

Interleukin-22 (IL-22) is produced by immune cells and promotes tissue repair and regeneration; however, in malignancy, IL-22 can promote tumor growth. Giannou et al. find that tissue resident iNKT17 cells produce IL-22 and promote cancer cell extravasation through regulation of aminopeptidase N. Neutralization of IL-22 inhibits metastasis formation, suggesting therapeutic avenues for cancer treatment.

Highlights

- *Il22*-deficient mice are protected against metastasis formation
- IL-22 neutralization blocks cancer cell extravasation
- IL-22 acts on endothelial cells, promoting cancer cell extravasation via ANPEP induction
- Tissue resident iNKT17 cells are the key IL-22 source during cancer cell extravasation

Giannou et al., 2023, Immunity *56*, 125–142
January 10, 2023
https://doi.org/10.1016/j.immuni.2022.12.014

CellPress

Immunity

CellPress
OPEN ACCESS

Article

Tissue resident iNKT17 cells facilitate cancer cell extravasation in liver metastasis via interleukin-22

Anastasios D. Giannou,[1,2,3,33,35,*] Jan Kempski,[1,2,4,5,33] Ahmad Mustafa Shiri,[1,2,33] Jöran Lücke,[1,2,3,34] Tao Zhang,[1,2,34] Lilan Zhao,[3,34] Dimitra E. Zazara,[6,7] Filippo Cortesi,[3] Kristoffer Riecken,[8] Maria Carolina Amezcua Vesely,[9,10] Jun Siong Low,[9,10] Hao Xu,[9,10] Eleanna Kaffe,[9,10] Laura Garcia-Perez,[1,2] Theodora Agalioti,[3] Yoshito Yamada,[11,12] Wolfgang Jungraithmayr,[12,13] Ehud Zigmond,[14,15] Karl-Frederick Karstens,[3] Babett Steglich,[1,2,3] Jonas Wagner,[3] Leonie Konczalla,[3,5] Antonella Carambia,[16] Kornelius Schulze,[16] Johann von Felden,[16] Peter May,[17] Daria Briukhovetska,[17] Tanja Bedke,[1,2] Leonie Brockmann,[1,2] Sarah Starzonek,[18] Tobias Lange,[18,19] Claudia Koch,[20]

(Author list continued on next page)

[1]Section of Molecular Immunology und Gastroenterology, I. Department of Medicine, University Medical Center Hamburg-Eppendorf, 20246 Hamburg, Germany
[2]Hamburg Center for Translational Immunology (HCTI), University Medical Center Hamburg-Eppendorf, 20246 Hamburg, Germany
[3]Department of General, Visceral and Thoracic Surgery, University Medical Center Hamburg-Eppendorf, 20246 Hamburg, Germany
[4]The Calcium Signalling Group, Department of Biochemistry and Molecular Cell Biology, University Medical Center Hamburg-Eppendorf, 20246 Hamburg, Germany
[5]Mildred Scheel Cancer Career Center HaTriCS4, University Medical Center Hamburg-Eppendorf, 20246 Hamburg, Germany
[6]Division for Experimental Feto-Maternal Medicine, Department of Obstetrics and Fetal Medicine, University Medical Center Hamburg-Eppendorf, 20246 Hamburg, Germany
[7]University Children's Hospital, University Medical Center Hamburg-Eppendorf, 20246 Hamburg, Germany
[8]Research Department Cell and Gene Therapy, Department of Stem Cell Transplantation, University Medical Center Hamburg-Eppendorf, 20246 Hamburg, Germany
[9]Department of Immunobiology, School of Medicine, Yale University, New Haven, CT 06520, USA
[10]Howard Hughes Medical Institute, Yale University School of Medicine, New Haven, CT 06520, USA
[11]Department of Thoracic Surgery, Kyoto University Hospital, Kyoto, Japan
[12]Department of Thoracic Surgery, University Hospital Zurich, Zurich, Switzerland

(Affiliations continued on next page)

SUMMARY

During metastasis, cancer cells invade, intravasate, enter the circulation, extravasate, and colonize target organs. Here, we examined the role of interleukin (IL)-22 in metastasis. Immune cell-derived IL-22 acts on epithelial tissues, promoting regeneration and healing upon tissue damage, but it is also associated with malignancy. *Il22*-deficient mice and mice treated with an IL-22 antibody were protected from colon-cancer-derived liver and lung metastasis formation, while overexpression of IL-22 promoted metastasis. Mechanistically, IL-22 acted on endothelial cells, promoting endothelial permeability and cancer cell transmigration via induction of endothelial aminopeptidase N. Multi-parameter flow cytometry and single-cell sequencing of immune cells isolated during cancer cell extravasation into the liver revealed iNKT17 cells as source of IL-22. iNKT-cell-deficient mice exhibited reduced metastases, which was reversed by injection of wild type, but not *Il22*-deficient, invariant natural killer T (iNKT) cells. IL-22-producing iNKT cells promoting metastasis were tissue resident, as demonstrated by parabiosis. Thus, IL-22 may present a therapeutic target for prevention of metastasis.

INTRODUCTION

Metastasis is a common cause of cancer-related death. What is known as the "metastatic cascade" describes the multi-step process of metastasis formation: invasion, intravasation, circulation, extravasation, and colonization of the target organs.[1] The cross-talk among the immune system, cancer cells, and tissue-specific stromal cells is thought to be the critical determinant in metastatic progression,[2] although specific insight into the cells and factors mediating this communication is limited. Tissue resident immune cells lodge in non-lymphoid tissues, providing continuous immune surveillance, and enable a prompt and efficient *in situ* response upon pathogen invasion.[3,4] Furthermore, tissue resident immune cells, and specifically $CD8^+$ T cells, innate lymphoid

Sabine Riethdorf,[20] Penelope Pelczar,[1,2] Marius Böttcher,[1,2] Morsal Sabihi,[1,2] Francis J. Huber,[1,2] Matthias Reeh,[3] Julia Kristin Grass,[3] Ramez Wahib,[3] Hannes Seese,[3] Björn-Ole Stüben,[3] Mohammad Fard-Aghaie,[3] Anna Duprée,[3] Pasquale Scognamiglio,[3] Gabriel Plitzko,[3] Jan Meiners,[3] Shiwa Soukou,[1,2] Agnes Wittek,[1,2] Caroline Manthey,[16] Ioannis C. Maroulis,[21] Petra C. Arck,[6] Daniel Perez,[3] Bin Gao,[22] Sotirios G. Zarogiannis,[23,24] Till Strowig,[25] Renata Pasqualini,[26] Wadih Arap,[27] Javier Suárez Gosálvez,[17] Sebastian Kobold,[17,28,29] Immo Prinz,[30,31] Andreas H. Guse,[4] Michael Tachezy,[3] Tarik Ghadban,[3] Asmus Heumann,[3] Jun Li,[3] Nathaniel Melling,[3] Oliver Mann,[3] Jakob R. Izbicki,[3] Klaus Pantel,[20] Udo Schumacher,[18,32] Ansgar W. Lohse,[16] Richard A. Flavell,[9,10] Nicola Gagliani,[1,2,3] and Samuel Huber[1,2,*]

[13]Department of Thoracic Surgery, Medical Center - University of Freiburg, Faculty of Medicine, University of Freiburg, Freiburg, Germany
[14]The Sackler Faculty of Medicine, Tel Aviv University, Tel Aviv, Israel
[15]The Research Center for Digestive Tract and Liver Diseases, Tel Aviv Sourasky Medical Center, Tel Aviv, Israel
[16]I. Department of Medicine, University Medical Center Hamburg-Eppendorf, Hamburg 20246, Germany
[17]Division of Clinical Pharmacology, Department of Medicine IV, Klinikum der Universität München, Munich, Germany
[18]Institute of Anatomy and Experimental Morphology, University Cancer Center Hamburg, University Medical Center Hamburg-Eppendorf, 20246 Hamburg, Germany
[19]Institute of Anatomy I, University Hospital Jena, 07743 Jena, Germany
[20]Department of Tumor Biology, University Medical Center Hamburg-Eppendorf, 20246 Hamburg, Germany
[21]Department of Surgery, University of Patras Medical School, Patras, Greece
[22]Laboratory of Liver Diseases, National Institute on Alcohol Abuse and Alcoholism, National Institutes of Health, Bethesda, MD, USA
[23]Department of Physiology, Faculty of Medicine, University of Thessaly, BIOPOLIS, Larissa, Greece
[24]Center for Pediatric and Adolescent Medicine, University Hospital Heidelberg, 69120 Heidelberg, Germany
[25]Department of Microbial Immune Regulation, Helmholtz Center for Infection Research, 38124 Braunschweig, Germany
[26]Rutgers Cancer Institute of New Jersey and Division of Cancer Biology, Department of Radiation Oncology, Rutgers New Jersey Medical School, Newark, NJ, USA
[27]Rutgers Cancer Institute of New Jersey and Division of Hematology/Oncology, Department of Medicine, Rutgers New Jersey Medical School, Newark, NJ, USA
[28]German Center for Translational Cancer Research (DKTK), Partner Site Munich, Munich, Germany
[29]Einheit für Klinische Pharmakologie (EKLiP), Helmholtz Zentrum München, German Research Center for Environmental Health (HMGU), Neuherberg, Germany
[30]Institute of Immunology, Hannover Medical School, Hannover, Germany
[31]Institute of Systems Immunology, Hamburg Center for Translational Immunology (HCTI), University Medical Center Hamburg-Eppendorf, 20246 Hamburg, Germany
[32]Medical School Berlin, 10117 Berlin, Germany
[33]These authors contributed equally
[34]These authors contributed equally
[35]Lead contact
*Correspondence: a.giannou@uke.de (A.D.G.), shuber@uke.de (S.H.)
https://doi.org/10.1016/j.immuni.2022.12.014

cells (ILCs), and innate-like T cells, perform an anti-tumorigenic function in the primary tumor in mice.[5,6] Tissue resident invariant natural killer T (iNKT) cells can also contribute to the anti-tumor response.[7] There are distinct subsets of iNKT cells, namely iNKT1, iNKT2, and iNKT17 cells, whose transcriptional profiles and signature cytokines are analog to Th1, Th2, and Th17 cell subsets among $CD4^+$ T cells. However, the role of tissue resident immune cells in the metastatic cascade is poorly understood.

Interleukin (IL)-22, a cytokine belonging to the IL-10 family, can be produced by tissue resident immune cells.[8] Furthermore, iNKT cells, and specifically iNKT17 cells, are able to produce IL-22.[9–12] IL-22 is also released by several other immune cell types, including ILCs and $CD4^+$ T lymphocytes.[13] Interestingly, cancer cells can directly induce IL-22 production *in vitro* and *in vivo*[14] and IL-22-producing Th17 cells accumulate in colon cancer tissues.[15] Accordingly, the number of infiltrating $CD4^+$ $IL17A^+$ $IL\text{-}22^+$ T cells is higher in human colorectal cancer (CRC), while $CD4^+IL17A^-IL\text{-}22^+$ T cells are not increased compared to healthy adjacent tissue.[16–18] Unlike other cytokines, IL-22 binds to non-immune cells expressing its specific receptor, IL-22RA1.[19] Thus, IL-22 may mediate the communication between the immune system and the tissue.

Interestingly, IL-22 has dual functions: short-term IL-22 exposure promotes intestinal integrity and protects intestinal stem cells against genotoxic stress.[19,20] However, uncontrolled and prolonged IL-22 activity promotes intestinal tumorigenesis.[21–23] IL-22 promotes cancer cell stemness[24,25] and facilitates tumor growth.[26,27] These data are further supported by human studies, which indicate a detrimental role of uncontrolled IL-22 activity in cancer.[28,29] Despite these data, the role of IL-22 during metastasis formation is still unclear.

In this study, we examined the role of IL-22 in metastasis formation. We found that tissue-resident iNKT17 cell-derived IL-22 acted directly on endothelial cells, thereby facilitating cancer cell extravasation via induction of endothelial aminopeptidase N (ANPEP) and, subsequently, liver metastasis formation. Our data present a rationale for targeting IL-22 in the clinic.

RESULTS

Il22-deficiency in mice protects against liver metastasis

First, we analyzed the role of IL-22 using a forced metastatic mouse model,[30] namely intrasplenic (i.s.) injection of CRC cells (MC38, murine colon adenocarcinoma cells). *Il22*-deficient mice were protected from metastasis formation compared to littermate

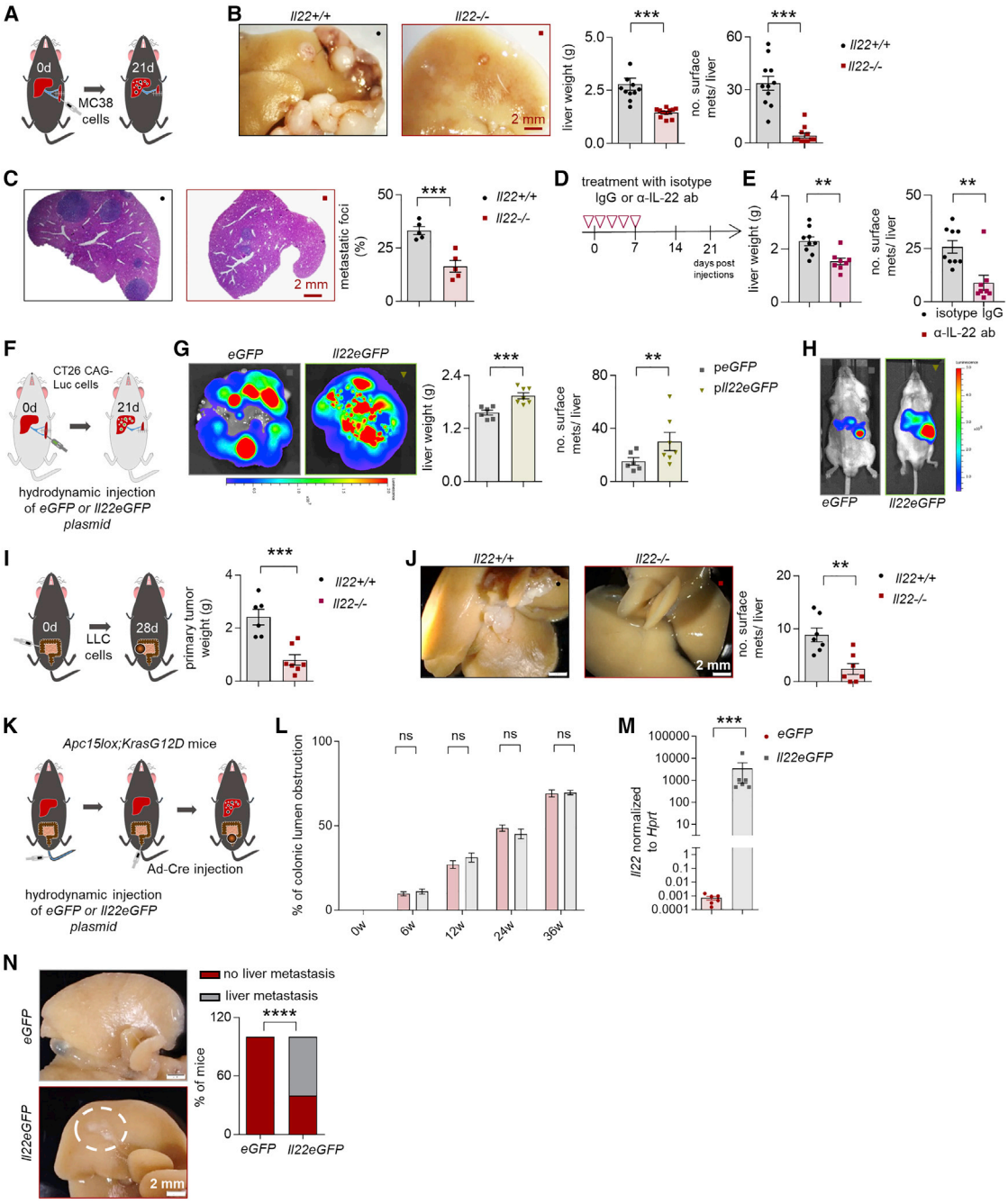

Figure 1. *Il22*-deficient mice are protected against liver metastasis

(A) Schematic overview of the experiment (i.s. injection of MC38 cells).

(B) Representative pictures, number of macroscopic liver metastases, and liver weight of $Il22^{+/+}$ mice compared to $Il22^{-/-}$ mice. n ≥ 11 mice per group.

(C) H&E staining and metastatic foci. n = 5 mice per group.

(D) Schematic overview of the experiment (i.s. injection of MC38 cells).

(E) Liver weight and number of macroscopic liver metastases in mice treated with an α-IL-22 or IgG control antibody. n ≥ 8 mice per group.

(F) Schematic overview of the experiment (i.s. injection of CT26CAG-Luc cells).

(G) *Ex vivo* bioluminescent imaging of livers after hydrodynamic overexpression of *eGFP* or *Il22eGFP* plasmid. Bioluminescent scale: 2×10^7–2×10^8 photons/sec/cm^2/sr. Liver weight and number of macroscopic liver metastases in Balb/c mice after hydrodynamic overexpression of *eGFP* or *Il22eGFP* plasmid. n ≥ 6 mice per group.

(H) Bioluminescent imaging of Balb/c mice after hydrodynamic overexpression of *eGFP* or *Il22eGFP* plasmid. Bioluminescent scale: 5×10^7–5×10^8 photons/sec/cm^2/sr. n ≥ 6 mice per group. Scale bar: 2 mm.

(I) Schematic overview of the experiment (injection of LLC cells into the cecum).

(J) Representative pictures and number of macroscopic liver metastases in $Il22^{+/+}$ and $Il22^{-/-}$ mice. n ≥ 6 mice per group.

(legend continued on next page)

controls (Figures 1A–1C). Likewise, IL-22 blockade protected mice from developing liver metastasis (Figures 1D and 1E). We then used a gain-of-function approach: *Il22tg8*^{Tg} transgenic mice overexpress IL-22 in the liver and also have increased serum IL-22 levels (≈6,000 pg/ml).[31] Indeed, we found an increased number of liver metastases in *Il22tg8*^{Tg} transgenic mice compared to littermate controls upon induction of forced liver metastasis (Figure S1A). The pro-metastatic function of IL-22 was seen also in *Balb/c* wild-type (WT) mice after hydrodynamic overexpression of IL-22 or control plasmid administration (*eGFP*) in the liver followed by an i.s. induction of liver metastasis with the CT26GAG-Luc colon cancer cell line (Figures 1F–1H and S1B–S1F).

We next examined the role of IL-22 in spontaneous metastasis models. To this end, we first injected C57BL/6 Lewis lung adenocarcinoma syngeneic cancer cells (Lewis lung carcinoma [LLC] cell line) into the cecum of *Il22*-deficient mice and littermate controls. *Il22*-deficient mice were largely protected from metastasis formation compared to littermate controls (Figures 1I and 1J). As a second model, we used *Apc*^{15lox};*Kras*^{G12D} mice,[32,33] a genetic model which spontaneously develops CRC and liver metastasis upon adenovirus, Ad-Cre (see STAR Methods), injection. Upon hydrodynamic overexpression of IL-22 in the liver, 60% of the mice developed liver metastases compared to no detectable metastases in mice with control (*Egfp*) gene transfer (Figures 1K–1N). There was no difference in the formation of the primary tumor in the colon. As a third spontaneous model, we used an intramucosal injection of CT26GAG-Luc cells in order to mimic human CRC development. This experimental setup resulted in liver metastasis formation only in *Balb/c* WT mice overexpressing IL-22 in their liver, while *Balb/c Il22*-deficient mice with a control hydrodynamic gene transfer did not develop any liver metastases (Figure S1G).

Thus, in various experimental models, IL-22 promoted liver metastasis formation.

IL-22 affects the host endothelium, thereby promoting metastasis

The next step was to identify the target cells of IL-22. We found that tumor cells (MC38 and LCC) express IL-22RA1 and can respond to IL-22 *in vitro* (Figures S2A–S2D). Furthermore, IL-22 increased cancer cell stemness, evidenced by enhanced tumor sphere formation *in vitro* (Figure S2E). To assess the relevance of this finding *in vivo*, we injected LLC-GFP (LLC-Green Fluorescent Protein) cancer cells into the cecum of mice or MC38-GFP cells intrasplenically. *Il22*-deficient mice showed lower circulating tumor cell (CTC) numbers in both models (Figures S2F–S2I). In order to test whether IL-22 acts directly on tumor cells *in vivo*, we silenced the expression of IL-22RA1 in MC38 cells (Figures S2J and S2K). We found no difference upon injection of *Il22ra1*-deficient and control MC38 cells when we used WT mice as recipients, suggesting that endogenous IL-22 levels are not sufficient to promote metastasis by acting on tumor cells directly. However, we observed reduced metastatic sites in *Il22tg8*^{Tg} transgenic mice receiving *Il22ra1*-deficient MC38 cells compared to the control group (Figures 2A and 2B), thus indicating that IL-22 in high concentrations can act on tumor cells *in vivo*. On this basis, we aimed to assess whether IL-22 could also act on non-tumor cells *in vivo*. To this end, we injected WT MC38 cells (which express IL-22RA1) intrasplenically into *Il22ra1*-deficient[19] and littermate control mice. *Il22ra1*-deficient mice exhibited lower liver weight and macroscopic metastases compared to WT littermate controls (Figures 2C and 2D). Thus, IL-22 can act on non-tumor cells, thereby promoting metastasis formation.

We next aimed to identify the non-tumor cell that would respond to IL-22. We did not detect expression of the IL-22RA1 receptor in CD45^{+} (immune) cells. However, we found that the liver sinusoidal endothelial cells (LSECs) highly expressed the IL22RA1 receptor (Figures 2E and 2F). Furthermore, IL-22 induced STAT3 phosphorylation in LSECs *in vitro* (Figure 2G). We further used a mouse model with conditional deletion of *Il22ra1* (Figures S2L, S2M, and S2O). This was crossed with *Cdh5*^{Cre} mice to obtain an endothelial-specific deletion,[34] and we observed Cre recombination in approximately 60% of endothelial cells (Figure S2O). As control, we used mice with a hepatocyte-specific driver, Albumin Cre (*Alb*^{Cre}), because hepatocytes can also respond to IL-22.[35] We did not observe a difference in the number of metastatic sites in *Il22ra1*$^{flox/flox}$;*Alb*$^{Cre+}$ mice compared to littermate controls upon i.s. injection of MC38 cells inducing liver metastasis (Figures 2H and 2I). In contrast, *Il22ra1*$^{flox/flox}$ *Cdh5*$^{Cre+}$ mice phenocopied *Il22ra1*-deficient mice by showing reduced forced liver metastases (Figures 2J and 2K).

Taken together, these findings indicate that IL-22 acts on the host endothelium, thereby promoting metastasis formation.

IL-22 signaling in endothelial cells promotes cancer cell extravasation

Next, we aimed to uncover the mechanism by which IL-22 signaling would promote metastasis formation. We hypothesized that this is due to altered endothelial adhesion of cancer cells, increased permeability of the endothelial layer allowing enhanced extravasation of cancer cells, or a combination of both. To test this, we used an *in vitro* adhesion assay and found that IL-22 did not increase the adhesion of CRC cells, HT-29 or MC38, to human umbilical vein endothelial cells (HUVECs) or LSECs, respectively (Figures S3A–S3C). As positive control, we used IL-1α and tumor necrosis factor (TNF)-α (Figures S3A–S3C). Additionally, IL-22 did not affect the expression of adhesion molecules such as E-Sel, P-Sel, ICAM-1, and VCAM-1 (Figures S3D–S3F). Next, we tested whether IL-22 would increase endothelial permeability and thus cancer cell extravasation. We found that IL-22 signaling enhanced the extravasation of tumor cells into the liver parenchyma, whereas this was decreased upon IL-22 blockade (Figures 3A–3F and S3G–S3K). Likewise, *Il22ra1*$^{flox/flox}$;*Cdh5*$^{Cre+}$ mice lacking IL-22 signaling on the endothelium showed reduced extravasation

(K) Schematic overview of the experiment (adenoviral infection of colonic epithelium for orthotopic colon cancer induction as a model of spontaneous liver metastasis).
(L) Endoscopic score of primary colon cancer of *Apc*^{15lox};*Kras*^{G12D} mice. n ≥ 6 mice per group.
(M) *Il22* mRNA levels in total liver of *Apc*^{15lox};*Kras*^{G12D} mice upon hydrodynamic liver overexpression of *eGFP* or *Il22eGFP* plasmid. n = 6 mice per group.
(N) Representative pictures and percentage of *Apc*^{15lox};*Kras*^{G12D} mice that developed macroscopic metastases. n = 6 mice per group. Scale bar: 2 mm. Data presented as mean ± SEM, not significant (ns): p > 0.05; *p < 0.05; **p ≤ 0.01; ***p ≤ 0.001 as assessed by Mann-Whitney U test or Fischer's exact test (K).

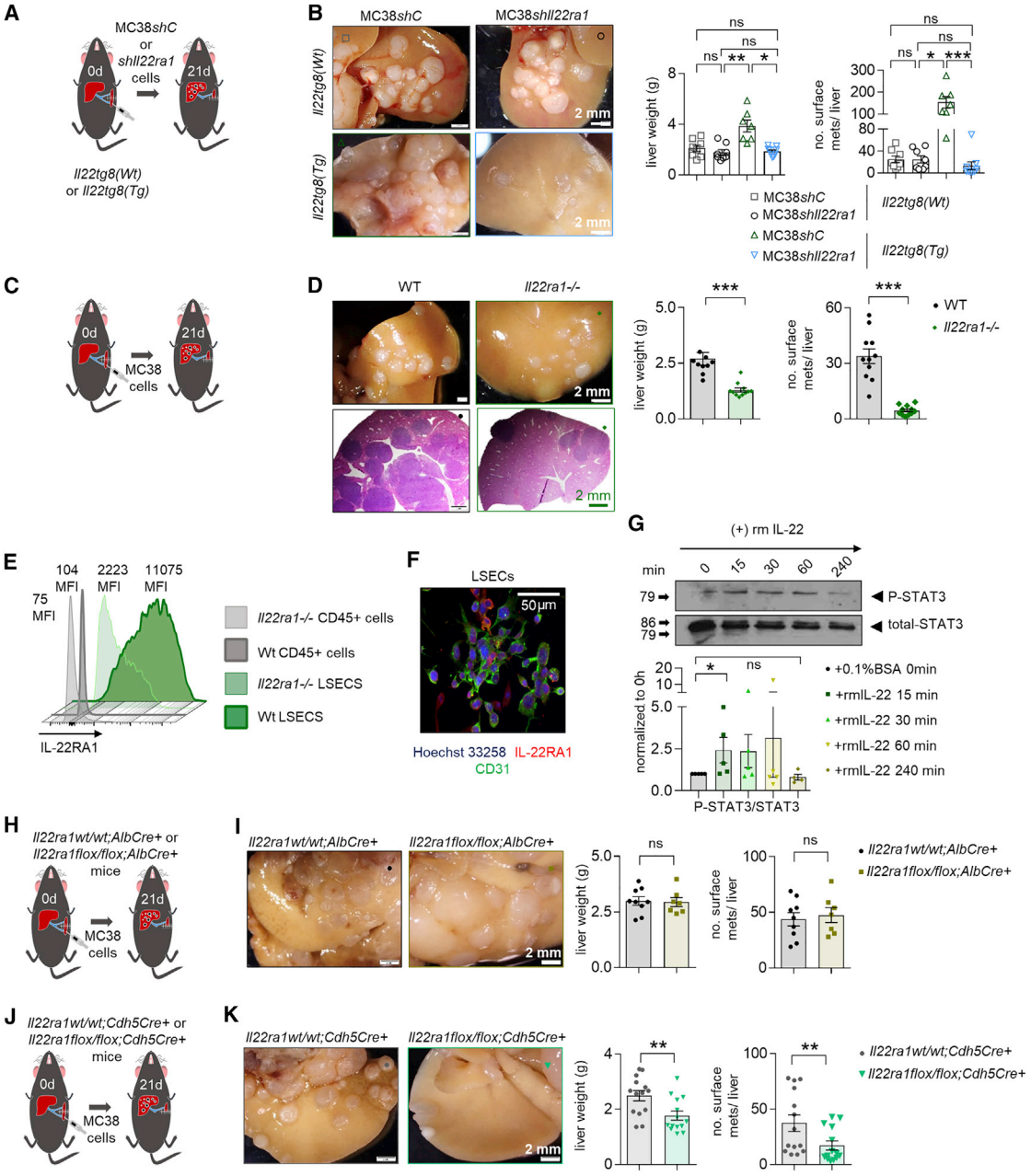

Figure 2. IL-22 affects the host endothelium, thereby promoting metastasis

(A) Schematic overview of the experiment (i.s. injection of MC38shC and MC38*shIl22ra1* cells in *Il22tg*$^{(wt)}$ and *Il22tg8*$^{(Tg)}$ mice).

(B) Liver weight and number of macroscopic liver metastases. n ≥ 7 mice per group.

(C) Schematic overview of the experiment (i.s. injection of MC38 cells in WT and *Il22ra1*−/− mice).

(D) Liver weight and number of macroscopic liver metastases. n ≥ 7 mice per group.

(E) IL-22RA1 expression in CD45^{+} cells and LSECs.

(F) Immunostaining of LSECs with CD31 (green) and IL-22RA1 (red). Scale bar, 50 µm.

(G) pSTAT3 levels in LSECs isolated from 6 WT mice and treated with recombinant murine (rm) IL-22.

(H) Schematic overview of the experiment (i.s. MC38 cell injection in *Il22ra1*$^{wt/wt}$;*Alb*$^{Cre+}$ and *Il22ra1*$^{flox/flox}$;*Alb*$^{Cre+}$ mice).

(I) Liver weight and number of macroscopic liver metastases. n ≥ 7 mice per group.

(J) Schematic overview of the experiment (i.s. MC38 cell injection in *Il22ra1*$^{wt/wt}$;*Cdh5*$^{Cre+}$ and *Il22ra1*$^{flox/flox}$;*Cdh5*$^{Cre+}$ mice).

(K) Liver weight and number of macroscopic liver metastases. n ≥ 14 mice per group. Scale bar, 2 mm (B, D, I, and K). Data presented as mean ± SEM, ns: $p > 0.05$; *$p < 0.05$; **$p \leq 0.01$; ***$p \leq 0.001$ as assessed by Mann-Whitney U test (C, D, I, and K) or one-way ANOVA with Bonferroni post hoc tests (B and G).

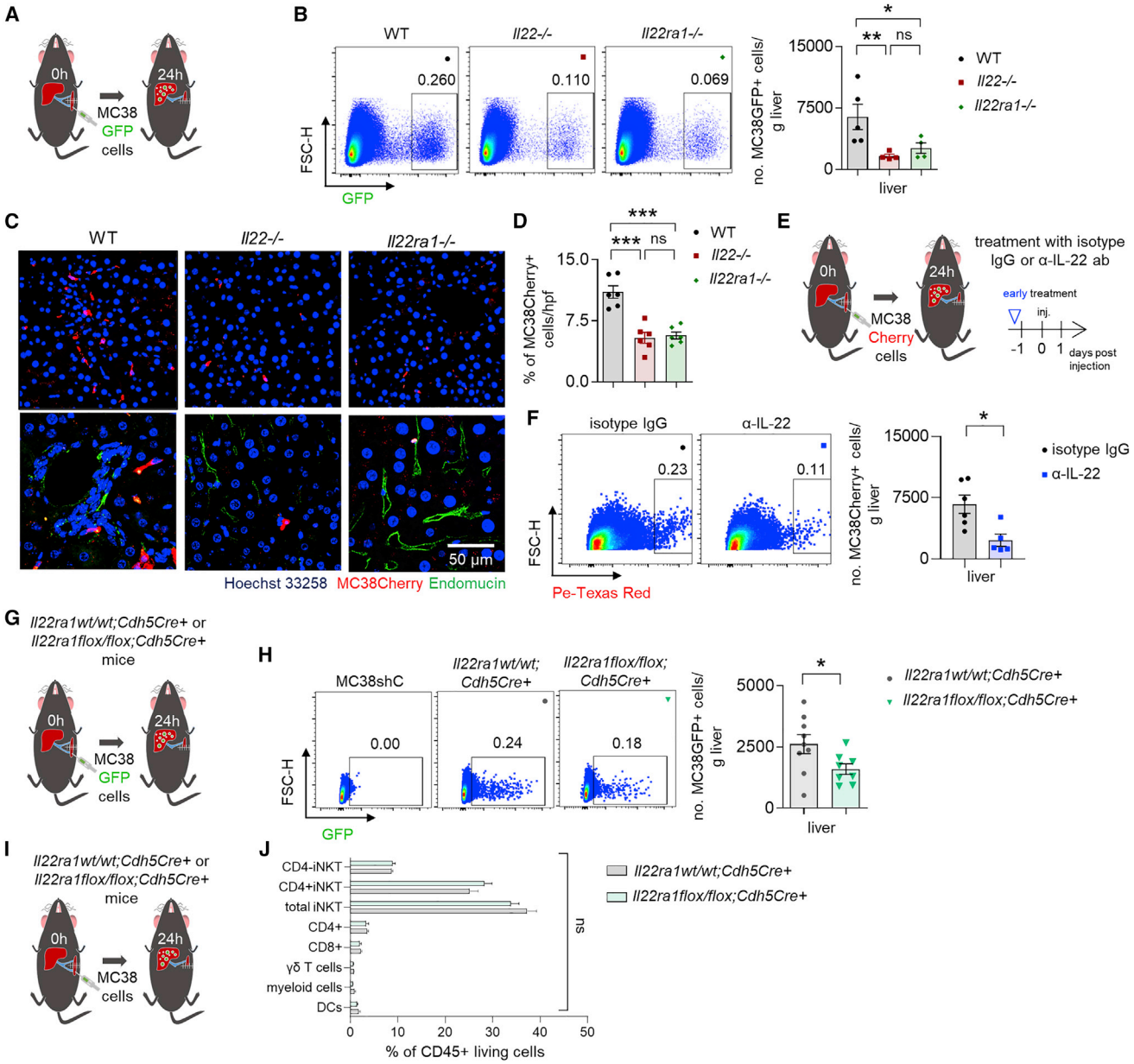

Figure 3. IL-22 signaling in endothelial cells is required for cancer cell extravasation

(A) Schematic overview of the experiment (i.s. injection of MC38 GFP-labelled cells in WT, *Il22*$^{-/-}$, and *Il22ra1*$^{-/-}$ mice [extravasation assay]). See also Figure S3.

(B) Representative FACS (fluorescence-activated cell sorting) plots and number of extravasated cancer cells 24 h post i.s. cancer cell injection. n ≥ 4 mice per group.

(C) Representative images of immunostaining of MC38 Cherry-labeled cells and endomucin (endothelial marker; green) 24 h post i.s. cancer cell injection. Scale bar, 50 µm.

(D) Number of extravasated cancer cells 24 h post i.s. injection. n = 6 mice per group.

(E) Schematic overview of the experiment (injection of MC38 Cherry-labeled cells in WT mice receiving an anti-IL-22 or IgG control antibody).

(F) Representative FACS plots and number of extravasated cancer cells from (E). n ≥ 5 mice per group.

(G) Schematic overview of the experiment (i.s. injection of MC38 GFP-labeled cells in *Il22ra1*$^{wt/wt}$;*Cdh5*$^{Cre+}$ and *Il22ra1*$^{flox/flox}$;*Cdh5*$^{Cre+}$ mice [extravasation assay]).

(H) Representative FACS plots and number of extravasated cancer cells 24 h post i.s. cancer cell injection. n ≥ 8 mice per group.

(I) Schematic overview of the experiment (i.s. injection of MC38 cells in *Il22ra1*$^{wt/wt}$;*Cdh5*$^{Cre+}$ and *Il22ra1*$^{flox/flox}$;*Cdh5*$^{Cre+}$ mice [extravasation assay]).

(J) Immune cell infiltration in the liver 24 h post i.s. injection. n ≥ 7 mice per group. Data presented as mean ± SEM, ns $p > 0.05$; *$p < 0.05$; **$p \leq 0.01$; ***$p \leq 0.001$ as assessed by one-way ANOVA with Bonferroni post hoc tests (B and D) or Mann-Whitney U test (F, H, and J).

(Figures 3G–3J). Finally, humanized MISTRG mice (*Rag2*$^{-/-}$*Il2rg*$^{-/-}$ mice in which the genes encoding human M-CSF, human IL-3 and GM-CSF, and human TPO are knocked in to their respective mouse loci; they also include a BAC-transgene encoding human SIRPα) that were engrafted with hCD34+ cells showed reduced extravasating human cancer cells (HCT-116, human CRC cells) into the liver parenchyma upon treatment with Fezakinumab, a human IL-22 antibody (Figures S3L and S3M).

Thus, these findings indicate that IL-22 blockade can be a therapeutic approach to prevent extravasation of tumor cells into the target organ.

IL-22 promotes increased endothelial expression of ANPEP and thereby cancer cell extravasation

In order to identify the molecular mechanisms underlying the effect of IL-22, we first used an *in vitro* assay. We found that LSEC exposure to rmIL-22 particularly induced the expression of three transcripts, namely *Anpep*, *Epas1*, and *Fgfr3 in vitro* (Figures 4A and S4A–S4E). We decided to focus on the aminopeptidase ANPEP, since ANPEP has been implicated in metastasis formation before[36] and the increased expression in LSECs could be verified by qPCR and immunoblotting (Figures 4B, 4C, and S4A–S4E). Additionally, MC38 cell i.s. injection in WT mice induced the expression of *Anpep* in LSECs 12 h after injection compared to *Il22*-deficient mice (Figure S4F). Indeed, ANPEP staining of WT LSECs isolated from a murine liver at the steady state revealed that the majority of CD31^{+} endothelial cells are positive for ANPEP (Figure 4D). Subsequently, we used two different *in vitro* endothelial cell assays. These experiments showed that IL-22 acts on the endothelium and affects cancer cell transmigration and vascular permeability (Figures 4E and 4F). We then silenced the ANPEP expression on HUVEC cells using lentiviral transduction (Figure 4H). This resulted in reduced cancer cell transmigration compared to respective controls (Figure 4I). Next, we used Ubenimex, which blocks aminopeptidase activity. Ubenimex-treated mice exhibited reduced metastatic sites compared to respective controls (Figures S4I and S4J). However, Ubenimex treatment also resulted in reduced tumor cell proliferation (Figures S4G and S4H). Thus, ubenimex might also act on cancer cells and have ANPEP-independent effects. Therefore, we next intrasplenically injected MC38 cells into ANPEP-deficient mice (*Cd13*$^{-/-}$ mice) and WT littermate controls. ANPEP-deficient mice showed reduced metastasis formation compared to littermate controls (Figures S4K and S4L). In order to further examine the role of the IL-22-ANPEP axis in the extravasation of tumor cells, we treated *Cd13*$^{-/-}$ mice with an anti-IL-22 neutralizing antibody and assessed the extravasation of tumor cells. WT mice, but not *Cd13*$^{-/-}$ mice, receiving anti-IL-22 neutralizing antibody showed a decreased extravasation of tumor cells compared to mice receiving IgG antibody (Figures 4J–4K).

Thus, IL-22 regulates ANPEP expression in endothelial cells *in vitro* and *in vivo*. Furthermore, the effect of IL-22 on cancer cell extravasation seems to depend at least in part on ANPEP.

IL-22 promotes lung metastasis by promoting cancer cell extravasation

On the basis of our data obtained in the liver, we next aimed to extend our findings to lung metastasis. We used two lung metastasis models and found in both models that *Il22*-deficient mice were protected from metastasis formation (Figures 5A and 5B). In contrast, *Il22tg8*^{Tg} mice showed increased lung metastasis (Figure S5A). In this model of forced lung metastasis, 60% of *Il22tg8*^{Tg} mice also developed liver metastasis, while this was not the case in any of their littermate controls (Figure S5B).

In line with our data in liver metastasis, *Il22ra1*$^{flox/flox}$*;Cdh5*$^{Cre+}$ mice (Figure S2) were also protected in a forced lung metastasis model (Figures 5C and 5D). To test the hypothesis that IL-22 acts on the endothelial cells in the target organ, we transplanted a single left lung from *Il22ra1*-deficient mice (*Il22ra1*$^{-/-}$) orthotopically into C57BL/6N *Il22ra1*-proficient mice (*Il22ra1*$^{+/+}$). Thus, an *Il22ra1*-proficient lung and an *Il22ra1*-deficient lung were in the same host. The mice subsequently underwent the forced metastasis model by intravenous (i.v.) administration of MC38 cells. We found that the orthotopically transplanted *Il22ra1*-deficient left lung from the donor was protected from metastasis compared to the host *Il22ra1*-proficient right lung (Figures 5E and 5F), indicating that IL-22 acts on the endothelial cells of the target organ.

To test whether IL-22 would increase the permeability of the endothelial layer, thereby allowing enhanced extravasation of cancer cells, we performed an *in vivo* extravasation assay. We found that *Il22*- and *Il22ra1*-deficient mice as well as mice treated with an α-IL-22 antibody showed less cancer cell extravasation compared to littermate WT controls (Figures 5G–5J). *Il22ra1*$^{flox/flox}$*;Cdh5*$^{Cre+}$ mice lacking IL-22 signaling on the endothelium showed reduced extravasation into the lung (Figures 5K and 5L). Finally, we exposed mouse primary lung endothelial cells to rmIL-22, which resulted in increased *Anpep* expression (Figure S5C).

Next, we aimed to investigate the identity of IL-22-producing cells that participate in cancer cell extravasation into the lung. Using flow cytometry, we found that the relative contribution of T and $\gamma\delta$ T cells of all IL-22-producing cells increased 12 h post cancer cell injection (Figure S5D). On this basis, we performed an extravasation assay in WT and *Rag1*$^{-/-}$ mice, which lack adaptive immune cells. We observed higher cancer cell extravasation in the lungs of WT compared to *Rag1*$^{-/-}$ mice, suggesting that adaptive immune cells affect cancer cell extravasation (Figures S5E and S5F). We then used *Il22*$^{flox/flox}$*;CD4*$^{Cre+}$ mice and found that T cell-derived IL-22 does not impact extravasation into the lung (Figures S5G and S5H). To test the role of iNKTs (invariant natural killer T cells), we used *Ja18*$^{-/-}$ mice, injected intravenously with MC38 Cherry-labeled cancer cells. No difference was observed in mice lacking iNKT cells compared to littermate controls (Figures S5I and S5J). Finally, we used diphtheria toxin-induced $\gamma\delta$ T cell-deficient mice (*Tcrd*$^{GDL/GDL}$ [GDL: GFP, human diphtheria toxin receptor, and luciferase knocked-in]) and found that these mice had reduced cancer cell extravasation into the lungs compared to controls (Figures S5K and S5L).

Taken together, IL-22 also acts on the lung endothelium, thereby inducing ANPEP and, consequently, cancer cell transmigration and metastasis formation.

IL-22-producing iNKT cells facilitate cancer cell extravasation into the liver parenchyma

Our next aim was to identify the source of IL-22 at the extravasation step of liver metastasis formation. To this end, we used an IL-22 reporter mouse model (*IL-22*^{sgBFP}*;IL-17A*^{eGFP}*;Foxp3*^{mRFP}) and analyzed IL-22 expression 12 h post i.s. cancer cell injection. IL-22

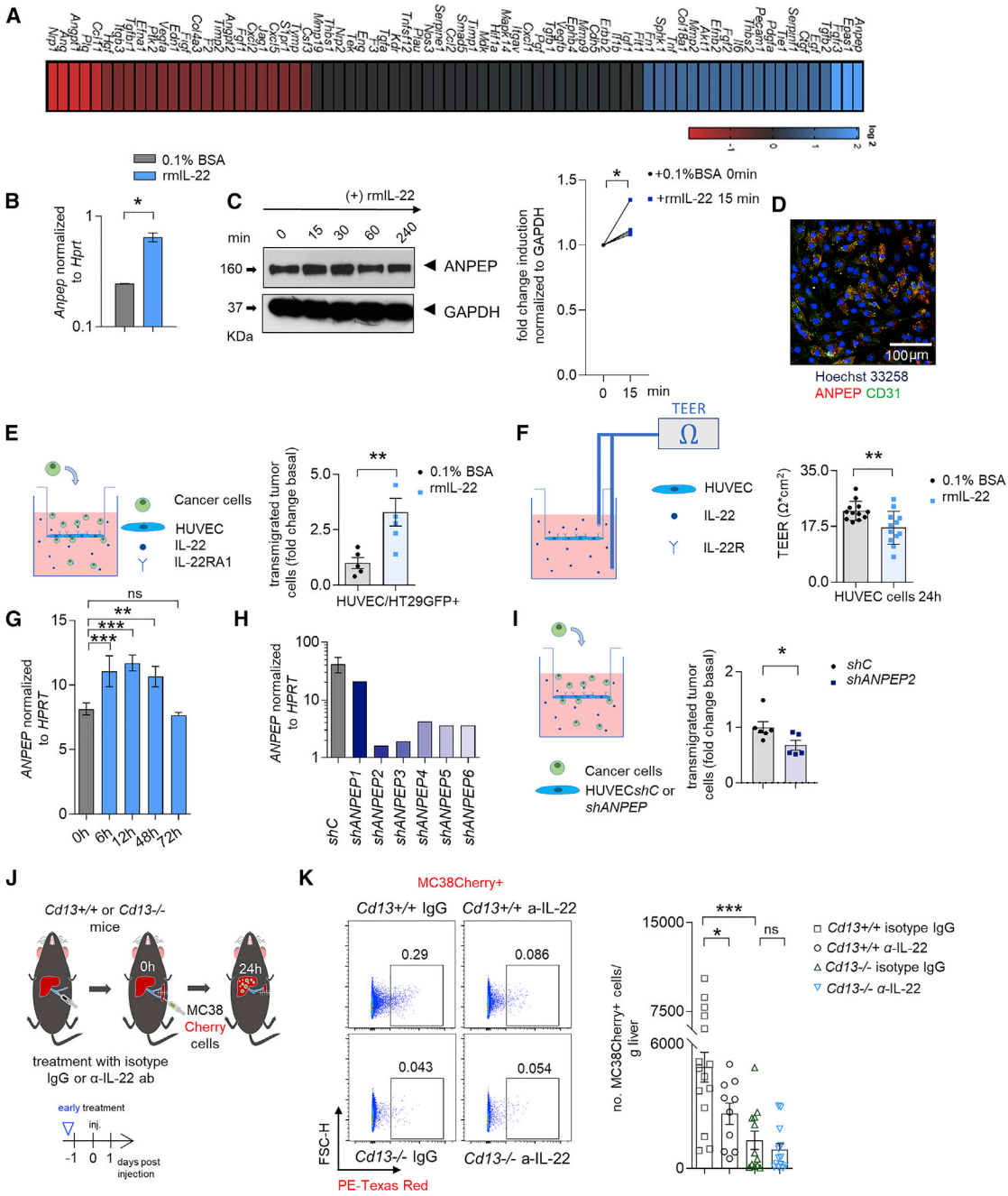

Figure 4. IL-22 increases endothelial ANPEP expression, thereby promoting endothelial permeability and cancer cell transmigration

(A) Gene expression analysis of LSECs upon rm IL-22 or PBS stimulation.

(B) *Anpep* expression in LSECs upon stimulation with rmIL-22.

(C) Immunoblotting analysis and quantification of ANPEP in LSECs upon rmIL-22 stimulation.

(D) Confocal microscopy pictures of *in vitro* cultured LSECs showing the CD31 (green) and ANPEP (red) expression.

(E) *In vitro* extravasation model of HT29 GFP-labeled cancer cells through HUVEC cells.

(F) TEER of HUVEC cell layers upon rmIL-22 stimulation.

(G) *ANPEP* RNA levels upon rmIL-22 stimulation.

(H) *ANPEP* RNA expression after shRNA silencing of *ANPEP* in different HUVEC clones.

(I) *In vitro* extravasation model of HT29 GFP-labeled cancer cells through *shC* or *shANPEP* HUVEC cells. n = 2 independent experiments.

(J) Schematic overview of the experiment (i.s. injection of MC38 Cherry cells in $Cd13^{+/+}$ or $Cd13^{-/-}$ mice receiving an α-IL-22 or IgG control antibody).

(K) Representative FACS plots and statistics. n ≥ 10 mice per group. Data presented as mean ± SEM, ns $p > 0.05$; *$p < 0.05$; **$p \leq 0.01$; ***$p \leq 0.001$ as assessed by one-way ANOVA with Bonferroni post hoc tests (D and K) or Mann-Whitney U test (B, E, F, and I).

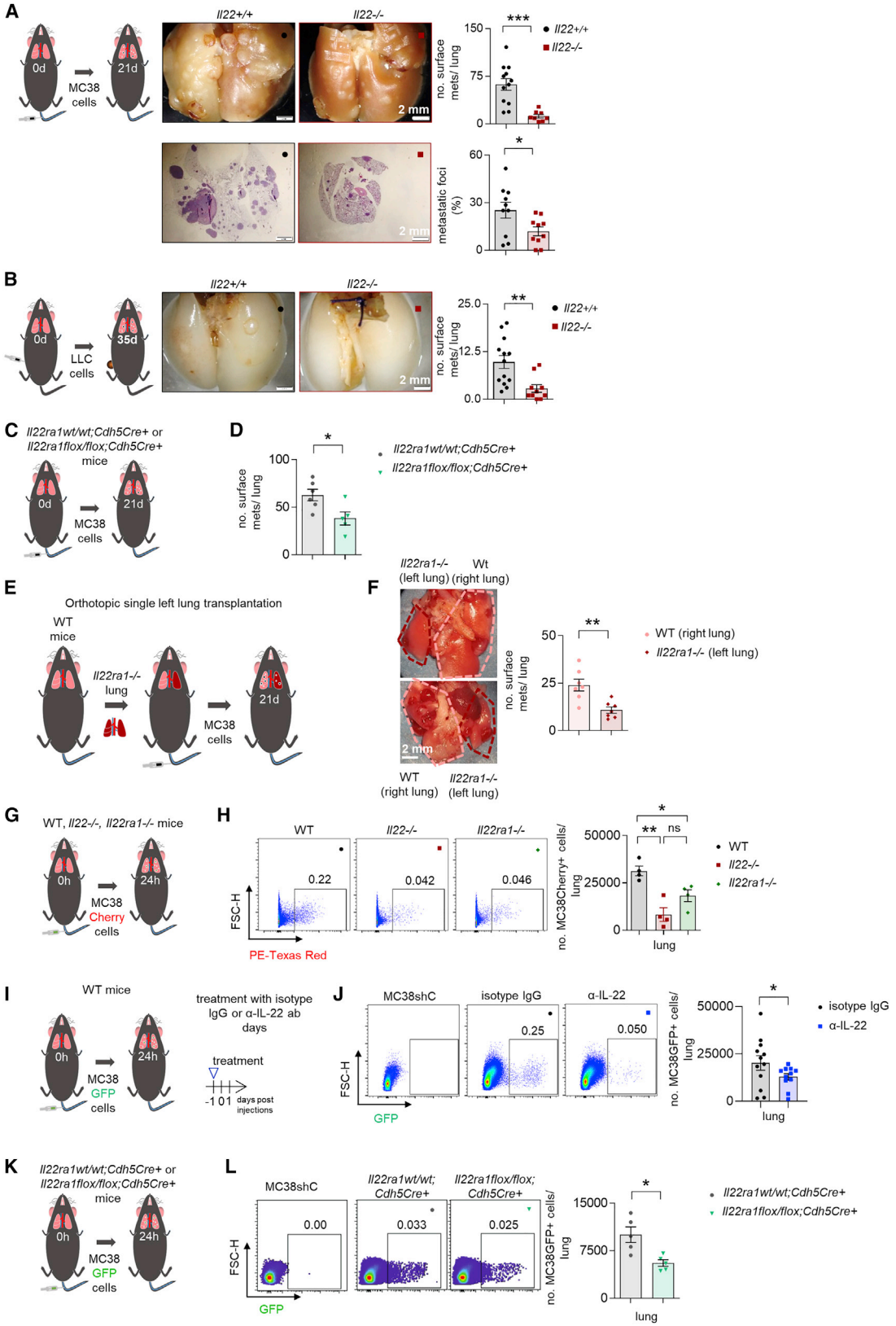

(legend on next page)

was already expressed in steady state and was further upregulated 12 h post cancer cell injection (Figures 6A and 6B). The highest IL-22 frequency was observed in $CD8^+$ T cells, but several other immune cells including $CD3^+CD4^-CD8^-$immune cells (Figures 6C, 6D, and S6A) and ILCs expressed IL-22 (Figures S6B–S6G). To test whether ILCs are a relevant source of IL-22 in cancer cell extravasation, we performed an extravasation assay in *Rag1*$^{-/-}$ mice, which lack adaptive immune cells, and WT mice with IgG or a neutralizing IL-22 antibody. Treatment of WT but not *Rag1*$^{-/-}$ mice with the neutralizing IL-22 antibody resulted in reduced cancer cell extravasation (Figures 6E and 6F). In line with these data, both *Rag1*$^{-/-}$ and *Rag1*$^{-/-}$*Il22*$^{-/-}$ mice showed a similar liver metastasis burden 21 days post cancer cell injection (Figure S6H). This finding suggests that adaptive immune cells promote cancer cell extravasation via IL-22. On this basis, we used *Il22*$^{flox/flox}$;*CD4*$^{Cre+}$ mice and found that IL-22 derived from $CD4^+$ or $CD8^+$ T cells does not impact cancer cell extravasation into the liver (Figures 6G and 6H). Based on these data, we hypothesized that a $CD3^+CD4^-CD8^-$cell, which is not present in *Rag1*$^{-/-}$ mice, might be the functionally relevant source of IL-22. This could, for example, be iNKT or γδ T cells. To test this hypothesis, we engrafted *Rag1*$^{-/-}$*Il22*$^{-/-}$ mice with the total population of iNKT or γδ T cells isolated from the livers of WT (*Il22*$^{+/+}$) or *Il22*-deficient mice (Figures 6I and S6I–S6L). Indeed, we found that *Rag1*$^{-/-}$*Il22*$^{-/-}$ mice harboring WT (*Il22*$^{+/+}$) iNKT cells exhibited increased extravasation compared to mice harboring *Il22*$^{-/-}$ iNKT cells 24 h upon i.s. injection of labeled tumor cells (Figures 6I and 6J). On the contrary, *Rag*$^{-/-}$*Il22*$^{-/-}$ mice receiving *Il22*$^{+/+}$ or *Il22*$^{-/-}$ γδ T cells did not show a difference in cancer cell extravasation (Figures S6M and S6Q). Thus, in contrast to our observations in lung tissues, absence of γδ T cells had no impact on cancer cell extravasation into the liver parenchyma (Figures S6M–S6Q). Next, we used *Ja18*-deficient mice, which lack iNKT cells. These mice were largely protected from metastasis formation compared to littermate controls (Figure S6R–S6S). We then engrafted *Ja18*-deficient mice with iNKT cells. Engraftment with iNKT cells isolated from the livers of WT (*Il22*$^{+/+}$) mice resulted in increased extravasation compared to mice harboring *Il22*$^{-/-}$ iNKT cells (Figures 6K and 6L). Finally, we aimed to examine whether iNKT cells would also express IL-22 in human liver metastasis (Figures S6T–S6V). Using flow cytometric analysis of human perimetastatic liver and liver metastasis from patients with primary CRC (M1, TNM staging), we found that iNKT cells were also able to produce IL-22 in human liver metastasis, particularly in the perimetastatic region (Figure S6V).

Thus, iNKT cells in the liver can produce IL-22 in mice and humans. Furthermore, IL-22 derived from iNKT cells plays a key functional role during cancer cell extravasation into the liver parenchyma.

Tissue resident iNKT17 IL-22-producing cells facilitate cancer cell extravasation

A tissue resident phenotype could explain why IL-22 is expressed in the target organ prior to metastasis formation. To test this, WT and IL-22 reporter mice were injected with MC38 cancer cells intrasplenically. 12 h post cancer cell injection, the mice received an α-CD45-AF700 antibody intravenously in order to label circulating immune cells and were sacrificed 2–3 min later. Using flow cytometric analysis, we found that the frequency of CD45-PeCy7 single-positive (infiltrating) cells increased upon cancer cell injection (Figures 7A and 7B). We then aimed to assess the relative contribution of IL-22-producing iNKT cells to the total amount of IL-22-producing $CD3^+$ cells. We found that the relative contribution of iNKT cells accounted for about 13% of all $CD3^+$IL-22-producing cells and increased to about 21% 12 h post cancer cell injection (Figures 7C and S7). There was a higher frequency of infiltrating iNKT cells producing IL-22 compared to circulating ones (Figures 7C and S7). We further assessed the contribution of IL-22-producing iNKT cells within IL-22-producing $CD45^+$ cells. The frequency of IL-22-producing iNKT cells, in particular the frequency of infiltrating IL-22-producing iNKT cells, also increased within this cell fraction, while the frequency of γδ T cells, which was measured as a control, stayed the same (Figures 7D, 7E, and S7). In order to better characterize the iNKT cells 12 h post i.s. injection, we used flow cytometry and single-cell sequencing. Using flow cytometry, we found that among iNKT cells, the production of IL-22 was almost exclusive to iNKT17 cells. Only a very small percentage of iNKT1 or iNKT2 cells produced IL-22. Furthermore, the single cell sequencing data demonstrated that iNKT cells express tissue resident markers, namely *Tmem176a and Tmem176b* (Figures 7F, 7G, and S7).[37] We could not test the iNKT17

Figure 5. IL-22 promotes lung metastasis by promoting cancer cell extravasation

(A) Schematic overview of the experiment (i.v. injection of MC38 cells for forced lung metastasis), representative pictures and number of macroscopic metastases, H&E staining, and metastatic foci percentage of *Il22*$^{+/+}$ and *Il22*$^{-/-}$ mice. n ≥ 10 mice per group.

(B) Schematic overview of the experiment (flank injection of MC38 cells for spontaneous lung metastasis), representative pictures, and number of macroscopic metastases. n ≥ 10 mice per group. Scale bar, 2 mm.

(C) Schematic overview of the experiment (i.v. injection of MC38 for forced lung metastasis in *Il22ra1*$^{wt/wt}$;*Cdh5*$^{Cre+}$ and *Il22ra1*$^{flox/flox}$;*Cdh5*$^{Cre+}$ mice).

(D) Number of macroscopic lung metastases. n ≥ 5 mice per group.

(E) Schematic overview of the experiment (i.v. MC38 cell injection following single left orthotopic lung transplantation using WT mice as recipients and *Il22ra1*$^{-/-}$ mice as donors).

(F) Representative pictures and quantification of lung metastases. n = 7 mice per group.

(G) Schematic overview of the experiment (i.v. injection of MC38 Cherry-labeled cells in WT, *Il22*$^{-/-}$ and *Il22ra1*$^{-/-}$ mice [extravasation assay]).

(H) Representative FACS plots and number of extravasated cancer cells 24 h post i.v. injection. n = 4 mice per group.

(I) Schematic overview of the experiment (i.v. injection of MC38 GFP-labeled cells in WT mice receiving an anti-IL-22 or IgG control antibody).

(J) Representative FACS plots and number of extravasated cancer cells. n ≥ 11 mice per group.

(K) Schematic overview of the experiment (i.v. injection of MC38 GFP-labeled cells in *Il22ra1*$^{wt/wt}$;*Cdh5*$^{Cre+}$ and *Il22ra1*$^{flox/flox}$;*Cdh5*$^{Cre+}$ mice [extravasation assay]).

(L) Representative FACS plots and number of extravasated cancer cells from *Il22ra1*$^{wt/wt}$;*Cdh5*$^{Cre+}$ and *Il22ra1*$^{flox/flox}$;*Cdh5*$^{Cre+}$ mice 24 h post i.v. injection. n = 5 mice per group. Data presented as mean ± SEM, ns $p > 0.05$; *$p < 0.05$; **$p \leq 0.01$; ***$p \leq 0.001$ as assessed by Mann-Whitney U test (A–D, J, and L), one-way ANOVA with Bonferroni post hoc tests (H), or two-tailed Wilcoxon matched-pairs signed rank test (F).

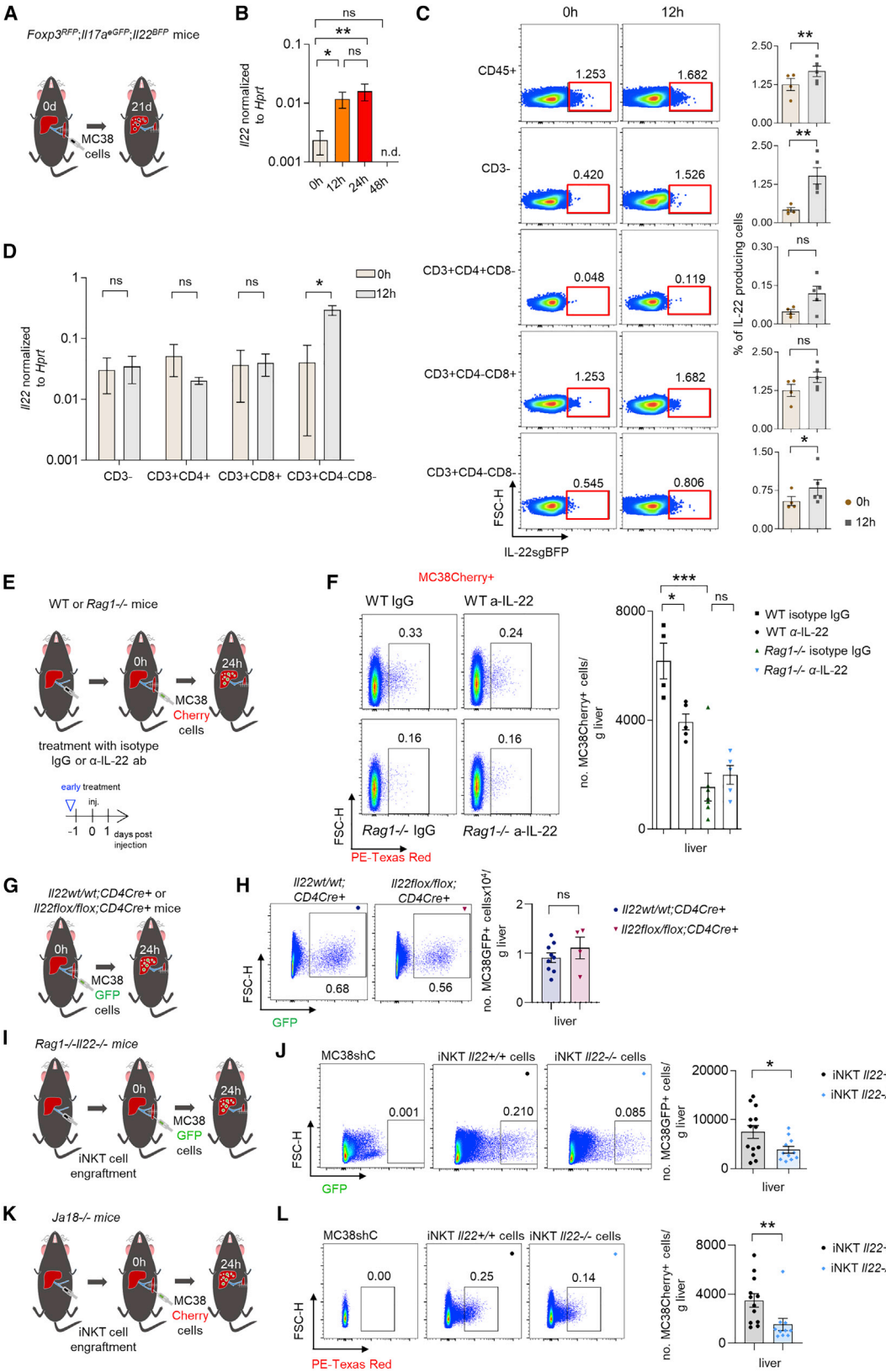

(legend on next page)

phenotype of the iNKT cells using the single-cell sequencing data, since *Il17a* and *Il22* were barely detectable and only a very small percentage of *Rorc*-positive cells were found (Figure S7). Finally, we performed parabiosis experiments, thereby creating parabiotic pairs between CD45.2 and CD45.½ mice.[38] Fourteen days post connection (Figure 7H), we injected MC38 cells or PBS into the portal vein of the CD45.2 members of the pairs (Figures 7I and 7J). Twelve hours post injection, we found that the majority of liver $CD45^{+}IL\text{-}22^{+}$ cells were in fact tissue resident cells (Figure 7K). In addition, we created pairs consisting of either two WT (littermate controls of *Il22*-deficient mice) mice or WT and *Il22*-deficient mice (Figure 7L). After 14 days, MC38 GFP-labeled cells were injected into the portal vein of both mice of the pair, which were then sacrificed 24 h later. *Il22*-deficient mice showed less extravasation compared to WT mice of the same pair (Figures 7M and 7N). WT mice paired with WT (littermate controls of $Il22^{-/-}$ mice) mice showed an equal extravasation number, suggesting that tissue-resident cell-derived IL-22 promotes extravasation of cancer cells.

Taken together, tissue resident iNKT17 cells are the functional relevant source of IL-22 during cancer cell extravasation.

DISCUSSION

Metastasis is responsible for the majority of cancer-related deaths worldwide.[39] The secondary tumor development and growth are influenced by tumor-infiltrating immune cells,[40] which can either promote or inhibit metastasis development.[41–43] However, the role of the immune cells that reside at the target site prior to its colonization with cancer cells in metastasis formation remains elusive. Thus, it is unclear whether tissue resident immune cells facilitate or inhibit metastasis. Consequently, it is unknown whether these cells and their cytokines could be targets for novel immunotherapies.

We report here that IL-22 is produced by tissue resident iNKT17 cells and mediates the immune system – cancer cell – tissue-specific stromal cell crosstalk, thereby facilitating cancer cell extravasation and thus liver metastasis formation. IL-22 increased endothelial permeability, thereby facilitating cancer cell extravasation. The consequence was tissue invasion, the critical step in metastasis formation. This effect was mediated by an IL-22-mediated upregulation of ANPEP expression in LSECs (see graphical abstract).

ANPEP is an aminopeptidase produced by a plethora of cells.[44] Interestingly, myeloid-derived ANPEP expression facilitates metastasis formation because *Anpep*-deficient mice show reduced lung metastases compared to *Anpep*-deficient mice transplanted with bone marrow from WT donors.[36] We extend this finding and we suggest that ANPEP aminopeptidase is an IL-22 target gene that increases endothelial permeability when expressed in the murine endothelium.

Several studies have reported that iNKT cells interact with liver sinusoids via the CXCL16-CXCR6 axis.[45,46] Interestingly, CXCL16 secretion by liver sinusoids has been linked to anti-tumor and anti-metastatic activity of iNKT cells in the liver.[46] Thus, we assessed whether this pathway also correlates with IL-22 production. However, this was not the case. Therefore, it seems that while the anti-tumorigenic functions of iNKT cells are linked to the CXCL16-CXCR6 axis, the pro-metastatic functions of iNKT cells shown here are linked to the IL-22-ANPEP axis. Interestingly, this effect of IL-22 as a promoter of cancer cell extravasation was not only found in the liver, but also in lung. The liver and the lungs both have extended endothelium, but their endothelial cells are markedly different.[47] In contrast to the lung, the liver is characterized by unique capillaries that differ from other capillaries in the body because of the presence of open pores. However, the endothelial permeability cannot fully explain the higher metastatic rates and metastatic organotropism exhibited by various forms of cancer. For example, primary CRC exhibits high metastatic rates both in the liver and the lung.[48] Regardless of these differences, our findings indicate that an IL-22 blockade could serve as a therapy to prevent both liver and lung metastasis. Indeed, from a therapeutic point of view, the extravasation process where the circulating cancer cells interact with the endothelium of the target organ is likely a rate-limiting step of metastasis formation. Here, cancer cell – endothelial cell interaction is required, and endothelial intercellular junctions are loosened in order to allow cancer cell transmigration into the stroma of the host organ.[49] IL-22 blockade could therefore have a major therapeutic effect. Indeed, we could show that Fezakinumab, a human monoclonal IL-22 antibody, which is already tested in Phase II trials for atopic dermatitis,[50] was able to block cancer cell extravasation in a humanized mouse model.[51]

Of note, cancer cells, like the endothelial cells, were responsive to IL-22, indicating that IL-22 can also mediate the communication between the immune system and the cancer cells.

Figure 6. iNKT cells promote cancer cell extravasation via IL-22

(A) Schematic overview of the experiment (i.v. injection of MC38 cells in IL-22 reporter mice).
(B) *Il22* mRNA levels in the liver at steady state, 12 and 24 h post i.s. MC38 cell injection.
(C) Representative concatenated FACS plots indicating mean and statistics of $CD45^{+}$, $CD3^{-}$, $CD3^{+}CD4^{+}$, $CD3^{+}CD8^{+}$, and $CD3^{+}CD4^{-}CD8^{-}$ IL-22-producing cells in the liver at 0 and 12 h post i.s. MC38 cell injection.
(D) *Il22* mRNA levels from indicated cell populations sorted from the liver at 0 and 12 h post i.s. MC38 cell injection.
(E) Schematic overview of the experiment (i.s. injection of MC38 GFP-labeled cells in WT and $Rag1^{-/-}$ mice, receiving an α-IL-22 or IgG control antibody).
(F) Representative FACS plots and statistics. $n \geq 4$ mice per group.
(G) Schematic overview of the experiment (i.s. injection of MC38 GFP-labeled cells in $Il22^{wt/wt}$;$CD4^{Cre+}$ and $Il22^{flox/flox}$;$CD4^{Cre+}$ mice). $n \geq 5$ mice per group.
(H) Representative FACS plots and number of extravasated cancer cells 24 h post i.s. injection. $n \geq 4$ mice per group.
(I) Schematic overview of the experiment (i.s. injection of MC38 GFP-labeled cells in $Rag^{-/-}Il22^{-/-}$ mice engrafted with $Il22^{+/+}$or $Il22^{-/-}$ iNKT cells).
(J) Representative FACS plots and number of extravasated cancer cells 24 h post i.s. injection. $n \geq 10$ mice per group.
(K) Schematic overview of the experiment (i.s. injection of MC38 Cherry-labeled cells in $Ja18^{-/-}$ mice engrafted with $Il22^{+/+}$or $Il22^{-/-}$ iNKT cells).
(L) Representative FACS plots and number of extravasated cancer cells 24 h post i.s. injection. $n \geq 10$ mice per group. Data presented as mean ± SEM, ns $p > 0.05$; *$p < 0.05$; **$p \leq 0.01$; ***$p \leq 0.001$ as assessed by one-way ANOVA with Bonferroni post hoc tests (B and F) or Mann-Whitney U test (C, D, H, J, and L).

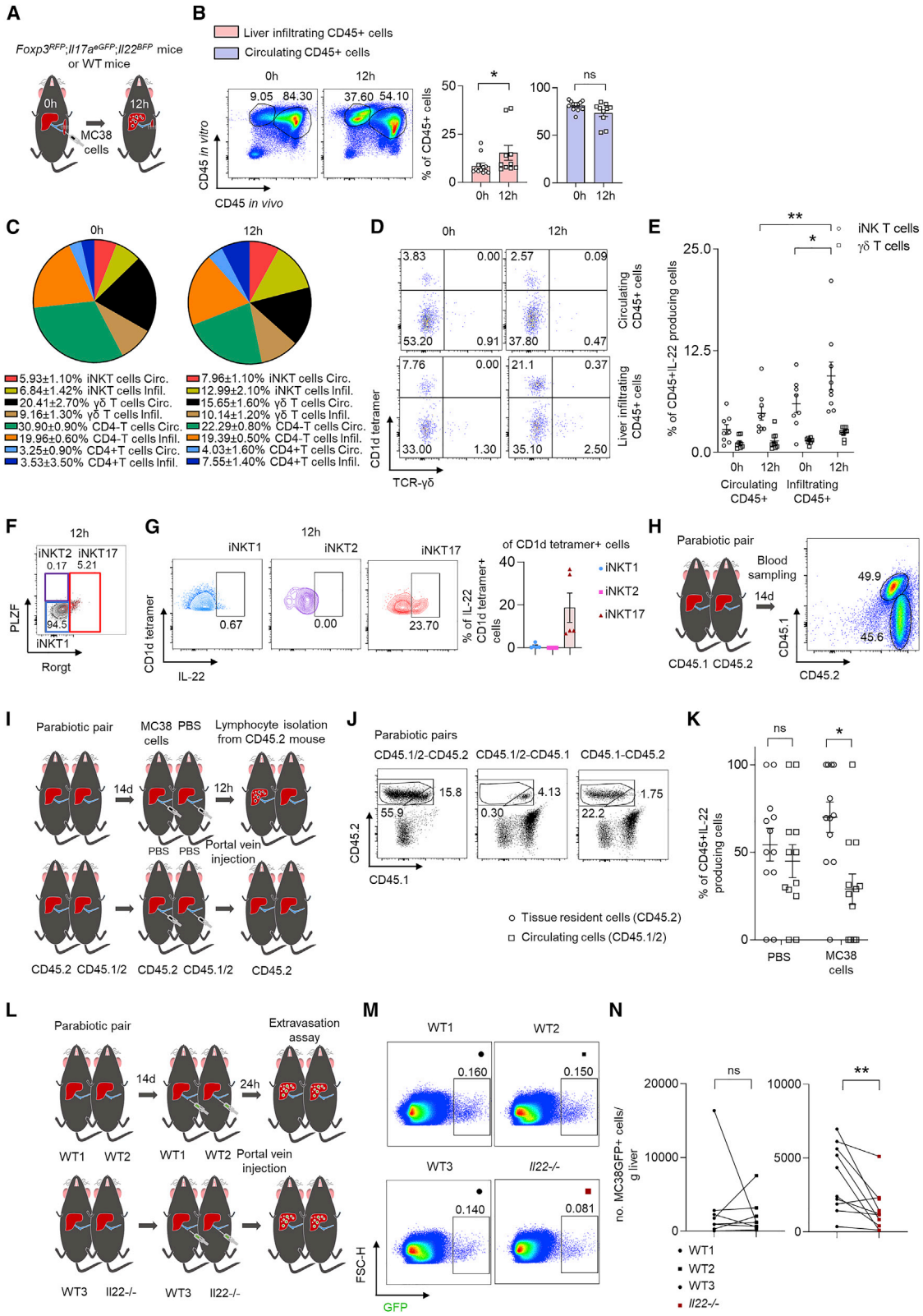

Figure 7. IL-22-producing iNKT17 cells are tissue resident and facilitate cancer cell extravasation

(A) Injection of an α-CD45 antibody intravenously after i.s. injection of MC38 cells.

(B) Representative FACS plots and statistics 0 and 12 h post i.s. injection. n ≥ 10 mice per group.

(legend continued on next page)

Indeed, IL-22RA1 silencing in cancer cells reduced the metastatic sites in an environment with high IL-22 levels. This finding shows an additive effect of IL-22 on cancer cells that express IL-22RA1. Thus, IL-22 promotes cancer cell extravasation. However, this does not exclude the fact that IL-22 has additional pro-metastatic effects. Indeed, other studies reported a direct tumorigenic effect of IL-22 on cancer cells, thereby promoting survival and proliferation.[52]

Many different cell types are able to produce IL-22 in liver metastasis. However, we found that tissue resident iNKT cells represent one major functionally relevant source of IL-22 in the early extravasation step of cancer cells. In this phase, iNKT17-cell-derived IL-22 acts on endothelial cells and increases their permeability to extravasating cancer cells. Importantly, our data indicate that iNKT cells control metastasis formation in the liver but not in the lungs. Indeed, we found low frequencies of IL-22-producing iNKT cells in the lung. Instead, we identified that γδ T cells represent the relevant cellular source of IL-22 in this setting and control the extravasation of cancer cells into the lungs. Thus, we speculate that, depending on the target organ, different cells can regulate the extravasation step of metastasis formation by producing IL-22. Interestingly, it has been reported before that NKT cells can have tissue residency and an effector-memory phenotype.[53,54] Indeed, we found here that IL-22-producing iNKT17 cells are tissue resident and play an essential role during cancer cell extravasation. It is tempting to speculate that this specific effect of iNKT17 cells is due to their tissue residency and presence in the liver even prior to the arrival of the circulating cancer cells.

NKT cells were best known for their anti-tumorigenic function.[46] However, emerging data involving innate-like T cells (NKT and MAIT [mucosal-associated invariant T cells]) indicate that these cells might also have a tumor-promoting function.[55] For example, it was published that invariant NKT cells are pro-tumorigenic in the colon,[56] but this activity disappears when a-GalCer is administered to the mice.[57] Furthermore, Molgora et al. showed that *Il1r8*$^{-/-}$ mice were protected from the development of liver metastasis.[58] Of note, these mice had increased numbers of NK cells and also a more mature NK cell phenotype. Furthermore, the adoptive transfer of *Il1r8*$^{-/-}$ NK cells also protected mice from the development of MC38 liver metastasis. Thus, *Il1r8*$^{-/-}$NK cells seem to play a protective role in metastasis. However, this study did not specifically investigate the role of tissue resident iNKT cells or the effect of IL-22 in this process. For our study, we wanted to address two points that remained open: whether IL-22-producing iNKT17 cells are tissue resident and, if so, whether they contribute to metastasis formation. Indeed, we found both to be affirmative. However, the mechanisms regulating IL-22 production in iNKT17 cells require further investigation.

In conclusion, our findings allowed us to identify the mechanisms by which tissue resident immune cells mediate the immune system – cancer cell – tissue-specific stromal cell crosstalk and revealed how tissue-resident iNKT-cell-derived IL-22 promotes extravasation during metastasis formation by acting on endothelial cells and inducing ANPEP expression. We would like to stress that the pro-metastatic effect of IL-22 can in fact be targeted therapeutically. When we neutralized IL-22 using an antibody, it blocked cancer cell extravasation and thus prevented metastasis formation in the target organ both in a murine model and also in a humanized mouse model. Based on these data, we propose targeting IL-22, e.g., by using Fezakinumab, as immunotherapy in patients suffering from established or impending metastasis.

LIMITATIONS OF THE STUDY

We found that IL-22 promotes both lung and liver metastasis. However, the cellular mechanism involving iNKT cells as IL-22 producers in aminopeptidase regulation on endothelial cells has only been shown for the hepatic environment. Therefore, further studies are critical to extend this finding to other organs. Indeed, in the lung, γδ T cells seem to be the functionally relevant source of IL-22 during metastasis. Thus, depending on the target organ, different cells may regulate metastasis formation. Further studies are required to test whether this difference is just due to different number, location, or function of iNKT and γδ T cells.

Other genes, besides ANPEP, known to promote cancer cell invasion and angiogenesis might also contribute to the effects of IL-22. We found that, besides ANPEP, NRP1 was also impacted by IL-22. Furthermore, we found that IL-22 can regulate VEGF (vascular endothelial growth factor) expression *in vitro*. Thus, we cannot exclude that other factors besides ANPEP may play an additional role in mediating the pro-metastatic effect of IL-22, and further studies will be critical in order to address this.

Blockade of IL-22 protected WT mice from developing forced liver metastasis. Testing this therapeutic regimen in *Apc*^{15lox}; *Kras*^{G12D} mice, which develop spontaneous cancer, was not feasible, since only mice with hydrodynamic overexpression of IL-22 in the liver and no control mice developed liver metastasis.

(C) Pie charts showing the proportion of infiltrating and circulating immune subsets among CD3$^+$IL-22$^+$ cells in murine liver 0 and 12 h post i.s. injection.
(D) Concatenated FACS plots of iNKT and γδ T cells gated on CD45$^+$IL-22$^+$ cells, including *in vivo* and *in vitro* CD45 staining. n ≥ 8 mice per group.
(E) Statistics of iNKT and γδ T cells gated on CD45$^+$IL-22$^+$ cells, including *in vivo* and *in vitro* CD45 staining. n ≥ 8 mice per group.
(F) Representative FACS plots showing the immune characterisation of iNKT cells gated on CD1d-tetramer$^+$IL-22$^+$ cells 12 h upon i.s. cancer cell injection.
(G) Representative FACS plots and statistics showing the immune subtypes (iNKT1, iNKT2, and iNKT17) of iNKT cells gated on CD1d-tetramer$^+$IL-22$^+$ cells 12 h upon i.s. cancer cell injection.
(H) CD45.2 reporter mice were connected together with CD45.1 (n = 3 mice per group) mice and the established blood chimerism was checked 14 days later.
(I) CD45.2 reporter mice were connected together with CD45.½ mice (n = 12 mice per group), followed by intraportal cancer cell injection after established blood chimerism.
(J) Representative FACS plots of CD45.½ and CD45.2 cells from parabiotic pairs.
(K) The proportion of CD45.½ and CD45.2 cells of parabiotic pairs was quantified.
(L) WT mice were connected with WT or *Il22*$^{-/-}$ mice (n ≥ 8 mice per group), followed by intraportal injection of MC38 GFP-labeled cells.
(M and N) Mice were sacrificed and the number of extravasated cancer cells was quantified. Data presented as mean ± SEM, ns $p > 0.05$; *$p < 0.05$; **$p \leq 0.01$; ***$p \leq 0.001$ as assessed by Mann-Whitney U test (B, E, and K) or two-tailed Wilcoxon matched-pairs signed rank test (N).

STAR★METHODS

Detailed methods are provided in the online version of this paper and include the following:

- KEY RESOURCES TABLE
- RESOURCE AVAILABILITY
  - Lead contact
  - Materials availability
  - Data and code availability
- METHOD DETAILS
  - Reagents
  - Cells
  - Animals
  - Isolation of hematopoietic cells from murine and human liver metastasis
  - Fluorescence-activated cell sorting
  - Mouse models of forced metastasis
  - Mouse models of spontaneous metastasis
  - Orthotopic colonic sub-mucosal implantation of CRC cells
  - Adenoviral infection of colonic epithelium for orthotopic colon cancer induction
  - Mouse colonoscopy
  - Immunoblotting
  - Hematoxylin and eosin (H&E) staining
  - Plasmids and transfections
  - Isolation of primary hepatocytes
  - Immunofluorescence
  - Isolation of LSECs
  - IL-22 ELISA
  - Adoptive transfer
  - Laminar flow adhesion assay
  - Extravasation assay
  - Circulating tumor cell isolation and quantification
  - Administration of antibody and aminopeptidase inhibitor treatment
  - IV injection of CD45 Ab
  - Parabiosis
  - Orthotopic single left lung transplantation (LuTx)
  - Endothelial gene assay
  - Measurement of the transendothelial electrical resistance (TEER)
  - *In vitro* transmigration assay
  - Lentiviral transfer of shRNAs into HUVEC cells
  - Bioluminescence imaging
  - Hydrodynamic injection of plasmid
  - Depletion of γδ T cells in *Tcrd*$^{GDL/GDL}$ mice
  - RNA analysis
  - scRNA-seq
  - Quantification and statistical analysis

SUPPLEMENTAL INFORMATION

Supplemental information can be found online at https://doi.org/10.1016/j.immuni.2022.12.014.

ACKNOWLEDGMENTS

The authors thank Elaine Hussey for reading the manuscript; Cathleen Haueis, Sandra Wende, and Tom Blankenburg for technical assistance; Gerrit Wolters-Eisfeld for Western blot antibodies; and Francesco Siracusa, the *in vivo* Optical Imaging Core Facility and the FACS Core Sorting Unit at the University Medical Center Hamburg-Eppendorf for their technical assistance. The PBS57-CD1d-tetramer was provided by the NIH tetramer core facility. Prof. Dr. Ron Smits, Erasmus University Medical Center, provided the *Apc*^{15lox} mice. We thank Dr. Guido Hegasy (www.hegasy.de) for designing the graphical abstract. This work was supported in part by the Deutsche Forschungsgemeinschaft (DFG) (SFB841 to S.H., N.G., A.W.L., K.R. [via B. Fehse]; SFB1328 to S.H., N.G.; grant 50552-1, SFB-TRR 338/1 2021–452881907 to S.K.; LA3373/6-1 to T.L.), the European Research Council (CoG 865466 to S.H., StG 756017 to S.K., ERC StG 715271 to N.G.), Else Kröner Memorial Stipendium (A.D.G.), Erich und Gertrud Roggenbuck-Stiftung (A.D.G.), Hamburger Krebsgesellschaft Stiftung (A.D.G.), the Jung Foundation for Science and Research (A.D.G.), and the Howard Hughes Medical Institute (R.A.F.). N.G. receives research grants from F. Hoffmann-La Roche and DZIF. S.H. has an endowed Heisenberg-Professorship awarded by the Deutsche Forschungsgemeinschaft. S.G.Z. acknowledges the Alexander von Humboldt Stiftung for an Experienced Researcher Fellowship. F.C. is supported by an iCARE-2 fellowship issued by AIRC and the European Union's Horizon 2020 grant 800924). K.P. received funding from the European Union Horizon 2020, grant No 765492, ERA-NET EU/TRANSCAN 2 JTC 2016 PROLIPSY, Deutsche Krebshilfe (Nr. 70112504), DFG SPP2084 μBone, and ERC Advanced Investigator Grant (Nr. 834974).

AUTHOR CONTRIBUTIONS

A.D.G., J.K., and A.M.S. conceived, designed, and carried out most experiments, analyzed data, and wrote the manuscript; J. Lücke, L.Z., and T.Z. carried out *in vivo* experiments and flow cytometry assays; D.E.Z. did immune labeling, confocal microscopy, *in vitro* transmigration assays and endothelial assays; F.C. helped with NKT characterization; K.R. and T.A. constructed expression vectors and performed transfection experiments; A.D.G., J.S.L., and M.C.A.V. carried out parabiosis experiments; H.X. carried out sorting; E.K. engrafted humanized mice; L.G.-P. performed ILC staining; A.D.G., Y.Y., and W.J. carried out single-left orthotopic lung transplantations; E.Z. established the intramucosal injection; K.F.K., L.K., K.S., J.V.F., M.R., and J.M. provided the human liver metastasis specimens; B.S. and J.W. carried out single-cell sequencing; A.C. isolated murine LSECs; P.M. and D.B. provided us with CRISPR for *Il22ra1* silencing; L.B. and T.B. performed fluorescence-activated cell sorting; S. Soukou and T.L. performed *in vitro* adhesion assays; C.K. and S.R. carried out CTC experiments; P.P., M.B., and M.S. performed *in vitro* experiments; F.J.H. performed *in vivo* experiments; S. Soukou characterized the *Il22ra1*$^{flox/flox}$;*Cdh5*$^{Cre+}$;*R26*^{YFP} mice; A.W. performed genotyping of *Il22ra1*$^{-/-}$, *Il22ra1*$^{flox/flox}$;*Alb*$^{Cre+}$ and *Il22ra1*$^{flox/flox}$;*Cdh5*$^{Cre+}$ mice; C.M. performed experiments of orthotopic colon cancer induction; B.G. provided the *Il22*$^{tg8+/-}$ mice; M.R., J.K.G., R.W., H.S., B.-O.S., M.F.A., A.D., G.P., I.C.M., D.P., P.S., M.T., T.G., A.H., J. Li, and N.M. provided the human liver metastasis specimens; S.G.Z. established the transendothelial electrical resistance (TEER) assay; T.S. provided *Il22ra1*$^{-/-}$ and *Il22ra1*$^{flox/flox}$ mice and provided critical intellectual input; R.P. and W.A. provided *Anpep*$^{-/-}$ mice and provided critical intellectual input; J.S.G. provided *Il22*$^{flox/flox}$;*CD4*$^{Cre+}$ mice and critical intellectual input; P.C.A., S.K., A.H.G., M.T., T.G., A.H., J. Li, N.M., O.M., J.R.I., K.P., U.S., A.W.L., and R.A.F. provided critical intellectual input; N.G. designed experiments, provided critical intellectual input, and edited the paper; and S.H. conceived the idea and supervised the study, designed experiments, and wrote the manuscript. All authors reviewed and concur with the submitted manuscript.

DECLARATION OF INTERESTS

S.K. declares honoraria from GSK, BMS, Novartis, and TCR2, Inc.; license fees from TCR2, Inc. and Carina Biotech; and research support from TCR2, Inc., Plectonic GmbH, Tabby Therapeutics, and Arcus Biosciences.

INCLUSION AND DIVERSITY

We support inclusive, diverse, and equitable conduct of research.

Received: August 22, 2022
Revised: September 9, 2022
Accepted: December 14, 2022
Published: January 10, 2023

REFERENCES

1. Bertocchi, A., Carloni, S., Ravenda, P.S., Bertalot, G., Spadoni, I., Lo Cascio, A., Gandini, S., Lizier, M., Braga, D., Asnicar, F., et al. (2021). Gut vascular barrier impairment leads to intestinal bacteria dissemination and colorectal cancer metastasis to liver. Cancer Cell *39*, 708–724.e11. https://doi.org/10.1016/j.ccell.2021.03.004.

2. Garner, H., and de Visser, K.E. (2020). Immune crosstalk in cancer progression and metastatic spread: a complex conversation. Nat. Rev. Immunol. *20*, 483–497. https://doi.org/10.1038/s41577-019-0271-z.

3. Bromley, S.K., Thomas, S.Y., and Luster, A.D. (2005). Chemokine receptor CCR7 guides T cell exit from peripheral tissues and entry into afferent lymphatics. Nat. Immunol. *6*, 895–901. https://doi.org/10.1038/ni1240.

4. Fernandez-Ruiz, D., Ng, W.Y., Holz, L.E., Ma, J.Z., Zaid, A., Wong, Y.C., Lau, L.S., Mollard, V., Cozijnsen, A., Collins, N., et al. (2016). Liver-resident memory CD8(+) T cells form a front-line defense against malaria liver-stage infection. Immunity *45*, 889–902. https://doi.org/10.1016/j.immuni.2016.08.011.

5. Park, S.L., Buzzai, A., Rautela, J., Hor, J.L., Hochheiser, K., Effern, M., McBain, N., Wagner, T., Edwards, J., McConville, R., et al. (2019). Tissue-resident memory CD8+ T cells promote melanoma–immune equilibrium in skin. Nature *565*, 366–371. https://doi.org/10.1038/s41586-018-0812-9.

6. Savas, P., Virassamy, B., Ye, C., Salim, A., Mintoff, C.P., Caramia, F., Salgado, R., Byrne, D.J., Teo, Z.L., Dushyanthen, S., et al. (2018). Single-cell profiling of breast cancer T cells reveals a tissue-resident memory subset associated with improved prognosis. Nat. Med. *24*, 986–993. https://doi.org/10.1038/s41591-018-0078-7.

7. Salio, M., Silk, J.D., Jones, E.Y., and Cerundolo, V. (2014). Biology of CD1- and MR1-Restricted T Cells. Annu. Rev. Immunol. *32*, 323–366. https://doi.org/10.1146/annurev-immunol-032713-120243.

8. Matos, T.R., O'Malley, J.T., Lowry, E.L., Hamm, D., Kirsch, I.R., Robins, H.S., Kupper, T.S., Krueger, J.G., and Clark, R.A. (2017). Clinically resolved psoriatic lesions contain psoriasis-specific IL-17-producing αβ T cell clones. J. Clin. Invest. *127*, 4031–4041. https://doi.org/10.1172/JCI93396.

9. Paget, C., Ivanov, S., Fontaine, J., Renneson, J., Blanc, F., Pichavant, M., Dumoutier, L., Ryffel, B., Renauld, J.C., Gosset, P., et al. (2012). Interleukin-22 is produced by invariant natural killer T lymphocytes during influenza A virus infection: potential role in protection against lung epithelial damages. J. Biol. Chem. *287*, 8816–8829. https://doi.org/10.1074/jbc.M111.304758.

10. Godfrey, D.I., Stankovic, S., and Baxter, A.G. (2010). Raising the NKT cell family. Nat. Immunol. *11*, 197–206. https://doi.org/10.1038/ni.1841.

11. Goto, M., Murakawa, M., Kadoshima-Yamaoka, K., Tanaka, Y., Nagahira, K., Fukuda, Y., and Nishimura, T. (2009). Murine NKT cells produce Th17 cytokine interleukin-22. Cell. Immunol. *254*, 81–84. https://doi.org/10.1016/j.cellimm.2008.10.002.

12. Yang, W., Yu, T., Huang, X., Bilotta, A.J., Xu, L., Lu, Y., Sun, J., Pan, F., Zhou, J., Zhang, W., et al. (2020). Intestinal microbiota-derived short-chain fatty acids regulation of immune cell IL-22 production and gut immunity. Nat. Commun. *11*, 4457. https://doi.org/10.1038/s41467-020-18262-6.

13. Rutz, S., Eidenschenk, C., and Ouyang, W. (2013). IL-22, not simply a Th17 cytokine. Immunol. Rev. *252*, 116–132. https://doi.org/10.1111/imr.12027.

14. Voigt, C., May, P., Gottschlich, A., Markota, A., Wenk, D., Gerlach, I., Voigt, S., Stathopoulos, G.T., Arendt, K.A.M., Heise, C., et al. (2017). Cancer cells induce interleukin-22 production from memory CD4(+) T cells via interleukin-1 to promote tumor growth. Proc. Natl. Acad. Sci. USA *114*, 12994–12999. https://doi.org/10.1073/pnas.1705165114.

15. Doulabi, H., Rastin, M., Shabahangh, H., Maddah, G., Abdollahi, A., Nosratabadi, R., Esmaeili, S.-A., and Mahmoudi, M. (2018). Analysis of Th22, Th17 and CD4+cells co-producing IL-17/IL-22 at different stages of human colon cancer. Biomed. Pharmacother. *103*, 1101–1106. https://doi.org/10.1016/j.biopha.2018.04.147.

16. Perez, L.G., Kempski, J., McGee, H.M., Pelzcar, P., Agalioti, T., Giannou, A., Konczalla, L., Brockmann, L., Wahib, R., Xu, H., et al. (2020). TGF-β signaling in Th17 cells promotes IL-22 production and colitis-associated colon cancer. Nat. Commun. *11*, 2608. https://doi.org/10.1038/s41467-020-16363-w.

17. Cui, G. (2019). TH9, TH17, and TH22 cell subsets and their main cytokine products in the pathogenesis of colorectal cancer. Front. Oncol. *9*, 1002. https://doi.org/10.3389/fonc.2019.01002.

18. Eyerich, S., Eyerich, K., Pennino, D., Carbone, T., Nasorri, F., Pallotta, S., Cianfarani, F., Odorisio, T., Traidl-Hoffmann, C., Behrendt, H., et al. (2009). Th22 cells represent a distinct human T cell subset involved in epidermal immunity and remodeling. J. Clin. Invest. *119*, 3573–3585. https://doi.org/10.1172/jci40202.

19. Gronke, K., Hernández, P.P., Zimmermann, J., Klose, C.S.N., Kofoed-Branzk, M., Guendel, F., Witkowski, M., Tizian, C., Amann, L., Schumacher, F., et al. (2019). Interleukin-22 protects intestinal stem cells against genotoxic stress. Nature *566*, 249–253. https://doi.org/10.1038/s41586-019-0899-7.

20. Lindemans, C.A., Calafiore, M., Mertelsmann, A.M., O'Connor, M.H., Dudakov, J.A., Jenq, R.R., Velardi, E., Young, L.F., Smith, O.M., Lawrence, G., et al. (2015). Interleukin-22 promotes intestinal-stem-cell-mediated epithelial regeneration. Nature *528*, 560–564. https://doi.org/10.1038/nature16460.

21. Kamanaka, M., Huber, S., Zenewicz, L.A., Gagliani, N., Rathinam, C., O'Connor, W., Jr., Wan, Y.Y., Nakae, S., Iwakura, Y., Hao, L., and Flavell, R.A. (2011). Memory/effector (CD45RB(lo)) CD4 T cells are controlled directly by IL-10 and cause IL-22-dependent intestinal pathology. J. Exp. Med. *208*, 1027–1040. https://doi.org/10.1084/jem.20102149.

22. Huber, S., Gagliani, N., Zenewicz, L.A., Huber, F.J., Bosurgi, L., Hu, B., Hedl, M., Zhang, W., O'Connor, W., Jr., Murphy, A.J., et al. (2012). IL-22BP is regulated by the inflammasome and modulates tumorigenesis in the intestine. Nature *491*, 259–263. https://doi.org/10.1038/nature11535.

23. Kirchberger, S., Royston, D.J., Boulard, O., Thornton, E., Franchini, F., Szabady, R.L., Harrison, O., and Powrie, F. (2013). Innate lymphoid cells sustain colon cancer through production of interleukin-22 in a mouse model. J. Exp. Med. *210*, 917–931. https://doi.org/10.1084/jem.20122308.

24. Kryczek, I., Lin, Y., Nagarsheth, N., Peng, D., Zhao, L., Zhao, E., Vatan, L., Szeliga, W., Dou, Y., Owens, S., et al. (2014). IL-22(+)CD4(+) T cells promote colorectal cancer stemness via STAT3 transcription factor activation and induction of the methyltransferase DOT1L. Immunity *40*, 772–784. https://doi.org/10.1016/j.immuni.2014.03.010.

25. Khosravi, N., Caetano, M.S., Cumpian, A.M., Unver, N., De la Garza Ramos, C., Noble, O., Daliri, S., Hernandez, B.J., Gutierrez, B.A., Evans, S.E., et al. (2018). IL22 promotes Kras-mutant lung cancer by induction of a protumor immune response and protection of stemness properties. Cancer Immunol. Res. *6*, 788–797. https://doi.org/10.1158/2326-6066.cir-17-0655.

26. Jiang, R., Tan, Z., Deng, L., Chen, Y., Xia, Y., Gao, Y., Wang, X., and Sun, B. (2011). Interleukin-22 promotes human hepatocellular carcinoma by activation of STAT3. Hepatology *54*, 900–909. https://doi.org/10.1002/hep.24486.

27. Jiang, R., Wang, H., Deng, L., Hou, J., Shi, R., Yao, M., Gao, Y., Yao, A., Wang, X., Yu, L., and Sun, B. (2013). IL-22 is related to development of human colon cancer by activation of STAT3. BMC Cancer *13*, 59. https://doi.org/10.1186/1471-2407-13-59.

28. McCuaig, S., Barras, D., Mann, E.H., Friedrich, M., Bullers, S.J., Janney, A., Garner, L.C., Domingo, E., Koelzer, V.H., Delorenzi, M., et al. (2020). The interleukin 22 Pathway interacts with mutant KRAS to promote poor

prognosis in colon cancer. Clin. Cancer Res. *26*, 4313–4325. https://doi.org/10.1158/1078-0432.ccr-19-1086.

29. Wen, Z., Liao, Q., Zhao, J., Hu, Y., You, L., Lu, Z., Jia, C., Wei, Y., and Zhao, Y. (2014). High expression of interleukin-22 and its receptor predicts poor prognosis in pancreatic ductal adenocarcinoma. Ann. Surg Oncol. *21*, 125–132. https://doi.org/10.1245/s10434-013-3322-x.
30. Giannou, A.D., Marazioti, A., Kanellakis, N.I., Giopanou, I., Lilis, I., Zazara, D.E., Ntaliarda, G., Kati, D., Armenis, V., Giotopoulou, G.A., et al. (2017). NRAS destines tumor cells to the lungs. EMBO Mol. Med. *9*, 672–686. https://doi.org/10.15252/emmm.201606978.
31. Feng, D., Wang, Y., Wang, H., Weng, H., Kong, X., Martin-Murphy, B.V., Li, Y., Park, O., Dooley, S., Ju, C., and Gao, B. (2014). Acute and chronic effects of IL-22 on acetaminophen-induced liver injury. J. Immunol. *193*, 2512–2518. https://doi.org/10.4049/jimmunol.1400588.
32. Hung, K.E., Maricevich, M.A., Richard, L.G., Chen, W.Y., Richardson, M.P., Kunin, A., Bronson, R.T., Mahmood, U., and Kucherlapati, R. (2010). Development of a mouse model for sporadic and metastatic colon tumors and its use in assessing drug treatment. Proc. Natl. Acad. Sci. USA *107*, 1565–1570. https://doi.org/10.1073/pnas.0908682107.
33. Robanus-Maandag, E.C., Koelink, P.J., Breukel, C., Salvatori, D.C.F., Jagmohan-Changur, S.C., Bosch, C.A.J., Verspaget, H.W., Devilee, P., Fodde, R., and Smits, R. (2010). A new conditional Apc -mutant mouse model for colorectal cancer. Carcinogenesis *31*, 946–952. https://doi.org/10.1093/carcin/bgq046.
34. Alva, J.A., Zovein, A.C., Monvoisin, A., Murphy, T., Salazar, A., Harvey, N.L., Carmeliet, P., and Iruela-Arispe, M.L. (2006). VE-Cadherin-Cre-recombinase transgenic mouse: A tool for lineage analysis and gene deletion in endothelial cells. Dev. Dyn. *235*, 759–767. https://doi.org/10.1002/dvdy.20643.
35. Kleinschmidt, D., Giannou, A.D., McGee, H.M., Kempski, J., Steglich, B., Huber, F.J., Ernst, T.M., Shiri, A.M., Wegscheid, C., Tasika, E., et al. (2017). A protective function of IL-22BP in ischemia reperfusion and acetaminophen-induced liver injury. J. Immunol. *199*, 4078–4090. https://doi.org/10.4049/jimmunol.1700587.
36. Dondossola, E., Rangel, R., Guzman-Rojas, L., Barbu, E.M., Hosoya, H., St John, L.S., Molldrem, J.J., Corti, A., Sidman, R.L., Arap, W., and Pasqualini, R. (2013). CD13-positive bone marrow-derived myeloid cells promote angiogenesis, tumor growth, and metastasis. Proc. Natl. Acad. Sci. USA *110*, 20717–20722. https://doi.org/10.1073/pnas.1321139110.
37. Drujont, L., Lemoine, A., Moreau, A., Bienvenu, G., Lancien, M., Cens, T., Guillot, F., Bériou, G., Bouchet-Delbos, L., Fehling, H.J., et al. (2016). RORγt+ cells selectively express redundant cation channels linked to the Golgi apparatus. Sci. Rep. *6*, 23682. https://doi.org/10.1038/srep23682.
38. Amezcua Vesely, M.C., Pallis, P., Bielecki, P., Low, J.S., Zhao, J., Harman, C.C.D., Kroehling, L., Jackson, R., Bailis, W., Licona-Limón, P., et al. (2019). Effector TH17 cells give rise to long-lived TRM cells that are essential for an immediate response against bacterial infection. Cell *178*, 1176–1188.e15. https://doi.org/10.1016/j.cell.2019.07.032.
39. Fares, J., Fares, M.Y., Khachfe, H.H., Salhab, H.A., and Fares, Y. (2020). Molecular principles of metastasis: a hallmark of cancer revisited. Signal Transduct. Target. Ther. *5*, 28. https://doi.org/10.1038/s41392-020-0134-x.
40. Qian, B.-Z., Li, J., Zhang, H., Kitamura, T., Zhang, J., Campion, L.R., Kaiser, E.A., Snyder, L.A., and Pollard, J.W. (2011). CCL2 recruits inflammatory monocytes to facilitate breast-tumour metastasis. Nature *475*, 222–225. https://doi.org/10.1038/nature10138.
41. Bindea, G., Mlecnik, B., Tosolini, M., Kirilovsky, A., Waldner, M., Obenauf, A.C., Angell, H., Fredriksen, T., Lafontaine, L., Berger, A., et al. (2013). Spatiotemporal dynamics of intratumoral immune cells reveal the immune landscape in human cancer. Immunity *39*, 782–795. https://doi.org/10.1016/j.immuni.2013.10.003.
42. Coffelt, S.B., Kersten, K., Doornebal, C.W., Weiden, J., Vrijland, K., Hau, C.-S., Verstegen, N.J.M., Ciampricotti, M., Hawinkels, L.J.A.C., Jonkers, J., and de Visser, K.E. (2015). IL-17-producing γδ T cells and neutrophils conspire to promote breast cancer metastasis. Nature *522*, 345–348. https://doi.org/10.1038/nature14282.
43. Mlecnik, B., Bindea, G., Angell, H.K., Maby, P., Angelova, M., Tougeron, D., Church, S.E., Lafontaine, L., Fischer, M., Fredriksen, T., et al. (2016). Integrative analyses of colorectal cancer show immunoscore is a stronger predictor of patient survival than microsatellite instability. Immunity *44*, 698–711. https://doi.org/10.1016/j.immuni.2016.02.025.
44. Guzman-Rojas, L., Rangel, R., Salameh, A., Edwards, J.K., Dondossola, E., Kim, Y.-G., Saghatelian, A., Giordano, R.J., Kolonin, M.G., Staquicini, F.I., et al. (2012). Cooperative effects of aminopeptidase N (CD13) expressed by nonmalignant and cancer cells within the tumor microenvironment. Proc. Natl. Acad. Sci. USA *109*, 1637–1642. https://doi.org/10.1073/pnas.1120790109.
45. Geissmann, F., Cameron, T.O., Sidobre, S., Manlongat, N., Kronenberg, M., Briskin, M.J., Dustin, M.L., and Littman, D.R. (2005). Intravascular immune surveillance by CXCR6+ NKT cells patrolling liver sinusoids. PLoS Biol. *3*, e113. https://doi.org/10.1371/journal.pbio.0030113.
46. Ma, C., Han, M., Heinrich, B., Fu, Q., Zhang, Q., Sandhu, M., Agdashian, D., Terabe, M., Berzofsky, J.A., Fako, V., et al. (2018). Gut microbiome-mediated bile acid metabolism regulates liver cancer via NKT cells. Science *360*, eaan5931. https://doi.org/10.1126/science.aan5931.
47. Paik, D.T., Tian, L., Williams, I.M., Rhee, S., Zhang, H., Liu, C., Mishra, R., Wu, S.M., Red-Horse, K., and Wu, J.C. (2020). Single-cell RNA sequencing unveils unique transcriptomic signatures of organ-specific endothelial cells. Circulation *142*, 1848–1862. https://doi.org/10.1161/circulationaha.119.041433.
48. Wang, J., Li, S., Liu, Y., Zhang, C., Li, H., and Lai, B. (2020). Metastatic patterns and survival outcomes in patients with stage IV colon cancer: A population-based analysis. Cancer Med. *9*, 361–373. https://doi.org/10.1002/cam4.2673.
49. Stoletov, K., Kato, H., Zardouzian, E., Kelber, J., Yang, J., Shattil, S., and Klemke, R. (2010). Visualizing extravasation dynamics of metastatic tumor cells. J. Cell Sci. *123*, 2332–2341. https://doi.org/10.1242/jcs.069443.
50. Guttman-Yassky, E., Brunner, P.M., Neumann, A.U., Khattri, S., Pavel, A.B., Malik, K., Singer, G.K., Baum, D., Gilleaudeau, P., Sullivan-Whalen, M., et al. (2018). Efficacy and safety of fezakinumab (an IL-22 monoclonal antibody) in adults with moderate-to-severe atopic dermatitis inadequately controlled by conventional treatments: A randomized, double-blind, phase 2a trial. J. Am. Acad. Dermatol. *78*, 872–881.e6. https://doi.org/10.1016/j.jaad.2018.01.016.
51. Rongvaux, A., Willinger, T., Martinek, J., Strowig, T., Gearty, S.V., Teichmann, L.L., Saito, Y., Marches, F., Halene, S., Palucka, A.K., et al. (2014). Development and function of human innate immune cells in a humanized mouse model. Nat. Biotechnol. *32*, 364–372. https://doi.org/10.1038/nbt.2858.
52. Wu, T., Cui, L., Liang, Z., Liu, C., Liu, Y., and Li, J. (2013). Elevated serum IL-22 levels correlate with chemoresistant condition of colorectal cancer. Clin. Immunol. *147*, 38–39. https://doi.org/10.1016/j.clim.2013.02.007.
53. Thomas, S.Y., Scanlon, S.T., Griewank, K.G., Constantinides, M.G., Savage, A.K., Barr, K.A., Meng, F., Luster, A.D., and Bendelac, A. (2011). PLZF induces an intravascular surveillance program mediated by long-lived LFA-1–ICAM-1 interactions. J. Exp. Med. *208*, 1179–1188. https://doi.org/10.1084/jem.20102630.
54. Salou, M., Legoux, F., Gilet, J., Darbois, A., du Halgouet, A., Alonso, R., Richer, W., Goubet, A.-G., Daviaud, C., Menger, L., et al. (2019). A common transcriptomic program acquired in the thymus defines tissue residency of MAIT and NKT subsets. J. Exp. Med. *216*, 133–151. https://doi.org/10.1084/jem.20181483.
55. Yan, J., Allen, S., McDonald, E., Das, I., Mak, J.Y.W., Liu, L., Fairlie, D.P., Meehan, B.S., Chen, Z., Corbett, A.J., et al. (2020). MAIT cells promote tumor initiation, growth, and metastases via tumor MR1. Cancer Discov. *10*, 124–141. https://doi.org/10.1158/2159-8290.CD-19-0569.
56. Wang, Y., Sedimbi, S., Löfbom, L., Singh, A.K., Porcelli, S.A., and Cardell, S.L. (2018). Unique invariant natural killer T cells promote intestinal polyps

by suppressing TH1 immunity and promoting regulatory T cells. Mucosal Immunol. *11*, 131–143. https://doi.org/10.1038/mi.2017.34.

57. Zhang, Y., Springfield, R., Chen, S., Li, X., Feng, X., Moshirian, R., Yang, R., and Yuan, W. (2019). α-GalCer and iNKT cell-based cancer immunotherapy: realizing the therapeutic potentials. Front. Immunol. *10*, 1126. https://doi.org/10.3389/fimmu.2019.01126.
58. Molgora, M., Bonavita, E., Ponzetta, A., Riva, F., Barbagallo, M., Jaillon, S., Popović, B., Bernardini, G., Magrini, E., Gianni, F., et al. (2017). IL-1R8 is a checkpoint in NK cells regulating anti-tumour and anti-viral activity. Nature *551*, 110–114. https://doi.org/10.1038/nature24293.
59. Weber, K., Bartsch, U., Stocking, C., and Fehse, B. (2008). A multicolor panel of novel lentiviral "Gene Ontology" (LeGO) vectors for functional gene analysis. Mol. Ther. *16*, 698–706. https://doi.org/10.1038/mt.2008.6.
60. Grabinger, T., Bode, K.J., Demgenski, J., Seitz, C., Delgado, M.E., Kostadinova, F., Reinhold, C., Etemadi, N., Wilhelm, S., Schweinlin, M., et al. (2017). Inhibitor of apoptosis protein-1 regulates tumor necrosis factor–mediated destruction of intestinal epithelial cells. Gastroenterology *152*, 867–879. https://doi.org/10.1053/j.gastro.2016.11.019.
61. Nittka, S., Krueger, M.A., Shively, J.E., Boll, H., Brockmann, M.A., Doyon, F., Pichler, B.J., and Neumaier, M. (2014). Radioimmunoimaging of liver metastases with PET using a 64Cu-labeled CEA antibody in transgenic mice. PLoS One *9*, e106921. https://doi.org/10.1371/journal.pone.0106921.
62. Brodbeck, T., Nehmann, N., Bethge, A., Wedemann, G., and Schumacher, U. (2014). Perforin-dependent direct cytotoxicity in natural killer cells induces considerable knockdown of spontaneous lung metastases and computer modelling-proven tumor cell dormancy in a HT29 human colon cancer xenograft mouse model. Mol. Cancer *13*, 244. https://doi.org/10.1186/1476-4598-13-244.
63. Bauer, R., Udonta, F., Wroblewski, M., Ben-Batalla, I., Santos, I.M., Taverna, F., Kuhlencord, M., Gensch, V., Päsler, S., Vinckier, S., et al. (2018). Blockade of myeloid-derived suppressor cell expansion with all-trans retinoic acid increases the efficacy of antiangiogenic therapy. Cancer Res. *78*, 3220–3232. https://doi.org/10.1158/0008-5472.CAN-17-3415.
64. Esplugues, E., Huber, S., Gagliani, N., Hauser, A.E., Town, T., Wan, Y.Y., O'Connor, W., Jr., Rongvaux, A., Van Rooijen, N., Haberman, A.M., et al. (2011). Control of TH17 cells occurs in the small intestine. Nature *475*, 514–518. https://doi.org/10.1038/nature10228.
65. Huber, S., Gagliani, N., Esplugues, E., O'Connor, W., Jr., Huber, F.J., Chaudhry, A., Kamanaka, M., Kobayashi, Y., Booth, C.J., Rudensky, A.Y., et al. (2011). Th17 cells express interleukin-10 receptor and are controlled by Foxp3^{-} and Foxp3+ regulatory CD4+ T cells in an interleukin-10-dependent manner. Immunity *34*, 554–565. https://doi.org/10.1016/j.immuni.2011.01.020.
66. Wan, Y.Y., and Flavell, R.A. (2005). Identifying Foxp3-expressing suppressor T cells with a bicistronic reporter. Proc. Natl. Acad. Sci. USA *102*, 5126–5131. https://doi.org/10.1073/pnas.0501701102.
67. Soares, K.C., Foley, K., Olino, K., Leubner, A., Mayo, S.C., Jain, A., Jaffee, E., Schulick, R.D., Yoshimura, K., Edil, B., and Zheng, L. (2014). A preclinical murine model of hepatic metastases. JoVE, 51677. https://doi.org/10.3791/51677.
68. Liao, H.-W., Hsu, J.-M., Xia, W., Wang, H.-L., Wang, Y.-N., Chang, W.-C., Arold, S.T., Chou, C.-K., Tsou, P.-H., Yamaguchi, H., et al. (2015). PRMT1-mediated methylation of the EGF receptor regulates signaling and cetuximab response. J. Clin. Invest. *125*, 4529–4543. https://doi.org/10.1172/JCI82826.
69. Pelczar, P., Witkowski, M., Perez, L.G., Kempski, J., Hammel, A.G., Brockmann, L., Kleinschmidt, D., Wende, S., Haueis, C., Bedke, T., et al. (2016). A pathogenic role for T cell–derived IL-22BP in inflammatory bowel disease. Science *354*, 358–362. https://doi.org/10.1126/science.aah5903.
70. Richter, U., Schröder, C., Wicklein, D., Lange, T., Geleff, S., Dippel, V., Schumacher, U., and Klutmann, S. (2011). Adhesion of small cell lung cancer cells to E- and P-Selectin under physiological flow conditions: implications for metastasis formation. Histochem. Cell Biol. *135*, 499–512. https://doi.org/10.1007/s00418-011-0804-4.
71. Jungraithmayr, W.M., Korom, S., Hillinger, S., and Weder, W. (2009). A mouse model of orthotopic, single-lung transplantation. J. Thorac. Cardiovasc. Surg. *137*, 486–491. https://doi.org/10.1016/j.jtcvs.2008.10.007.
72. Giannou, A.D., Marazioti, A., Spella, M., Kanellakis, N.I., Apostolopoulou, H., Psallidas, I., Prijovich, Z.M., Vreka, M., Zazara, D.E., Lilis, I., et al. (2015). Mast cells mediate malignant pleural effusion formation. J. Clin. Invest. *125*, 2317–2334. https://doi.org/10.1172/JCI79840.
73. Butler, A., Hoffman, P., Smibert, P., Papalexi, E., and Satija, R. (2018). Integrating single-cell transcriptomic data across different conditions, technologies, and species. Nat. Biotechnol. *36*, 411–420. https://doi.org/10.1038/nbt.4096.
74. Hafemeister, C., and Satija, R. (2019). Normalization and variance stabilization of single-cell RNA-seq data using regularized negative binomial regression. Genome Biol. *20*, 296. https://doi.org/10.1186/s13059-019-1874-1.
75. Stuart, T., Butler, A., Hoffman, P., Hafemeister, C., Papalexi, E., Mauck, W.M., 3rd, Hao, Y., Stoeckius, M., Smibert, P., and Satija, R. (2019). Comprehensive Integration of Single-Cell Data. Cell *177*, 1888–1902.e21. https://doi.org/10.1016/j.cell.2019.05.031.
76. Szabo, P.A., Miron, M., and Farber, D.L. (2019). Location, location, location: tissue resident memory T cells in mice and humans. Sci. Immunol. *4*, eaas9673. https://doi.org/10.1126/sciimmunol.aas9673.

STAR★METHODS

KEY RESOURCES TABLE

REAGENT or RESOURCE	SOURCE	IDENTIFIER
Antibodies		
Anti-human CD45	BioLegend	Cat# 304010; RRID: AB_314398
Anti-human CD3	BD Bioscience	Cat# 564307; RRID: AB_2744390
Anti-human CD4	BioLegend	Cat# 357410; RRID: AB_2565662
Anti-human IL-22	eBioscience	Cat# 12-7229-42; RRID: AB_1834463
Human PBS57-loaded CD1d tetramer	NIH tetramer core facility	N/A
Anti-mouse CD45	BioLegend	Cat# 103149; RRID: AB_2564590
Anti-mouse CD45	BioLegend	Cat# 103114; RRID: AB_312979
Anti-mouse CD45	BioLegend	Cat# 147716; RRID: AB_2750449
Anti-mouse CD45.1	BioLegend	Cat# 110714; RRID: AB_313503
Anti-mouse CD45.2	BioLegend	Cat# 109830; RRID: AB_1186098
Anti-mouse CD3	BioLegend	Cat# 100216; RRID: AB_493697
Anti-mouse CD3	BioLegend	Cat# 100206; RRID: AB_312663
Anti-mouse CD3	eBioscience	Cat# 35-0031-82; RRID: AB_11219266
Anti-mouse CD8	BioLegend	Cat# 100722; RRID: AB_312761
Anti-mouse CD4	BD Bioscience	Cat# 563790; RRID: AB_2738426
Anti-mouse TCR γ/δ	BioLegend	Cat# 118116; RRID: AB_1731813
Anti-mouse IL-22RA1	R&D	Cat# FAB42941P; RRID: AB_1964624
Anti-mouse IgG	R&D	Cat# IC006P; RRID: AB_357256
Anti-mouse pSTAT3	BD Bioscience	Cat# 560312; RRID: AB_1645327
Anti-mouse Lin-1	BioLegend	Cat# 133313; RRID: AB_2715571
Mouse PBS57-loaded CD1d tetramer	NIH tetramer core facility	N/A
Anti-mouse CD90.1	BioLegend	Cat# 202526; RRID: AB_1595470
Anti-mouse CD90.1	BioLegend	Cat# 202537; RRID: AB_2562644
Anti-mouse CD90.1	BioLegend	Cat# 202518; RRID: AB_1659223

(*Continued on next page*)

Continued

REAGENT or RESOURCE	SOURCE	IDENTIFIER
Anti-mouse CD90.1	BioLegend	Cat# 202529; RRID: AB_10899572
Anti-mouse CD90.2	BioLegend	Cat# 105320; RRID: AB_493725
Anti-mouse CD90.2	BioLegend	Cat# 105343; RRID: AB_10643586
Anti-mouse CD90.2	BioLegend	Cat# 140310; RRID: AB_2632889
Anti-mouse IL-7Ra	BioLegend	Cat# 135020; RRID: AB_1937209
Anti-mouse IL-7Ra	BioLegend	Cat# 135014; RRID: AB_1937265
Anti-mouse CD3	BioLegend	Cat# 100303; RRID: AB_312668
Anti-mouse CD4	BioLegend	Cat# 100507; RRID: AB_312710
Anti-mouse CD5	BioLegend	Cat# 100603; RRID: AB_312732
Anti-mouse CD8	BioLegend	Cat# 100703; RRID: AB_312742
Anti-mouse CD11b	BioLegend	Cat# 101203; RRID: AB_312786
Anti-mouse CD11c	BD Bioscience	Cat# 553800; RRID: AB_395059
Anti-mouse CD19	BioLegend	Cat# 115503; RRID: AB_313638
Anti-mouse CD49b	BioLegend	Cat# 103521; RRID: AB_2566365
Anti-mouse GR-1	BioLegend	Cat# 108403; RRID: AB_313368
Anti-mouse NK1.1	BioLegend	Cat# 108703; RRID: AB_313390
Anti-mouse TCR gd	BioLegend	Cat# 118103; RRID: AB_313827
Anti-mouse TCRb	BioLegend	Cat# 109203; RRID: AB_313426
Anti-mouse Ter119	BioLegend	Cat# 116204; RRID: AB_313705
Anti-Fc- γ receptors	Samuel Huber Lab, UKE, Germany	clone 2.4G2
Streptavidin	BD Bioscience	Cat# 564176
Anti-GFP rabbit	Life-technologies	Cat# A11122; RRID: AB_221569
AF488 donkey anti-mouse IgG	Life-technologies	Cat# A21202; RRID: AB_141607
AF488 goat anti-rat IgG	Invitrogen	Cat# A21208; RRID: AB_141709
AF568 goat anti-chicken IgG	Life-technologies	Cat# A11041; RRID: AB_2534098
AF568 goat anti-rat IgG	Life-technologies	Cat# A11077; RRID: AB_2534121
AF568 donkey anti-goat IgG	Life-technologies	Cat# A11057; RRID: AB_2534104
AF568 donkey anti-rabbit IgG	Life-technologies	Cat# A10042; RRID: AB_2534017

(*Continued on next page*)

Continued

REAGENT or RESOURCE	SOURCE	IDENTIFIER
AF633 goat anti-rat IgG	Life-technologies	Cat# A21094; RRID: AB_2535749
CD31	Abcam	Cat# ab24590; RRID: AB_448167
Endomucin	Santa Cruz	Cat# sc-53941 RCID: AB_2100037
rat anti-mouse CD31	BD Bioscience	Cat# 550274; RRID: AB_393571
CD31 Rat anti-mouse	BD Bioscience	Cat# 553369; RRID: AB_394815
anti-IL-22 ab	Genentech	Cat# 8E11.9; RRID: AB_2651129
IgG control ab	Genentech	Cat# 10E7
GAPDH (6C5) mouse	Santa Cruz Biotechnology	Cat# sc-32233; RRID: AB_627679
anti-rabbit IgG HRPlinked Antibody	Cell Signaling	Cat# 7074; RRID: AB_2099233
Stat3 (124H6) mouse	Cell Signaling	Cat# 9139; RRID: AB_331757
pStat3 (Y705) rabbit	Cell Signaling	Cat# 9131; RRID: AB_331586
ANPEP	Merck Millipore	Cat# MABC950
Polyclonal Swine anti-Rabbit Immunoglobulins/HRP	Dako	Cat# P0214
Polyclonal Rabbit anti-Mouse Immunoglobulins/HRP	Dako	Cat# P0161
Bacterial and virus strains		
Stellar™ Competent Cells	Clontech	Cat# 636763
Adenovirus Cre	Cell Biolabs	ADV-005
Chemicals, peptides, and recombinant proteins		
rmIL-22 (recombinante murine IL-22)	PeproTech	Cat# 210-22
rmIL-6 (recombinante murine IL-6)	BioLegend	Cat# 715202
IL-1α	PeproTech	Cat# 211-11A
TNF-α	Peprotech	Cat# 315-01A
Agarose	Biozym Scientific GmbH	Cat# 849004
IGEPAL® CA-630	Sigma-Aldrich	Cat# I3021
Formaldehyde	Sigma-Aldrich	Cat# F8775
Ubenimex	Sigma-Aldrich	Cat# B8385
BSA	Biomol	Cat# 9048-46-8
Lumisensor Chemiluminescent HRP Substrate	Genscript	Cat# L00221V300
DNase	AppliChem	Cat# A3778
Collagenase	Sigma-Aldrich	Cat# C2139
AccuCount Blank Particles 8.0–12.9 μm	Spherotech	Cat# ACBP-100-10
Ionomycin	Sigma-Aldrich	Cat# I9657
Monensin A	BioLegend	Cat# 420701
PMA (phorbol 12-myristate 13-acetate)	Sigma-Aldrich	Cat# P8139
peqGOLD TriFast™	Peqlab	Cat# 30-2010

(*Continued on next page*)

Continued

REAGENT or RESOURCE	SOURCE	IDENTIFIER
peqGOLD TriFast™ FL	Peqlab	Cat#30-2110
DMSO	Invitrogen	Cat# C34557
Tamoxifen	Sigma-Aldrich	Cat# T5648
Luciferin	Biosynth	Cat# FL08608
Hoechst 33,258	Sigma-Aldrich	Cat# 94403
Zombie UV™ Fixable Viability	BioLegend	Cat# 423108
Fixable Viability Dye eFluor™ 506	Invitrogen	Cat# 65-0866-14
EcoRI	New England Biolabs	Cat# R0101S
Superscript III reverse transcriptase	Invitrogen	Cat# 18080044
Phusion® Hot Start Flex DNA polymerase	New England Biolabs	Cat#M0535S
In-Fusion® HD Cloning Plus	Takara	Cat# 638916
TransIT®-LT1 reagent	Mirus	Cat# MIR2300
Transwell Permeble Supports	Costar	Cat# 3464
Transwell Permeble Supports	Costar	Cat# 3470
Macherey-Nagel™ NucleoSpin™ Gel and PCR Clean-up Kit	Macherey-Nagel™	Cat# 740609.50
GeneJet plasmid mini prep kit	ThermoFischer	Cat# K0503
Percoll	GE Healthcare	Cat# GE17-0891-01
Polyvinylidene difluoride membranes	Merck Millipore	Cat# IPFL00010
IL-22-ELISA	Peprotech	Cat# 900-K257
ECL substrate	Merck Millipore	Cat# WBULS0100
Liberase	Roche Diagnostics	Cat# 05578566001
O.C.T.	Sakura	Cat# 4583
FBS	Life Technologies	Cat# 16000044
Critical commercial assays		
CytoSelect Tumor-endothelium adhesion assay	Cell Biolabs	Cat# CBA-215
RT^2 Profiler™ PCR Array Mouse Angiogenesis	Qiagen	PAMM-024Z
Colonoscopy system	Karl Storz	custom-made
stereoscope	Olympus Corporation	custom-made
Axio Vert.A1- inverted microscope	Zeiss	custom-made
SP5-confocal microscope	Leica	custom-made
small-animal ventilator	UNO Apparatus	Cat# 55-0000
epithelial Ohm-voltmeter	Merck Millipore	Cat# MERS00002
ibidiTreat μ-slide IV0.4	ibidi GmbH	Cat# 80606
Experimental models: Cell lines		
Mouse: MC38	Brunner Lab Neumaier Lab	University of Konstanz, Germany University of Heidelberg
Mouse: MC38-*eGFP* (peGFP-C1)	This paper	N/A
Mouse: MC38-*mCherry* (LeGO-C2)	This paper	N/A
Mouse: MC38*shC*	This paper	N/A
Mouse: MC38*shIl22ra1* clone 1	This paper	N/A
Mouse: MC38shIl22ra1 clone 1	This paper	N/A
Mouse: CT26-Luc-GFP-12-	TRON-University Mainz	N/A
Mouse: LLC	ATCC	CRL-1642, RRID: CVCL_4358
Human: HT29	Schumacher Lab – UKE Hamburg, Germany	HTB-38, RRID: CVCL_0320

(*Continued on next page*)

Continued

REAGENT or RESOURCE	SOURCE	IDENTIFIER
Human: HT29GFP (pEGFPC1)	This paper	N/A
Human: HUVEC	Loges Lab – UKE Hamburg, Germany	#CRL-1730, RRID: CVCL_2959
Human: HUVEC*shC*	This paper	N/A
Human: HUVEC*shANPEP1*	This paper	N/A
Human: HUVEC*shANPEP2*	This paper	N/A
Human: HUVEC*shANPEP3*	This paper	N/A
Human: HUVEC*shANPEP4*	This paper	N/A
Human: HUVEC*shANPEP5*	This paper	N/A
Human: HUVEC*shANPEP6*	This paper	N/A
Human: HEK293T	ATCC	#CRL-3216, RRID: CVCL_0063
Human: HEK293T-Il22eGFP (*pIl22eGFP*)	This paper	N/A
Human: HEKT293GFP (*peGFPC1*)	This paper	N/A
Experimental models: Organisms/strains		
Mouse: C57BL/6J	Jackson Laboratories	Stock:000,664; RRID:IMSR_JAX:000,664
Mouse: BALB/c: Balb/cAnNCrl	Charles River	Stock:028; RRID:IMSR_CRL:028
Mouse: *Il22−/−: B6;129SvF1-Il22^{tm1Flv}/J*	Flavell Lab – Yale University, USA	RRID:MGI:3761616
Mouse: *Rag1−/−: B6.129S7-Rag1^{tm1Mom}/J*	Flavell Lab – Yale University, USA	Stock:002,216; RRID:MGI:3582299
Mouse: *CD4Cre+: B6.Cg-Tg(Cd4-cre)1Cwi/BfluJ*	Flavell Lab – Yale University, USA	Stock:022,071; RRID:IMSR_JAX:022,071
Mouse: *Il22flox/flox: B6;129S5-Il22$^{tm1.1Lex}$/Mmucd*	MMRRC, Lexicon Genetics	Stock:036745-UCD; RRID: MMRRC_036745-UCD
Mouse: *Il17ACre+: B6.129(SJL)-Il17atm1.1(icre)Stck/RthsnJ*	Flavell Lab – Yale University, USA	Stock:034,347; RRID:IMSR_JAX:034,347
Mouse: *Il22ra1flox/flox: B6.Cg-Il22ra1$^{tm1.1Koll}$/J*	Strowig Lab - Helmholtz-Centre for Infection Research, Germany	Stock:031,003; RRID:IMSR_JAX:031,003
Mouse: *Foxp3RFP: B6.Cg-Foxp3^{tm1Flv}/J*	Flavell Lab – Yale University, USA	Stock:008,374; RRID:IMSR_JAX:008,374
Mouse: *Il17aeGFP: B6.Cg-Il17a$^{tm1.1Flv}$/J*	Flavell Lab – Yale University, USA	RRID:MGI:5006666
Mouse: *Il17aFP635*	Flavell Lab – Yale University, USA	N/A
Mouse: *Il22sgBFP*	Flavell Lab – Yale University, USA	N/A
Mouse: *Il10eGFP: B6.Cg-Il10^{tm1Flv}/J*	Flavell Lab – Yale University, USA	Stock:008,379; RRID:IMSR_JAX:008,379
Mouse: *Cdh5Cre+: B6.FVB-Tg(Cdh5-cre)7Mlia/J* (backcrossed with C57BL/6 for at least 12 generations)	Herkel Lab – UKE Hamburg, Germany	Stock:006,137; RRID:IMSR_JAX:006,137
Mouse: *AlbCre+: B6.FVB(129)-Tg(Alb1-cre)1Dlr/J* (backcrossed with C57BL/6 for at least 12 generations)	Herkel Lab – UKE Hamburg, Germany	Stock:016,832; RRID:IMSR_JAX:016,832
Mouse: *KrasG12D: B6.129S4-Kras^{tm4Tyj}/J*	Jackson Laboratories	Stock:008,179; RRID:IMSR_JAX:008,179
Mouse: *Apc15lox: B6.129P2-Apc^{tm1Rsmi}/RfoJ*	Ron Smits - Erasmus University Medical Center	Stock:029,275; RRID:IMSR_JAX:029,275
Mouse: *RosaYFP: B6.129X1-Gt(ROSA)26Sor$^{tm1(EYFP)Cos}$/J*	Jackson Laboratories	Stock:006,148; RRID:IMSR_JAX:006,148
Mouse: *Il22tg8(Tg)*:	(B6N Background)	Gao, NIH

(*Continued on next page*)

Continued

REAGENT or RESOURCE	SOURCE	IDENTIFIER
Mouse: *Cd13−/−*	Renata Pasqualini Lab- Rutgers Cancer Institute of New Jersey and Division New Jersey, USA	N/A
Mouse: *Ja18−/−: B6(Cg)-Traj18$^{tm1.1Kro}$/J*	Paolo Dellabona Lab- Experimental Immunology Unit, San Raffaele Scientific Institute, Milano	Stock:030,524 RRID:IMSR_JAX: 030,524
Mouse: *Il22ra1−/−*:	Till Strowig Lab-Helmholtz Center for Infection Research, Braunschweig, Germany	N/A
Mouse: CD45.1: *B6.SJL-Ptprc^{a} Pepc^{b}/BoyJ*	Flavell Lab – Yale University, USA	Stock:002,014; RRID:IMSR_JAX:002,014
Mouse: MISTRG: C; 129S4-*Rag2$^{tm1.1Flv}$Csf1$^{tm1(CSF1)Flv}$Csf2/Il3$^{tm1.1(CSF2,IL3)Flv}$Thpo$^{tm1.1(TPO)Flv}$Il2rg$^{tm1.1Flv}$* Tg(SIRPA)1Flv/J	Flavell Lab – Yale University, USA	Stock:017,712 RRID:IMSR_JAX:017,712
Oligonucleotides		
Oligonucleotides for qPCR, PCR and cloning	This paper	See Table S1
Oligonucleotides for sgRNA cloning	This paper	See Table S2
Recombinant DNA		
Plasmid: pCMV-EGFP C1	Clontech	This plasmid has been discontinued by Clontech
Plasmid: peGFP-C1	Clontech	This plasmid has been discontinued by Clontech
Plasmid: pIl22*eGFP*	This paper	N/A
Plasmid: pGEM®-T Easy vector	Promega	A1360
Plasmid: GAC.Luc-puro	Addgene[30]	RRID:Addgene_74409
Plasmid: LeGO-C2	Addgene[59]	RRID:Addgene_27339
Software and algorithms		
Adobe Illustrator CC 2017	Adobe	https://www.adobe.com/de/products/illustrator.html
Flowjo 10	Tree Star	https://www.flowjo.co
GraphPad Prism 8.0	GraphPad	https://www.graphpad.com
ImageJ 1.52.	ImageJ	https://imagej.nih.gov/ij/
Image Lab 5.2	BioRad	https://www.bio-rad.com/
CapImage software V8.6	Dr. Heinrich Zeintl	http://www.drzeintl.de
SteponeSoftware 2.1	Thermfischer	https://www.thermofisher.com/de/de/home.html
Microsoft Office 2016	Microsoft	https://products.office.com
BD FACSDiva	BD Biosciences	https://www.bdbiosciences.com/en-in
Snapgene	GSL Biotech	https://www.snapgene.com/
SnapGene Viewer	GSL Biotech	https://www.snapgene.com/
G*power	HHU Düsseldorf	http://www.gpower.hhu.de/
Cell Ranger v3.1.0	10x Genomics	https://www.10xgenomics.com
R	R Core	https://www.r-project.org/

RESOURCE AVAILABILITY

Lead contact

Further information and requests for reagents may be directed to, and will be fulfilled by, the lead contact, Anastasios Giannou (a.giannou@uke.de).

Materials availability

All data necessary to understand and assess the conclusions of the manuscript are available in the body of the paper and in the supplementary materials. *Il22*$^{-/-}$ (VG437) mice are available under a material transfer agreement with Regeneron. *Il22*^{flox} mice are available under a material transfer agreement with Lexicon and Genentech. α-IL-22 treatment antibody was kindly provided by Genentech under a material transfer agreement with the University Medical Center Hamburg-Eppendorf. *Apc*^{15lox} mice are available under a material transfer agreement with Prof. Dr. Ron Smits from Erasmus University Medical Center. *Ja18*$^{-/-}$ mice were kindly provided by Dr. Paolo Dellabona at Ospedale San Raffaele - Milano (Italy). *MISTRG* (humanized mice) were kindly provided by Dr. Richard Flavell as part of an ongoing collaboration. All reagents generated or used in this study are available on request from the lead contact with a completed Materials Transfer Agreement. Information on reagents used in this study is available in the key resources table.

Further information and requests for resources and reagents should be directed to Anastasios Giannou (a.giannou@uke.de) and Samuel Huber (s.huber@uke.de).

Data and code availability

All the data supporting the findings of the article are available within the main text or supplemental information. The published article includes datasets generated during this study. Original single cell RNA-seq data has been deposited in GEO: GSE217223.

METHOD DETAILS

Reagents

IL-22 neutralizing antibodies and IgG2a control were provided by Genentech (San Francisco, CA). rmIL-22 and rmTNF-α were from Peprotech (London, UK), rmIL-1a and rhIL-22 from R&D Systems (Minneapolis, MN), ELISA kits from Peprotech, R&D or Antigenix America and Boyden chambers from Millipore (Billerica, MA).

Cells

Lewis lung carcinoma (LLC), human cell line expressing mutant version of the SV40 large T antigen (HEK293T) (ATCC, Manassas, VA), colon adenocarcinoma (MC38) syngenic for C57BL/6 mice, colon adenocarcinoma (CT26) syngenic for Balb/c mice,[60,61] human colon carcinoma (HT29)[62] and Human Umbilical Vein Endothelial (HUVEC) cells[63] were cultured and tested as described in the Supplemental Experimental Procedures.

Animals

C57BL/6J, C57BL/6N, Balb/c Il22$^{+/+}$, *Il22*$^{-/-}$, *Il22ra1*$^{-/-}$, *Il22tg8*^{Tg}, *Apc*^{15lox};*LSL-Kras*^{G12D}, *IL-22*^{sgBFP};*IL-17A*^{sgGFP};*Foxp3*^{mRFP}, *IL-22*^{sgBFP};*IL-17A*^{Katushka};*Foxp3*^{mRFP};*IL-10*^{sgGFP}, *Il22ra1*$^{flox/flox}$;*Alb*$^{Cre+}$, *Il22ra1*$^{flox/flox}$;*Cdh5*$^{Cre+}$, *Cd13*$^{-/-}$ *(Anpep knock out), MISTRG (humanized mice), Il22ra1*$^{flox/flox}$;*Cdh5*$^{Cre+}$;*R26*^{YFP}, *Il22*$^{flox/flox}$;*CD4*$^{Cre+}$, *Ja18*$^{-/-}$, *Rag*$^{-/-}$ and *Rag*$^{-/-}$;*Il22*$^{-/-}$, *Tcrd*$^{GDL/GDL}$ *and Tcrd*$^{+/+}$ mice[64–66] were bred and housed under specific pathogen-free conditions in the animal facility of the University Medical Center Hamburg Eppendorf. *Ja18*$^{-/-}$ mice were kindly provided by Dr. Paolo Dellabona at Ospedale San Raffaele - Milano (Italy). *MISTRG* (humanized mice) were kindly provided by Dr. Richard Flavell as part of an ongoing collaboration. Age- and sex-matched littermates between 8 and 16 weeks of age were used. Animal experiments were carried out in accordance with the Institutional Animal Care and Use Committee of Yale University or the Institutional Review Board "Behörde für Justiz und Verbraucherschutz, Lebensmittelsicherheit und Veterinärwesen" (Hamburg, Germany).

Isolation of hematopoietic cells from murine and human liver metastasis

Hematopoietic cells were isolated from macroscopically healthy human liver, perimetastatic liver and human liver metastasis or murine liver or lung metastasis. Human tissues were obtained freshly after surgical removal of metastases from patients diagnosed with CRC and liver metastasis. Human studies were approved by the local ethical committee (Ethik-Kommission der Ärztekammer Hamburg). To isolate the lymphocytes, the human or murine tissues were cut into small pieces and minced using a scalpel. The healthy liver or metastasis tissue was incubated for 30 min at 37°C on a shaking incubator in HBSS (with Ca^{2+} and Mg^{2+}) with Collagenase (1 mg/mL) and DNase I (10 U/ml) and supernatant was collected. Leukocytes were further enriched by Percoll gradient centrifugation (GE Healthcare, Chicago, IL).[35]

Fluorescence-activated cell sorting

Fc-γ receptors were blocked using a mAb (clone 2.4G2). The cells were stained with fluorochrome-conjugated antibodies. BD LSRFortessa and FACSAria (BD Biosciences, San Jose, CA) were used for cell analysis and cell sorting, respectively. Data were analyzed using FlowJo v.6.1 (TreeStar, Ashland, OR).

Mouse models of forced metastasis

Intrasplenic (i.s.) injection (forced liver metastasis). For induction of forced liver metastases, mice received 250 μL PBS containing $3x10^5$ cancer cells i.s. The injection was performed in hemi-spleen which was removed 3 min after cancer cell injection. The mice were sacrificed after 3 weeks. Macroscopic liver metastases were counted using a stereoscope (Olympus Corporation, Germany).[30,67]

Intraportal (in.p.) injection (forced liver metastasis). Mice were anesthetized using continuous isoflurane, and their abdomens were sterilized. After administration of analgesic agents, median laparotomy (10 mm) was performed, and the incision site was held open using a retractor. After exposure of the peritoneal cavity, the intestines were located and exteriorized onto a sterile field surrounding the incision site to visualize the portal vein. Throughout the procedure, the intestines were kept hydrated with sterile PBS that was pre-warmed at 37°C. For intraportal injection, sterile PBS or MC38 cancer cells ($3x10^5$ suspended in 250 μL of sterile PBS) were injected into the portal vein via a 30-gauge needle. Successful injection was confirmed by partial blanching of the liver. After the injection, a sterile coagulation gauge was then held over the injection site for 1 min to ensure that no injected contents would leak into the peritoneal cavity. Afterward, the intestines were placed back into the peritoneal cavity, and the peritoneum and skin were closed with a suture and autoclips, respectively. The mice were sacrificed after 24 h. Livers were harvested and an extravasation assay was performed.

Intravenous (i.v.) injection (forced lung metastasis). For induction of forced lung metastases, mice received 100 μL PBS containing $2.5x10^5$ cancer cells i.v. The mice were sacrificed after 3 weeks. Macroscopic metastases in harvested lungs were counted using a stereoscope.

Mouse models of spontaneous metastasis

Flank model (spontaneous lung and liver metastasis). For induction of solid tumors, mice were anesthetized using isoflurane inhalation and received subcutaneous injection of 100 μL PBS containing $5x10^5$ LLC cells. Three vertical tumor dimensions (δ1, δ2, and δ3) were monitored longitudinally and tumor volume was calculated using the formula π *δ1 *δ2 *δ3/6. Both models were described elsewhere.[30] The tumors were resected after 2 weeks. The mice were sacrificed 4 weeks after tumor resection and macroscopic metastases in lungs were counted using a stereoscope.

Cecum model (spontaneous liver metastasis). The cecum of anesthetized mice was exteriorized through an abdominal laparotomy. 1×10^6 LLC cells were injected into the cecal wall between the mucosa and the muscularis externa layers using a 30-gauge needle. A proper implantation into the cecum was confirmed at day 0 by a localized bubble in the cecal wall. The mice were sacrificed after 4 weeks and macroscopic metastases in livers were counted using a stereoscope.[68]

Orthotopic colonic sub-mucosal implantation of CRC cells

Mice were anesthetized using isoflurane. Sub-mucosal injections were accomplished using stainless flexible stainless steel; 8 inch long, 30 gauge and 45° bevel hypodermic needles custom made according to our specification (Cadence Inc. U.S.A). The needle was inserted through Luer lock (Söllner, GmbH) screwed on the working channel of the scope to avoid air leakage. Subsequently, the scope was inserted into the mouse colon and following its inflation the needle was brought through the working channel to the scope's front. The CRC cell implantation procedure was performed by two coordinated persons; one person was navigating the colonoscopy while the other person was operating the injection maneuver. The injection was performed under observation by a very gentle sub-mucosal penetration with the open side of the bevel heading up in a flat angle. 50 μL PBS containing $1.5x10^5$ CRC tumor cells were then injected into the colonic sub-mucosa.

Adenoviral infection of colonic epithelium for orthotopic colon cancer induction

Apc^{15lox};LSL-Kras^{G12D} mice were fasted overnight and anesthetized using 2% isoflurane. A midline incision was performed and the distal colon was clamped 3 cm from the anus. After washing with PBS, 100 μL trypsin were injected into the colon for 10 min. The lining of the distal colon was then mechanically abraded using a small caliber brush. After washing with PBS, 10^9 pfu of adenovirus in 100 μL PBS were injected into the colon for 30 min. For all incubations, a second clamp was placed 1 cm from the anus to ensure localization during the entire incubation period. After the infection period, both clamps were removed and the abdominal wall was closed in two layers. These procedures were well tolerated by all animals. Ad5CMV^{Cre} and adenoviruses were obtained from the Cellbiolabs (San Diego, USA). Mice developed CRC after 6– 8 weeks and were sacrificed after 8 months. The primary tumors and macroscopic liver metastases were quantified by colonoscopy or using a stereoscope, respectively.

Mouse colonoscopy

Mice were fasted overnight and anesthetized using 2% isoflurane. A custom-made colonoscopy system (Karl Storz) was used as previously described.[69] Air was carefully insufflated into the colon to allow full visualization but avoid perforation. Endoscopic images and movies were saved for later offline analysis with ImageJ software to calculate the ratio of the tumor area relative to that of the lumen. Tumor sizes were graded from 1 to 5. Tumors observed during endoscopy were counted to obtain the total number of tumors per animal. The total tumor score per mouse was calculated as the sum of all tumor sizes.

Immunoblotting

To analyze protein activation and expression, LSECs or hepatocyte lysates were separated in a 10% SDS-PAGE assay, transferred to polyvinylidene difluoride membranes (Merck Millipore), probed with specific antibodies, and were visualized by enhanced chemiluminescence. Band density was determined by incubation with the appropriate HRP-conjugated secondary Abs (Dako, Carpintera, CA) and were visualized with the ECL substrate (Merck Millipore).

Hematoxylin and eosin (H&E) staining

Liver or lung specimens were fixed in 4% buffered formalin, embedded in paraffin or OCT (Sakura, Tokyo, Japan), and stored at −80°C. Tissue sections (4 μm) were prepared and stained with H&E. Metastatic lesion areas were quantified using ImageJ (ImageJ, U.S. National Institutes of Health, Bethesda, MD).

Plasmids and transfections

The coding sequences for IL-22 were cloned via reverse transcription and PCR from murine C57BL/6 intestinal total RNA with the corresponding primers (primer set A), Superscript III reverse transcriptase (Invitrogen) and Phusion Hot Start Flex DNA polymerase (New England Biolabs). After cleanup and addition of 3′ A overhangs, the PCR product was cloned in pGEM-T Easy vector (Promega). A second PCR product using the pGEM-T Easy-IL-22 construct template with Phusion Hot Start Flex DNA polymerase and primer set B was performed that was sub-cloned into pCMV-EGFP C1 (Clontech) mammalian expression vector by the InFusion ligation system (Takara). The IL22 expressing construct was verified by standard Sanger sequencing.

The construct expressing the sgRNA against IL-22RA1 was a kind gift of Dr Sebastian Kobold. Chemiluminescent MC38 cells stably expressing the sgRNA against IL-22RA1 protein were obtained as follows: MC38 CRC cells were transfected with TransIT-LT1 reagent (Mirus) instructions and a mixture of 1:5 of GAC.Luc-puro Plasmid (Addgene Number# 74409): *Il22ra1*sgRNA encoding vector. Briefly, 1.5x10^5/mL MC38 cells were plated in full DMEM medium for overnight incubation in 5 cm diameter cell culture plates. On the next day, the plasmids and TransIT-LT1 reagent were each diluted in 100 μL OptiMEM (Gibco) and left for 5 min at room temperature (RT). The plasmid and reagent solutions were then combined, mixed briefly by vortex and were left for 15 min at RT. The medium was removed from MC38 cells leaving approximately 800 μL at the plate. The plasmid and reagent solution was carefully overlaid on the cells and the plates were incubated overnight at 37°C in a 5% CO_2 humidified incubator. 24 h later, 1–3 mL DMEM medium supplemented with 10% FBS was added into the cell culture medium. Cells were collected 48 h after transfection, washed twice with PBS, trypsinized and splitted into three 10 cm diameter plates containing 5, 10 and 15 μg/ml puromycin. After 5 days, stable visible clones were individually picked into a 96-well plate and assessed for pSTAT3 and chemiluminescence. Correct clones were expanded for liver metastasis induction.

Isolation of primary hepatocytes

For the isolation of primary hepatocytes, the liver was digested with Liberase (Roche Diagnostics) and was then gently disrupted to free residual cells. Single-cell suspension was filtered through a 100-μm cell strainer and the cells were allowed to settle by gravity for 20 min. Subsequently, parenchymal cells were separated by 10 min centrifugation in a 90% Percoll gradient (GE Healthcare). For primary hepatocyte culture, William's E + GlutaMAX-I medium (Life Technologies, Karlsruhe, Germany) was supplemented with 10% FBS (Life Technologies), 1% penicillin/streptomycin (Life Technologies) and 1% L-glutamine (Life Technologies). The cells were incubated overnight at 37°C, 40% O_2. Subsequently, the hepatocytes were washed and incubated with 100 ng/mL rmIL-22 or rmIL-6 for 15 min (eBioscience; R&D Systems; Peprotech, respectively). Finally, the cells were harvested and the RNA was extracted.

Immunofluorescence

Primary LSECs were fixed for 10 min in 4% paraformaldehyde at RT. Sections (5 μm) were washed with PBS and incubated in PBS-Triton 0.3% for 5 min. After washing, sections or cells were incubated for 60 min in blocking buffer. Samples were stained overnight with specific antibodies at 4°C. After washing, secondary antibody staining was performed (1 h, RT) followed by 5 min staining with Hoechst 33,258 (1:5000). As control, the primary Ab was omitted. Bright-field and fluorescent microscopy was carried out using either an Axio Vert.A1 (Zeiss, Jena, Germany) inverted microscope or an SP5 (Leica, Heidelberg, Germany) confocal microscope.

Isolation of LSECs

For the isolation of LSECs, a slit was cut in the left ventricle of the heart. The liver was perfused with PBS and then with∼ 5 mL 0.05% collagenase through the portal vein and vena cava, until it was clear of blood. After perfusion, the liver tissues were collected in complete medium on ice. Afterward, the liver was sliced into small pieces of approximately 0.5 cm. Two livers per genotype were digested in collagenase with 1% collagen and 0.83% DNase at 37°C for 25 min, while shaking. The remaining liver pieces were filtered through a 200-μm cell strainer and further centrifuged to remove the hepatocytes. The supernatant was again centrifuged. The pellet was resolved with maximum 5 mL PBS and added to 2 mL Optiprep. On top, 1 mL PBS was carefully pipetted and then centrifuged. The white interphase was collected in a new tube and washed with PBS. Single-cell suspension was filtered through a 40-μm cell strainer and centrifuged. For isolating the LSECs, the magnetic activated cell sorting was used. IMDM complete medium was used in order to culture the LSECs on collagen-coated plates at 37°C.

IL-22 ELISA

IL-22 serum levels were measured using a mouse IL-22 ELISA kit (Antigenix America) according to the manufacturer's instructions.

Adoptive transfer

INKT cells were isolated from livers using fluorescent activated cell sorting (see Sorting panel in Figures S6H and S6I). *Rag1*$^{-/-}$*Il22*$^{-/-}$ or *Ja18*$^{-/-}$ mice were engrafted with 10^5 iNKT or γδ T cells by intraportal injection. After 5–7 days, an *in vivo* extravasation assay was performed.

Laminar flow adhesion assay

The dynamic adhesion of human HT29 and mouse MC38 tumor cells to endothelial cells under physiological flow conditions was analyzed in a laminar flow adhesion assay as previously described.[70] In short, HUVEC cells (PromoCell, Heidelberg) or LSECs were seeded in ibidiTreat μ-slide IV0.4 (ibidi GmbH, Germany) flow chambers and after confluence to monolayers, endothelial cells were stimulated with 10 ng/mL recombinant human or murine IL-1α (R&D Systems, Minneapolis, MN), 10 ng/mL recombinant human or murine TNFα or 20 to 100 ng/mL human or murine IL-22 for 4 h prior to the flow assay (tumor cell suspension: 1x10^5 cells/ml; flow rate: 8.5 mL/h; shear stress: 0.25 dyn/cm^2). Non-stimulated endothelial cells served as negative controls. Data were acquired and evaluated with CapImage software (version 8.6, Dr. Heinrich Zeintl, Heidelberg). The adhesive events on the endothelium were distinguished into firm adhesion, rolling and tethering and counted in three separate regions of interest for 1 min each.

Extravasation assay

For the *in vivo* extravasation assay, mice received 250 μL PBS containing 1x10^6 MC38 GFP-labelled cells i.s. The mice were sacrificed after 24 h and their livers were weighed. To isolate the MC38 GFP-labelled cells, the murine livers were cut in small pieces and minced using a scalpel. The tissue was incubated for 30 min at 37°C on a shaking incubator in HBSS (with Ca^{2+} and Mg^{2+}) with Collagenase (1 mg/mL) and DNase I (10 U/ml) and supernatant was collected. Then, the supernatants were centrifuged for 4 min at 40 g. We repeated this step twice more. After 3 centrifugations, the hepatocytes were removed and the cells were diluted in PBS 1x. One-fifth of the cells were mixed with beads in 1:10 dilution and were analyzed by flow cytometry. In every extravasation assay, we used a mouse injected with not labeled cells in order to set up the gate of GFP + or Cherry + cells.

Circulating tumor cell isolation and quantification

6 mL Ficoll (Ficoll Paque PLUS, endotoxin tested, Cytiva, Uppsala, Sweden) were placed in a 15 mL Falcon tube and overlayed with the mouse blood (2 mL)/PBS (5 mL) mixture. After centrifugation for 30 min at 400 x g (rotor brake inactivated), supernatant and interphase were carefully removed and transferred to a 50 mL Falcon tube using a serological pipette and mixed with 30 mL PBS. Erythrocytes were lysed by adding 1 mL Flow Cytometry Human Lyse Buffer (R&D systems), mixing and incubating for 1 min. Subsequently, the sample was centrifuged for 10 min at 400 x g (rotor brake activated). Supernatant was discarded and the cell pellet was resuspended in 3 mL PBS. Cytospins with 500.000 cells per slide were prepared by spinning the appropriate volume for 3 min at 150 x g (Swing out rotor 1626, 1100 rpm, Hettich ROTOFIX 32) and air-drying. All steps were performed at RT.

Administration of antibody and aminopeptidase inhibitor treatment

For administration of antibodies, the abdomen of mice was sterilized, and anti-IgG or anti-IL-22 (50 μg in 200 μL PBS; Genentech, California, USA) were suspended in 200 μL of sterile PBS. For administration of Ubenimex, 20 mg/kg was diluted and injected for 7 days.

IV injection of CD45 Ab

To distinguish between circulating CD45$^+$ cells and CD45$^+$ cells infiltrating into the liver parenchyma, we injected fluorochrome labeled antibody specific for PeCy7 conjugated anti-CD45 Ab (30-F11) into the bloodstream of mice. Briefly, mice received 5 μg PeCy7 conjugated anti-CD45 Ab (30-F11) in PBS intravenously, and were euthanized after 3 min. For *in vitro* CD45 staining, an A-700 conjugated anti-CD45 antibody was used. In all the experiments blood staining controls were used and around 96–99% of CD45$^+$ T cells were labeled.

Parabiosis

In short, females were anesthetized with a mixture of ketamine/xylazine (100 mg/kg and 10 mg/kg, respectively). After shaving the corresponding lateral aspects of each mouse, matching skin incisions were made from behind the ear to the hip and sutured together with nylon and collagen (5-0 Ethicon, Vicryl) absorbable suture. Then, these areas were clipped with 7-mm stainless-steel wound clips (Reflex7).[38]

Orthotopic single left lung transplantation (LuTx)

Orthotopic LuTxes were performed as described previously with minor modifications.[71] No immunosuppression was applied to any of the transplanted mice. *Il22ra1*$^{-/-}$ mice were used as donors, and WT mice were used as recipients. Briefly, donors were anesthetized with isoflurane anesthesia. The pulmonary artery, bronchus, and pulmonary vein were carefully separated from one another with blunted forceps, prior to cuffing with 24-, 20-, and 22-gauge cuffs, respectively. The left lung graft was stored for less than 20 min

before its implantation. The recipient mouse was anesthetized with isoflurane anesthesia, intubated and ventilated using a small-animal ventilator (UNO Apparatus) at a respiratory rate of 120 bpm and a tidal volume of 300 μL. The chest was opened on the left side between the third and fourth ribs and the native left lung was retracted with a clamp. The hilar structures were carefully separated from one another with blunted forceps. After arrest of the blood and air flow toward the left lung, the cuffed graft pulmonary artery, bronchus, and pulmonary vein were inserted into the recipient counterparts and ligated with 10-0 sutures. The native left lung was removed and the incision in the chest was closed with a 6-0 suture, after removing all potential air bubbles from the chest. The mice were extubated. After the operation, the recipient mice were allowed to recover at 30°C overnight and received buprenorphine for 3 days. The mice were sacrificed at indicated time points according to the experimental plan.

Endothelial gene assay

Endothelial gene RNA levels were measured using a RT^2 profiler PCR assay (Qiagen) according to the manufacturer's instructions. The altered genes were verified by qPCR analysis

Measurement of the transendothelial electrical resistance (TEER)

HUVEC cells were seeded onto collagen-coated supported polycarbonate and polyester porous (0.4 μm pores) membranes (Transwell and Transwell Clear; Corning-Costar, Corning, NY) and cultured at 37°C and 5% CO_2 in HUVEC complete medium to promote proliferation. Media were changed every 2 days and TEER was measured using an epithelial Ohm-voltmeter (Millicell ERS 2, Merck Millipore, Darmstadt, Germany). After reaching a plateau of TEER, we exposed HUVEC cells to recombinant human (rh) IL-22 (100 ng/ml). 0 and 24 h after exposure to rh IL-22, TEER was measured in every well.

In vitro transmigration assay

HUVEC cells ($1x10^5$) were seeded onto collagen-coated supported polycarbonate and polyester porous (0.4 μm pores) membranes (Transwell and Transwell Clear; Corning-Costar, Corning, NY) and cultured at 37°C and 5% CO_2 in HUVEC complete medium to promote proliferation and creating monolayer. Media were changed every 2 days and TEER) was measured using an epithelial Ohm-voltmeter (Millicell ERS 2, Merck Millipore, Darmstadt, Germany) to check the monolayer induction. $5x10^4$ HT-29 GFP-labelled cells were then seeded in the transwell inserts with an endothelial monolayer in HUVEC medium with 2% FBS in presence of 0.1% BSA or rh IL-22 (100 ng/ml). 24 h after seeding, cells were washed and fixed with 4% paraformaldehyde. Cells on the apical side of each insert were scraped off and the migration to the basolateral side was visualized using a Zeiss fluorescence microscope.

Lentiviral transfer of shRNAs into HUVEC cells

Lentiviral vectors expressing shRNAs under control of the human U6 promoter (MISSION pLKO.1-puro) directed against human ANPEP (TRCN0000050238, TRCN0000050239, TRCN0000050240, TRCN0000050241, TRCN0000050242, TRCN0000435991, TRCN0000418482, TRCN0000425830) and a non-targeted control shRNA (SHC002) were obtained from Sigma-Aldrich (Munich, Germany). Production of lentiviral particles was described in detail earlier[59] and protocols are available online (http://www.LentiGO-Vectors.de). Selection of successfully transduced cells with 1 μg/mL puromycin in the culture medium was started two days after transduction.

Bioluminescence imaging

Cells and mice were imaged after addition of 300 μg/mL D-luciferin to culture media or i.v. delivery of 1 mg D-luciferin on a Xenogen Lumina II. Data were analyzed on Living Image v.4.2 (Perkin-Elmer, Waltham, MA).[72]

Hydrodynamic injection of plasmid

For hydrodynamic injection of plasmid, mice were anesthetized using continuous isoflurane, and their tail was sterilized. Subsequently, 10 μg of plasmid (*eGFP* or *Il22eGFP*) diluted in PBS (volume of 9% of mouse weight) were injected into the tail vein.

Depletion of γδ T cells in *Tcrd*$^{GDL/GDL}$ mice

γδ T cells in *Tcrd*$^{GDL/GDL}$ mice were depleted using a single intraperitoneal diphtheria toxin injection (50 ng/g bodyweight). Experiments using these mice always included WT littermates injected with diphtheria toxin and *Tcrd*$^{GDL/GDL}$ mice injected with PBS as correct controls.

RNA analysis

Total RNA was extracted from tissue and cells of colon, lymph nodes, liver and spleen using TRIzol Reagent (Invitrogen). The High capacity cDNA synthesis Kit (Applied Biosystems) was used for cDNA synthesis. Primers and probes were purchased from Applied Biosystems. Real-time PCR was performed using the Kapa Probe Fast qPCR Master Mix (Kapa Biosystems) on the StepOne Plus system (Applied Biosystems). For both human and mouse, relative expression was normalized to HPRT and calculated using the $2^{-\Delta\Delta Ct}$ method.

scRNA-seq

Droplet-based single-cell RNA sequencing (10x Chromium single cell 5′ solution v1.1, 10x Genomics) experiments were performed according to the manufacturer's protocol. In brief, after sorting, cells were centrifuged and loaded onto the chip for GEM generation. The droplets were recovered and reverse transcription as well as cell barcoding were performed. The cDNA was recovered using Dynabeads MyOne SILANE (ThermoFisher Scientific). Afterward, cDNA was amplified and the quality was checked with a Bioanalyzer 2100 (Agilient Technologies). For the gene expression library construction, cDNA was fragmented and end-repaired, followed by further amplification with index primers. The libraries were sequenced on a Illumina NovaSeq 6000. After demultiplexing, the Cellranger pipeline (v. 3.0.1, 10x Genomics) was used to process fastq files, aligning the reads to the mm10 mouse genome draft. The resulting barcode-read count matrices were processed in R, using the Seurat package v. 4.0.4.[73] Briefly, low quality and suspected doublet cells were removed, resulting in 7065 $CD45^{+}IL\text{-}22^{-}$ cells and 277 $CD45^{+}IL\text{-}22^{+}$ cells before injection, as well as 9730 $CD45^{+}$ $IL\text{-}22^{-}$ cells and 1302 $CD45^{+}$ IL-22 + cells 12 h after injection. All four samples were normalized using the SCTransform function,[74] followed by integration as described previously.[75] PCA was ran on the integrated expression values, followed by UMAP based on the top 30 PCs and shared nearest neighbor prediction on the top 20 PCs. 23 clusters were found which were grouped into 11 higher level clusters based on cell type markers (see heatmap in Figure S7). To compute the tissue residency score, the AddModuleScore function was used based on the following marker genes: *Cd69*, *Cxcr3*, *Cxcr6*, *Itgal*, *Itga1*, *Pdcd1*, *Cd101*, *Selplg*, *Itgb2*, *Ccr10*, *Zfp683*, *Prdm1*, *Runx3*.[76]

Quantification and statistical analysis

Sample size was calculated using G*power (http://www.gpower.hhu.de/) assuming $\alpha = 0.05$, $\beta = 0.8$, and $\rho = 0.3$. No data were excluded. Animals were allocated to treatments by alternation and transgenic animals were enrolled case-control-wise. Data acquisition was blinded on samples previously coded by a non-blinded investigator.

Statistical analysis was performed using GraphPad Prism Software (GraphPad Software, San Diego, CA, USA). For paired group comparison, the non-parametric two-sided Mann-Whitney test was used. Multiple comparisons testing was examined by one-way ANOVA with Bonferroni post-hoc tests. Paired group comparison test was carried out using two-tailed Wilcoxon matched-pairs signed rank test. Sample size (*n*) refers to biological replicates. The mRNA expression of the cytokines was transformed using a base 10 logarithm. The significance level α was set to 0.05.

Immunity, Volume *56*

Supplemental information

Tissue resident iNKT17 cells facilitate cancer cell extravasation in liver metastasis via interleukin-22

Anastasios D. Giannou, Jan Kempski, Ahmad Mustafa Shiri, Jöran Lücke, Tao Zhang, Lilan Zhao, Dimitra E. Zazara, Filippo Cortesi, Kristoffer Riecken, Maria Carolina Amezcua Vesely, Jun Siong Low, Hao Xu, Eleanna Kaffe, Laura Garcia-Perez, Theodora Agalioti, Yoshito Yamada, Wolfgang Jungraithmayr, Ehud Zigmond, Karl-Frederick Karstens, Babett Steglich, Jonas Wagner, Leonie Konczalla, Antonella Carambia, Kornelius Schulze, Johann von Felden, Peter May, Daria Briukhovetska, Tanja Bedke, Leonie Brockmann, Sarah Starzonek, Tobias Lange, Claudia Koch, Sabine Riethdorf, Penelope Pelczar, Marius Böttcher, Morsal Sabihi, Francis J. Huber, Matthias Reeh, Julia Kristin Grass, Ramez Wahib, Hannes Seese, Björn-Ole Stüben, Mohammad Fard-Aghaie, Anna Duprée, Pasquale Scognamiglio, Gabriel Plitzko, Jan Meiners, Shiwa Soukou, Agnes Wittek, Caroline Manthey, Ioannis C. Maroulis, Petra C. Arck, Daniel Perez, Bin Gao, Sotirios G. Zarogiannis, Till Strowig, Renata Pasqualini, Wadih Arap, Javier Suárez Gosálvez, Sebastian Kobold, Immo Prinz, Andreas H. Guse, Michael Tachezy, Tarik Ghadban, Asmus Heumann, Jun Li, Nathaniel Melling, Oliver Mann, Jakob R. Izbicki, Klaus Pantel, Udo Schumacher, Ansgar W. Lohse, Richard A. Flavell, Nicola Gagliani, and Samuel Huber

SUPPLEMENTAL INFORMATION

Tissue resident iNKT17 cells facilitate cancer cell extravasation in liver metastasis via IL-22

Anastasios D. Giannou, Jan Kempski, Ahmad Mustafa Shiri, Jöran Lücke, Tao Zhang, Lilan Zhao, Dimitra E. Zazara, Filippo Cortesi, Kristoffer Riecken, Maria Carolina Amezcua Vesely, Jun Siong Low, Hao Xu, Eleanna Kaffe, Laura Garcia-Perez, Theodora Agalioti, Yoshito Yamada, Wolfgang Jungraithmayr, Ehud Zigmond, Karl-Frederick Karstens, Babett Steglich, Jonas Wagner, Leonie Konczalla, Antonella Carambia, Kornelius Schulze, Johann von Felden, Peter May, Daria Briukhovetska, Tanja Bedke, Leonie Brockmann, Sarah Starzonek, Tobias Lange, Claudia Koch, Sabine Riethdorf, Penelope Pelczar, Marius Böttcher, Morsal Sabihi, Francis J. Huber, Matthias Reeh, Julia Kristin Graß, Ramez Wahib, Hannes Seese, Ole Stüben, Mohammad Fard-Aghaie, Anna Duprée, Pasquale Scognamiglio, Gabriel Plitzko, Jan Meiners, Shiwa Soukou, Agnes Wittek, Caroline Manthey, Ioannis C. Maroulis, Petra C. Arck, Daniel Perez, Bin Gao, Sotirios G. Zarogiannis, Till Strowig, Renata Pasqualini, Wadih Arap, Javier Suárez Gosálvez, Sebastian Kobold, Immo Prinz, Andreas H. Guse, Michael Tachezy, Tarik Ghadban, Asmus Heumann, Jun Li, Nathaniel Melling, Oliver Mann, Jakob R. Izbicki, Klaus Pantel, Udo Schumacher, Ansgar W. Lohse, Richard A. Flavell, Nicola Gagliani, and Samuel Huber

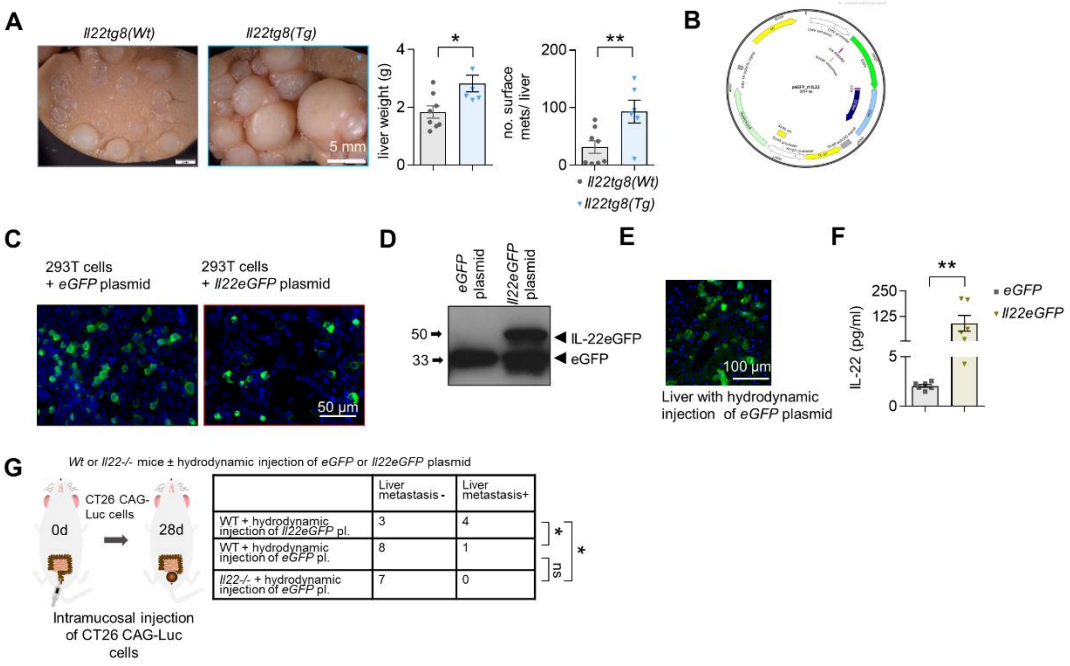

	Liver metastasis -	Liver metastasis+	
WT + hydrodynamic injection of *Il22eGFP* pl.	3	4	*
WT + hydrodynamic injection of *eGFP* pl.	8	1	ns
Il22-/- + hydrodynamic injection of *eGFP* pl.	7	0	*

Figure S1, related to Figure 1. High IL-22 levels promote liver metastasis

(A) Representative pictures, liver weight and number of macroscopic metastases in total liver of mice with normal (*Il22tg8*$^{(Wt)}$) or high (*Il22tg8*$^{(Tg)}$) levels of IL-22. n ≥ 5 mice per group. Scale bar: 5 mm. (B) Map of *Il22eGFP* plasmid. (C) *In vitro* cultured 293T cells transfected with *eGFP* (left) and *Il22eGFP* (right) plasmid. Scale bar: 50µm. (D) 293T cells were transfected with *peGFP* and *pIl22eGFP* plasmid. GFP levels were measured using immunoblotting. (E) Representative picture of liver tissue upon hydrodynamic injection of *peGFP* plasmid. Scale bar: 100µm. (F) IL-22 serum levels in mice hydrodynamically injected with *eGFP* or *Il22eGFP* plasmid. n ≥ 6 mice per group. (G) Schematic overview and incidence of liver metastases in mice with no (*Il22-/-* mice upon hydrodynamic injection of eGFP plasmid), normal (WT upon hydrodynamic injection of eGFP plasmid) or high (WT upon hydrodynamic injection of Il22eGFP plasmid) levels of IL-22 using hydrodynamic overexpression of eGFP or Il22eGFP plasmid and intramucosal injection of CT26 CAG-Luc cells. n ≥ 7 mice per group. Data presented as mean ± SEM. ns>0.05; *:p<0.05; **:p≤0.01; ***:p≤0.001 as assessed by Mann-Whitney U test (A, F) or Fischer´ s exact test (G).

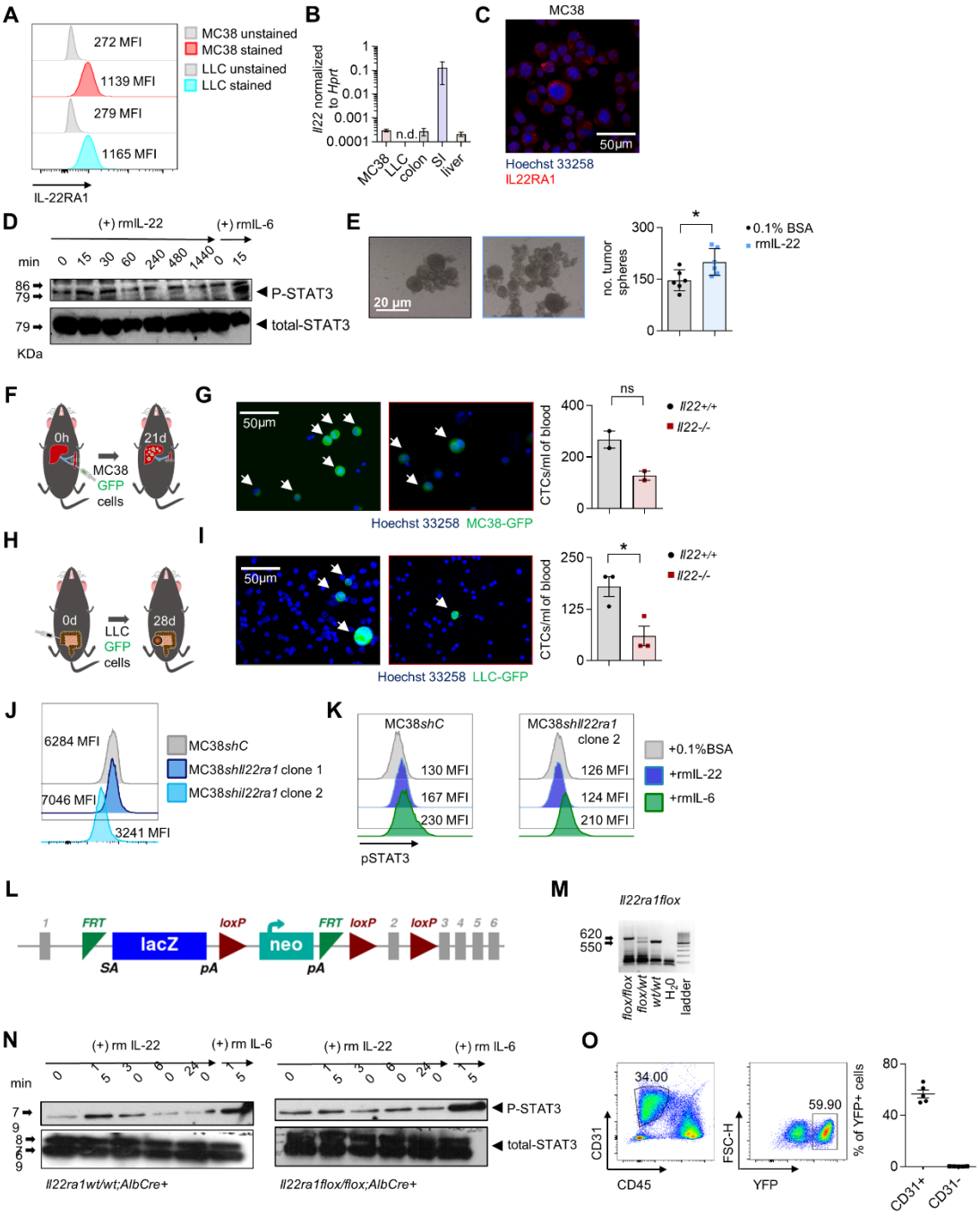
A
272 MFI
1139 MFI
279 MFI
1165 MFI
MC38 unstained
MC38 stained
LLC unstained
LLC stained
IL-22RA1
B
Il22 normalized to Hprt
n.d
MC38
LLC
colon
SI
liver
C
MC38
50µm
Hoechst 33258
IL22RA1
D
(+) rmIL-22
(+) rmIL-6
min
0 15 30 60 240 480 1440 0 15
86
79
P-STAT3
79
total-STAT3
KDa
E
20 µm
no. tumor spheres
0.1% BSA
rmIL-22
F
0h
21d
MC38 GFP cells
G
50µm
Hoechst 33258 MC38-GFP
CTCs/ml of blood
ns
Il22+/+
Il22-/-
H
0d
28d
LLC GFP cells
I
50µm
Hoechst 33258 LLC-GFP
CTCs/ml of blood
Il22+/+
Il22-/-
J
6284 MFI
7046 MFI
3241 MFI
MC38shC
MC38shIl22ra1 clone 1
MC38shil22ra1 clone 2
K
MC38shC
130 MFI
167 MFI
230 MFI
MC38shIl22ra1 clone 2
126 MFI
124 MFI
210 MFI
+0.1%BSA
+rmIL-22
+rmIL-6
pSTAT3
L
1
FRT
lacZ
loxP
neo
FRT
loxP
2
loxP
3 4 5 6
SA
pA
pA
M
Il22ra1flox
620
550
flox/flox
flox/wt
wt/wt
H2O
ladder
N
(+) rm IL-22
(+) rm IL-6
(+) rm IL-22
(+) rm IL-6
min
0 1 5 30 60 240 0 1 5
0 1 5 30 60 240 0 1 5
7
9
8
6
9
P-STAT3
total-STAT3
Il22ra1wt/wt;AlbCre+
Il22ra1flox/flox;AlbCre+
O
34.00
CD31
CD45
59.90
FSC-H
YFP
% of YFP+ cells
CD31+
CD31-

Figure S2, related to Figure 2. IL-22 signaling increases cancer cell stemness

(A) IL-22RA1 surface protein levels in MC38 and LLC cancer cells measured using FACS (B) *Il22* mRNA levels in MC38, LLC cancer cells as well as murine colon, small intestine (SI) and liver (RNA extracts from total tissue). (C) Immunostaining of IL-22RA1 in MC38 cells. Scale bar: 50µm. (D) Immunoblotting of p-STAT3 on MC38 cells upon IL-22 exposure in different time points. (E) Representative pictures and number of tumor spheres after exposure to 0.1% BSA or rmIL-22. Scale bar: 20 µm. (F) Schematic overview of intrasplenic injection of MC38 GFP-labelled cells for forced liver metastasis induction. (G) Representative pictures and number of GFP-labelled CTCs in $Il22^{+/+}$ and $Il22^{-/-}$ mice. n=2 independent experiments with 5 mice per group each time. Scale bar: 50 µm. (H) Schematic overview of cecum injection of LLC-GFP cells for spontaneous liver metastasis induction in $Il22^{+/+}$ and $Il22^{-/-}$ mice (I) Representative pictures and number of GFP-labelled CTCs in $Il22^{+/+}$ and $Il22^{-/-}$ mice. n=3 independent experiments with 6 mice per group each time. Scale bar: 50 µm. (J) Validation of silencing of *Il22ra1* in MC38 cancer cells by FACS. (K) Functional assay of silencing of *Il22ra1* in MC38 cancer cells by analyzing the pSTAT3 levels upon IL-22 exposure. (L) Construct map of $Il22ra1^{flox/flox}$ mice. (M) Genotyping PCR of $Il22ra1^{-/-}$ and $Il22ra1^{flox/flox}$ mice. (N) Hepatocytes were isolated from $Il22ra1^{wt/wt};Alb^{Cre+}$ and $Il22ra1^{flox/flox};Alb^{Cre+}$ mice and treated with 50 ng/ml recombinant murine (rm) IL-22 for 15 min, 30 min, 60 min and 240 min. IL-6 was used as a positive control. pSTAT3 levels were measured using immunoblotting. n=2 mice per group. (O) Gating strategy for identification of YFP+ LSECs isolated from liver of $Il22ra1^{flox/flox};Cdh5^{Cre+}$ mice and respective quantification. Data presented as mean ± SEM. ns:p>0.05; *:p<0.05; **:p≤0.01; ***:p≤0.001 as assessed by Mann-Whitney U test (E, G).

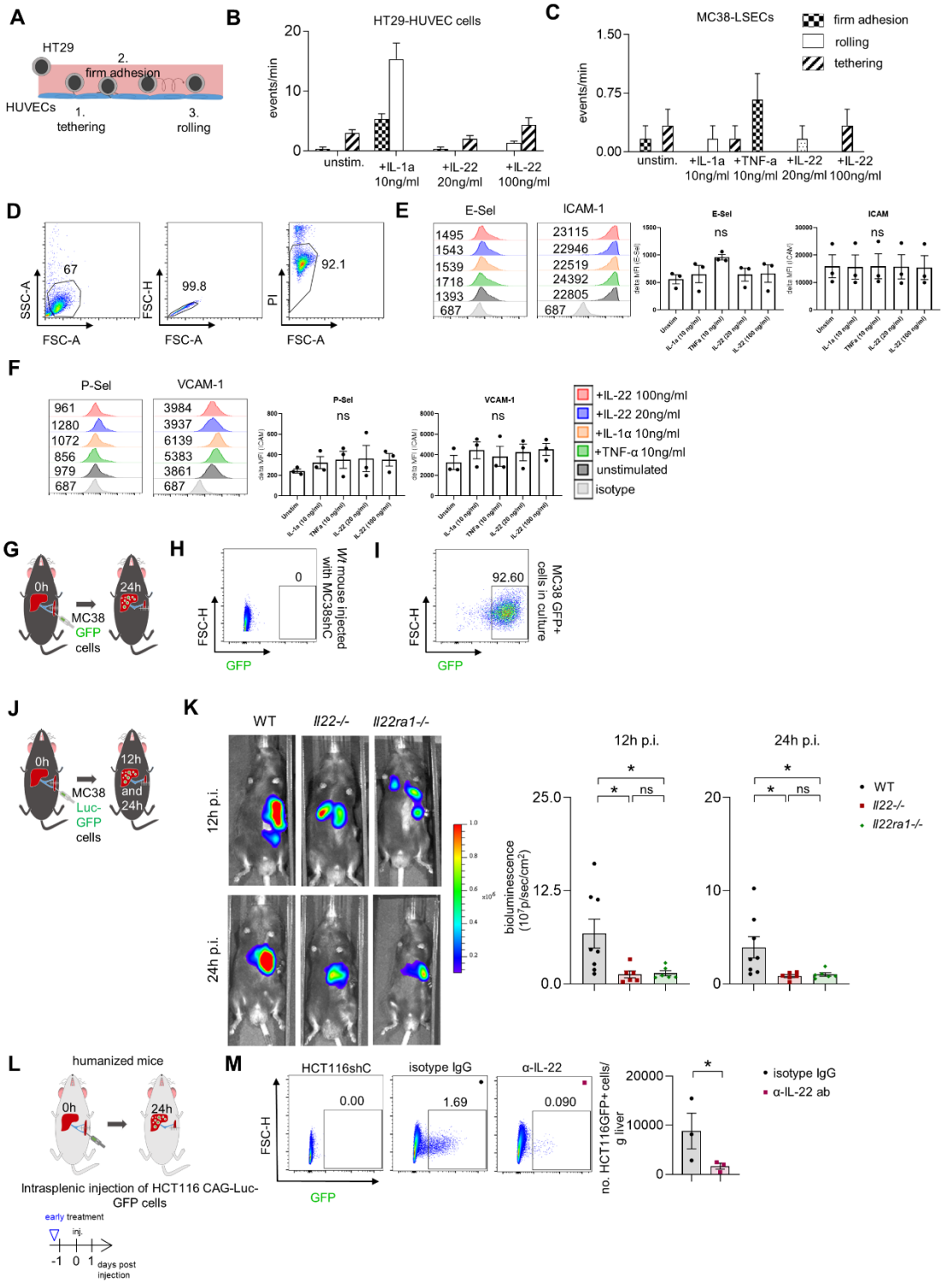
A
HT29
2.
firm adhesion
HUVECs
1.
tethering
3.
rolling
B
HT29-HUVEC cells
events/min
unstim.
+IL-1a 10ng/ml
+IL-22 20ng/ml
+IL-22 100ng/ml
C
MC38-LSECs
firm adhesion
rolling
tethering
events/min
unstim.
+IL-1a 10ng/ml
+TNF-a 10ng/ml
+IL-22 20ng/ml
+IL-22 100ng/ml
D
SSC-A
FSC-A
67
FSC-H
99.8
PI
92.1
E
E-Sel
ICAM-1
1495
1543
1539
1718
1393
687
23115
22946
22519
24392
22805
687
ns
F
P-Sel
VCAM-1
961
1280
1072
856
979
687
3984
3937
6139
5383
3861
687
ns
+IL-22 100ng/ml
+IL-22 20ng/ml
+IL-1α 10ng/ml
+TNF-α 10ng/ml
unstimulated
isotype
G
0h
24h
MC38 GFP cells
H
0
FSC-H
GFP
Wt mouse injected with MC38shC
I
92.60
FSC-H
GFP
MC38 GFP+ cells in culture
J
0h
12h and 24h
MC38 Luc-GFP cells
K
WT
Il22-/-
Il22ra1-/-
12h p.i.
24h p.i.
bioluminescence (10⁷p/sec/cm²)
ns
WT
Il22-/-
Il22ra1-/-
L
humanized mice
0h
24h
Intrasplenic injection of HCT116 CAG-Luc-GFP cells
early treatment
inj.
-1 0 1 days post injection
M
HCT116shC
isotype IgG
α-IL-22
0.00
1.69
0.090
FSC-H
GFP
no. HCT116GFP+ cells/ g liver
isotype IgG
α-IL-22 ab

Figure S3, related to Figure 3. IL-22 does not affect cancer cell endothelial adhesion, but cancer cell extravasation

(A) Schematic overview of the *in vitro* adhesion assay of endothelial HUVEC and HT-29 cancer cells. (B) HT-29 cancer cells were perfused over HUVEC cells (flow rate 8 mL/h) and retaining cells were counted. (C) MC38 cancer cells were perfused over LSECs (flow rate 8 mL/h) and retaining cells were counted. (D-F) FACS plots and histograms showing the expression of adhesion molecules, namely E-Sel, P-Sel, ICAM-1, VCAM-1, on LSECs upon stimulation with TNF-α, IL-1α and IL-22 in two different concentrations. (G) Schematic overview of intrasplenic injection of MC38 GFP-labelled cells in WT mice (extravasation assay). (H) FACS plot of liver of Wt mouse after intrasplenic injection of MC38 shC cells (I) FACS plot of MC38 GFP-labelled cells in culture. (J) Schematic overview of intrasplenic injection of MC38 Luc-GFP-labelled cells in WT, *Il22*$^{-/-}$ and *Il22ra1*$^{-/-}$ mice (extravasation assay). (K) Bioluminescent imaging and quantification of bioluminescent signal of WT, *Il22*$^{-/-}$ and *Il22ra1*$^{-/-}$ mice 12 and 24 hours after intrasplenic injection of MC38 Luc-GFP cells. Bioluminescent scale: $1x10^5$-$1x10^6$ photons/sec/cm^2/sr. (L) Injection of HCT116 CAG-Luc-GFP-labelled cells in humanized mice receiving a treatment with Fezakinumab (a human α-IL-22 antibody) or IgG control antibody. (M) Representative FACS plots showing the percentage of extravasated GFP+ cancer cells in the liver and bar plots showing the total number of extravasated cancer cells from (L). Data presented as mean ± SEM. ns>0.05; *:p<0.05; **:p≤0.01 as assessed by one-way ANOVA with Bonferroni post hoc tests (B, C, E, F and K) or Mann-Whitney U test (M).

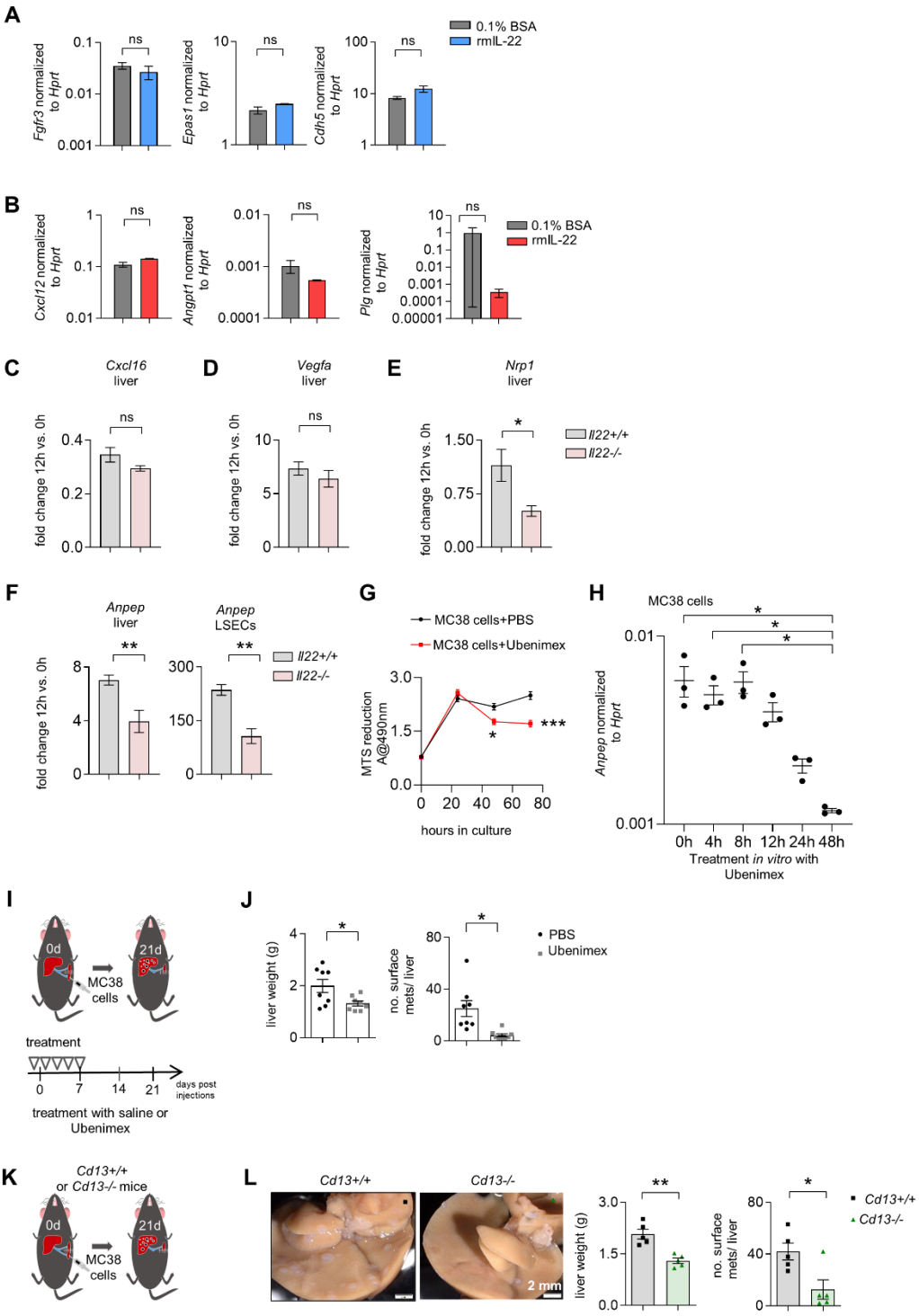
A
Fgfr3 normalized to Hprt
Epas1 normalized to Hprt
Cdh5 normalized to Hprt
ns
0.1% BSA
rmIL-22
B
Cxcl12 normalized to Hprt
Angpt1 normalized to Hprt
Plg normalized to Hprt
C
Cxcl16 liver
D
Vegfa liver
E
Nrp1 liver
fold change 12h vs. 0h
Il22+/+
Il22-/-
F
Anpep liver
Anpep LSECs
G
MC38 cells+PBS
MC38 cells+Ubenimex
MTS reduction A@490nm
hours in culture
H
MC38 cells
Anpep normalized to Hprt
Treatment in vitro with Ubenimex
I
0d
21d
MC38 cells
treatment
days post injections
treatment with saline or Ubenimex
J
liver weight (g)
no. surface mets/ liver
PBS
Ubenimex
K
Cd13+/+ or Cd13-/- mice
L
Cd13+/+
Cd13-/-
2 mm

Figure S4, related to Figure 4. Inhibition of aminopeptidases reduces liver metastasis formation

(A) *Fgfr3, Epas1* and *Cdh5* expression in LSECs upon stimulation with rmIL-22**.** (B) *Cxcl12, Angpt1,* and *Plg* expression in LSECs upon stimulation with rmIL-22**.** (C, D, E) Fold change of C*xcl16, Vegfa* and *Nrp1* expression in the liver tissue 12h post intrasplenic injection of MC38 cells in *Il22*$^{+/+}$ and *Il22*$^{-/-}$ mice compared to 0h. (F) Fold change of *Anpep* expression in LSECs and liver tissue 12h post intrasplenic injection of MC38 cells in WT and *Il22*$^{-/-}$ mice (G) MTS assay of MC38 cells upon Ubenimex treatment in different time points of culture. (H) *Anpep* expression of MC38 cells upon Ubenimex treatment in different time points of culture. (I) Schematic overview of intrasplenic injection of MC38 cells for forced liver metastasis induction in mice receiving a control or Ubenimex treatment, respectively. (J) Liver weight and number of macroscopic metastases in total liver of mice treated with PBS or Ubenimex. n ≥ 8 mice per group. (K) Schematic overview of intrasplenic injection of MC38 cells for forced liver metastasis induction in *Cd13*$^{+/+}$ and *Cd13*$^{-/-}$ mice. (L) Representative pictures, number of macroscopic metastases in total liver and liver weight of *Cd13*$^{+/+}$ mice compared to *Cd13*$^{-/-}$ mice. n = 5 mice per group. Data presented as mean ± SEM. ns>0.05; *:p<0.05; **:p≤0.01 as assessed by one-way (H, K, L) or two-way ANOVA with Bonferroni post hoc tests (G) or Mann-Whitney U test (A-F, J).

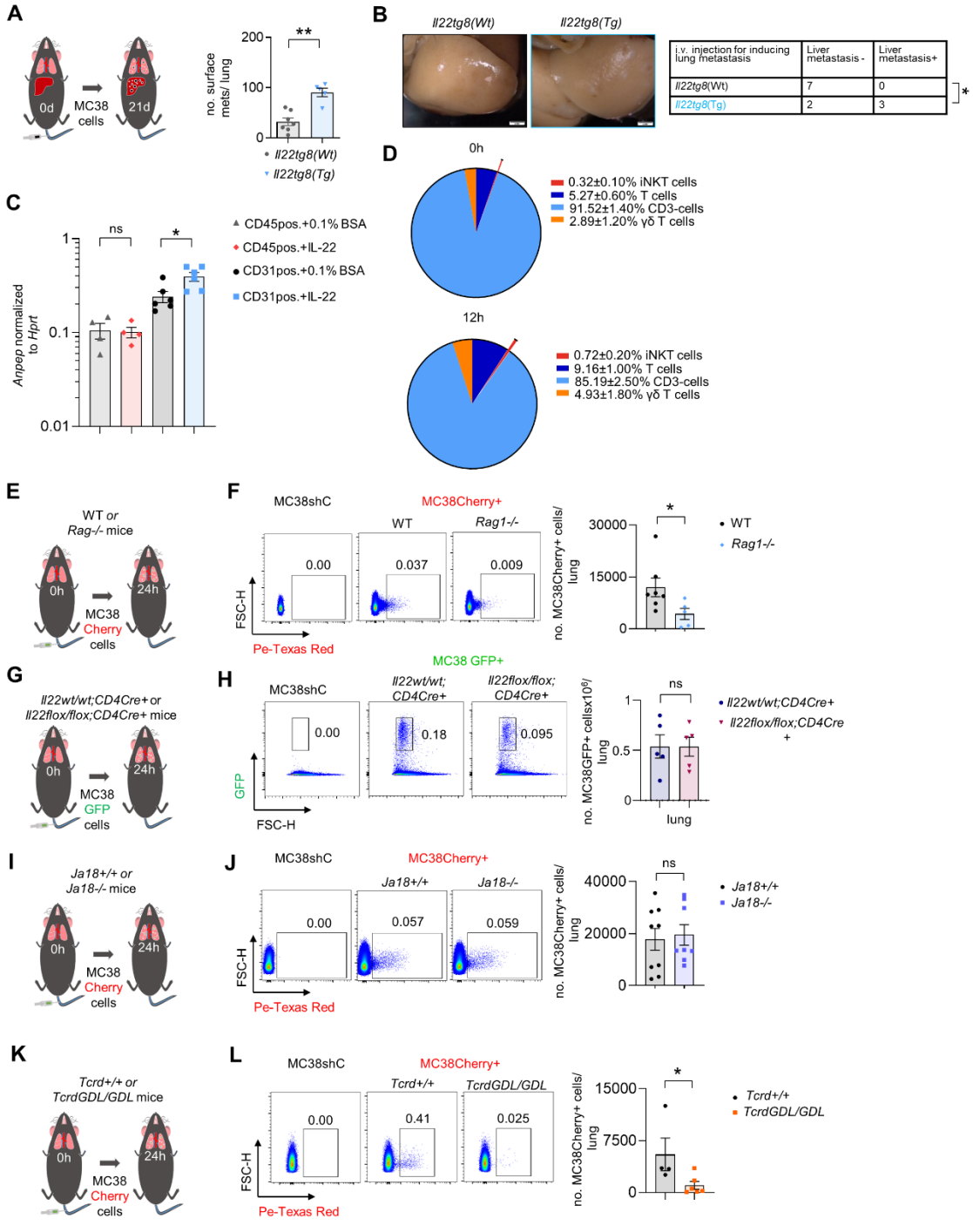
A
0d
MC38 cells
21d
no. surface mets/ lung
200
100
0
**
Il22tg8(Wt)
Il22tg8(Tg)
B
Il22tg8(Wt)
Il22tg8(Tg)
i.v. injection for inducing lung metastasis
Liver metastasis -
Liver metastasis+
Il22tg8(Wt)
7
0
Il22tg8(Tg)
2
3
*
C
ns
*
1
0.1
0.01
Anpep normalized to Hprt
CD45pos.+0.1% BSA
CD45pos.+IL-22
CD31pos.+0.1% BSA
CD31pos.+IL-22
D
0h
0.32±0.10% iNKT cells
5.27±0.60% T cells
91.52±1.40% CD3-cells
2.89±1.20% γδ T cells
12h
0.72±0.20% iNKT cells
9.16±1.00% T cells
85.19±2.50% CD3-cells
4.93±1.80% γδ T cells
E
WT or Rag-/- mice
0h
24h
MC38 Cherry cells
F
MC38shC
MC38Cherry+
WT
Rag1-/-
0.00
0.037
0.009
FSC-H
Pe-Texas Red
no. MC38Cherry+ cells/ lung
30000
15000
0
*
WT
Rag1-/-
G
Il22wt/wt;CD4Cre+ or Il22flox/flox;CD4Cre+ mice
0h
24h
MC38 GFP cells
H
MC38shC
MC38 GFP+
Il22wt/wt; CD4Cre+
Il22flox/flox; CD4Cre+
0.00
0.18
0.095
GFP
FSC-H
no. MC38GFP+ cellsx10⁶/ lung
1
0.5
0
ns
lung
Il22wt/wt;CD4Cre+
Il22flox/flox;CD4Cre+
I
Ja18+/+ or Ja18-/- mice
0h
24h
MC38 Cherry cells
J
MC38shC
MC38Cherry+
Ja18+/+
Ja18-/-
0.00
0.057
0.059
FSC-H
Pe-Texas Red
no. MC38Cherry+ cells/ lung
40000
20000
0
ns
Ja18+/+
Ja18-/-
K
Tcrd+/+ or TcrdGDL/GDL mice
0h
24h
MC38 Cherry cells
L
MC38shC
MC38Cherry+
Tcrd+/+
TcrdGDL/GDL
0.00
0.41
0.025
FSC-H
Pe-Texas Red
no. MC38Cherry+ cells/ lung
15000
7500
0
*
Tcrd+/+
TcrdGDL/GDL

Figure S5, related to Figure 5. IL-22 producing γδ T cells affect cancer cell extravasation into the lung via ANPEP induction

(A) Schematic overview of intravenous injection of MC38 cells for forced lung metastasis induction and number of macroscopic metastases in total lungs of mice with normal (*Il22tg8*$^{(Wt)}$) or high (*Il22tg8*$^{(Tg)}$) levels of IL-22. n ≥ 5 mice per group. (B) Representative pictures and percentage of mice with normal (*Il22tg8*$^{(Wt)}$) or high (*Il22tg8*$^{(Tg)}$) levels of IL-22 which develop macroscopic liver metastases. n ≥ 5 mice per group. (C) *Anpep* expression of sorted CD45+ and CD31+ cells upon stimulation with rmIL-22 (100 ng/µl). (D) Diagram showing the proportion of different immune subtypes of CD45+IL-22+ cells in murine lung 0 and 12 hours upon intravenous injection of MC38 cells. (E) Schematic overview of intravenous injection of MC38 Cherry-labelled cells in WT and *Rag1*$^{-/-}$ mice. (F) Representative FACS plots and statistics of MC38 Cherry-labelled extravasated cells in Wt and *Rag1*$^{-/-}$ mice. n ≥ 4 mice per group. (G) Schematic overview of intravenous injection of MC38 GFP-labelled cells in *Il22*$^{wt/wt}$*;CD4*$^{Cre+}$ and *Il22*$^{flox/flox}$*;CD4*$^{Cre+}$ mice (extravasation assay). n ≥ 5 mice per group. (H) Representative FACS plots and number of extravasated cancer cells from *Il22*$^{wt/wt}$*;CD4*$^{Cre+}$ and *Il22*$^{flox/flox}$*;CD4*$^{Cre+}$ mice 24h post intravenous injection. n ≥ 4 mice per group (I) Schematic overview of intravenous injection of MC38 Cherry-labelled cells in *Ja18*$^{+/+}$ and *Ja18*$^{-/-}$ mice. n ≥ 8 mice per group. (J) Representative FACS plots and number of extravasated cancer cells from *Ja18*$^{+/+}$ or *Ja18*$^{-/-}$ mice 24h post intravenous injection. Mice were sacrificed and the number of extravasated cancer cells in the lungs was quantified. (K) Schematic overview of intravenous injection of MC38 Cherry-labelled cells in *Tcrd*$^{GDL/GDL}$ and *Tcrd*$^{+/+}$ mice following DT (Diphtheria toxin) injection (DT injection in *Tcrd*$^{GDL/GDL}$ mice leads to γδ T cell depletion). n ≥ 4 mice per group. (L) Representative FACS plots and number of extravasated cancer cells from *Tcrd*$^{GDL/GDL}$ or *Tcrd*$^{+/+}$ mice 24h post intravenous injection. Mice were sacrificed and the number of extravasated cancer cells in the lungs were quantified. Data presented as mean ± SEM. ns>0.05; *:p<0.05; **:p≤0.01; ***:p≤0.001 as assessed by Mann-Whitney U test (C, F, H, J and L) or Fischer´ s exact test (B).

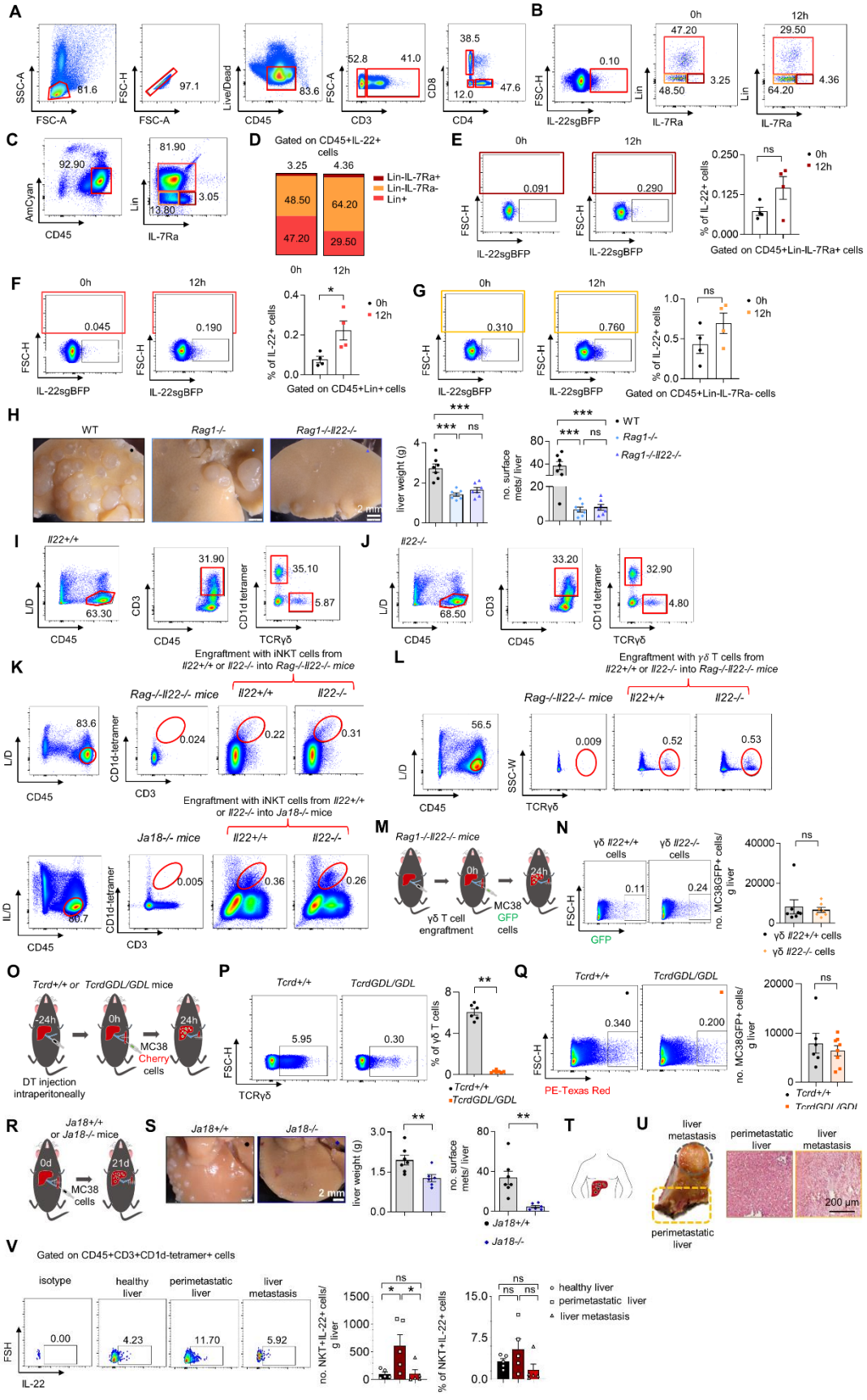
A
SSC-A
FSC-A
81.6
FSC-H
FSC-A
97.1
Live/Dead
CD45
83.6
FSC-A
CD3
52.8
41.0
CD8
CD4
38.5
12.0
47.6
B
0h
12h
FSC-H
IL-22sgBFP
0.10
Lin
IL-7Ra
47.20
48.50
3.25
29.50
64.20
4.36
C
AmCyan
CD45
92.90
Lin
IL-7Ra
81.90
3.05
13.80
D
Gated on CD45+IL-22+ cells
3.25
4.36
48.50
64.20
47.20
29.50
Lin-IL-7Ra+
Lin-IL-7Ra-
Lin+
0h
12h
E
0h
12h
FSC-H
IL-22sgBFP
0.091
0.290
% of IL-22+ cells
ns
0h
12h
Gated on CD45+Lin-IL-7Ra+ cells
F
0h
12h
FSC-H
IL-22sgBFP
0.045
0.190
% of IL-22+ cells
*
Gated on CD45+Lin+ cells
G
0h
12h
FSC-H
IL-22sgBFP
0.310
0.760
% of IL-22+ cells
ns
Gated on CD45+Lin-IL-7Ra- cells
H
WT
Rag1-/-
Rag1-/-Il22-/-
2 mm
liver weight (g)
***
ns
no. surface mets/ liver
WT
Rag1-/-
Rag1-/-Il22-/-
I
Il22+/+
L/D
CD45
63.30
CD3
31.90
CD1d tetramer
35.10
5.87
TCRγδ
J
Il22-/-
L/D
CD45
68.50
CD3
33.20
CD1d tetramer
32.90
4.80
TCRγδ
K
Engraftment with iNKT cells from Il22+/+ or Il22-/- into Rag-/-Il22-/- mice
Rag-/-Il22-/- mice
Il22+/+
Il22-/-
L/D
CD45
83.6
CD1d-tetramer
CD3
0.024
0.22
0.31
Engraftment with iNKT cells from Il22+/+ or Il22-/- into Ja18-/- mice
Ja18-/- mice
Il22+/+
Il22-/-
IL/D
CD45
60.7
CD1d-tetramer
CD3
0.005
0.36
0.26
L
Engraftment with γδ T cells from Il22+/+ or Il22-/- into Rag-/-Il22-/- mice
Rag-/-Il22-/- mice
Il22+/+
Il22-/-
L/D
CD45
56.5
SSC-W
TCRγδ
0.009
0.52
0.53
M
Rag1-/-Il22-/- mice
0h
24h
γδ T cell engraftment
MC38 GFP cells
N
γδ Il22+/+ cells
γδ Il22-/- cells
FSC-H
GFP
0.11
0.24
no. MC38GFP+ cells/ g liver
ns
γδ Il22+/+ cells
γδ Il22-/- cells
O
Tcrd+/+ or TcrdGDL/GDL mice
-24h
0h
24h
MC38 Cherry cells
DT injection intraperitoneally
P
Tcrd+/+
TcrdGDL/GDL
FSC-H
TCRγδ
5.95
0.30
% of γδ T cells
**
Tcrd+/+
TcrdGDL/GDL
Q
Tcrd+/+
TcrdGDL/GDL
FSC-H
PE-Texas Red
0.340
0.200
no. MC38GFP+ cells/ g liver
ns
Tcrd+/+
TcrdGDL/GDL
R
Ja18+/+ or Ja18-/- mice
0d
21d
MC38 cells
S
Ja18+/+
Ja18-/-
2 mm
liver weight (g)
**
no. surface mets/ liver
**
Ja18+/+
Ja18-/-
T
U
liver metastasis
perimetastatic liver
perimetastatic liver
liver metastasis
200 μm
V
Gated on CD45+CD3+CD1d-tetramer+ cells
isotype
healthy liver
perimetastatic liver
liver metastasis
FSH
IL-22
0.00
4.23
11.70
5.92
no. NKT+IL-22+ cells/ g liver
ns
% of NKT+IL-22+ cells
ns
healthy liver
perimetastatic liver
liver metastasis

Figure S6, related to Figure 6. IL-22 producing iNKT cells, but not T, γδ T and Lin- cells, affect cancer cell extravasation into the liver parenchyma (A) Gating strategy used to assess the IL-22 expression in different immune subtypes upon intrasplenic injection of MC38 cells. (B) Gating strategy used to assess the Lin-IL-7Ra+IL-22+, Lin-IL-7Ra-IL-22+ and Lin+IL-22+ cells isolated from murine liver 0 and 12h upon intrasplenic injection of MC38 cells. (C) Gating strategy used to assess the Lin-IL-7Ra+, Lin-IL-7Ra- and Lin+ cells isolated from murine liver 0 and 12h after intrasplenic injection of MC38 cells. (D) Diagram showing the proportion of different subtypes of CD45+IL-22+ cells in murine liver 0 and 12h after intrasplenic injection of MC38 cells. (E, F, G) FACS plots showing the production of IL-22 in the Lin-IL-7Ra+, Lin-IL-7Ra- and Lin+ cells isolated from murine liver 0 and 12h after intrasplenic injection of MC38 cells. n ≥ 4 mice per group. (H) Liver weight and number of macroscopic liver metastases post intrasplenic injection of MC38 cells in WT, *Rag*$^{-/-}$ *and Rag*$^{-/-}$*;Il22*$^{-/-}$ mice. n ≥ 6 mice per group. (I, J) FACS plots showing the gating strategy used for the sorting of iNKT and γδ T cells from *Il22*$^{+/+}$ and *Il22*$^{-/-}$ mice. (K) Engraftment with iNKT cells (total population) from *Il22*$^{+/+}$ or *Il22*$^{-/-}$ into *Rag1*$^{-/-}$ and *Ja18*$^{-/-}$ mice. (L) Engraftment with γδ T cells from *Il22*$^{+/+}$ into *Rag1*$^{-/-}$*Il22*$^{-/-}$ mice. (M) Schematic overview of intrasplenic injection of MC38 GFP-labelled cells in *Rag*$^{-/-}$*Il22*$^{-/-}$ mice engrafted with *Il22*$^{+/+}$or *Il22*$^{-/-}$ γδ T cells (extravasation assay). (N) Representative FACS plots and number of extravasated cancer cells from *Rag*$^{-/-}$*Il22*$^{-/-}$ mice engrafted with *Il22*$^{+/+}$or *Il22*$^{-/-}$ γδ T cells 24h postintrasplenic injection. n ≥ 7 mice per group. (O) Schematic overview of intrasplenic injection of MC38 GFP-labelled cells in *Tcrd*$^{GDL/GDL}$ *and Tcrd*$^{+/+}$ mice following DT (Diphtheria toxin) injection (DT injection in *Tcrd*$^{GDL/GDL}$ mice leads to γδ T cell depletion). n ≥ 7 mice per group. (P) Representative FACS plots and quantification of γδ T cells of *Tcrd*$^{GDL/GDL}$ *and Tcrd*$^{+/+}$ mice upon DT injection. (Q) Representative FACS plots and number of extravasated cancer cells from *Tcrd*$^{GDL/GDL}$ or *Tcrd*$^{+/+}$ mice 24h post intrasplenic injection. (R) Schematic overview of intrasplenic injection of MC38 cells for forced liver metastasis induction in *Ja18*$^{+/+}$ and *Ja18*$^{-/-}$ mice. (S) Representative pictures, number of macroscopic metastases in total liver and liver weight of *Ja18*$^{+/+}$ mice compared to *Ja18*$^{-/-}$ mice. n ≥ 6 mice per group. (T) Schematic overview of human liver metastasis. (U) Fresh specimen from resected liver metastasis and hematoxylin & eosin staining of perimetastatic and metastatic human liver. (V) Flow cytometry of perimetastatic and metastatic human liver and diagram showing the proportion of iNKT IL-22-producing cells in perimetastatic and metastatic human liver. Cells were isolated from fresh perimetastatic and metastatic liver tissue and analyzed using flow cytometry. n = 5 patients. Scale bar: 200μm. Data presented as mean ± SEM. ns>0.05; *:p<0.05; **:p≤0.01; ***:p≤0.001 as assessed by one-way ANOVA with Bonferroni post hoc tests (H, V) or Mann-Whitney U test (E, F, G, N, P, Q, S).

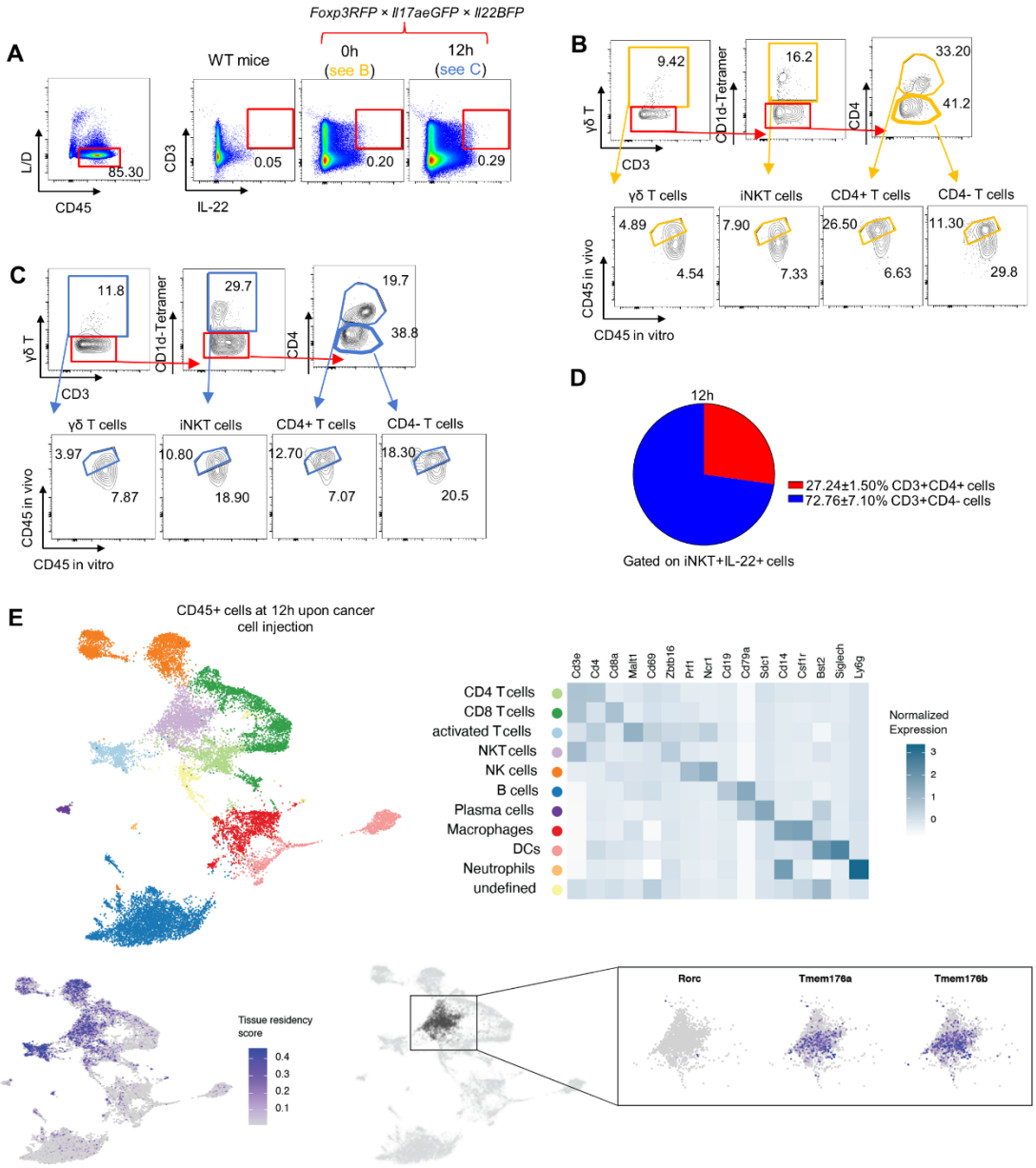
Foxp3RFP × Il17aeGFP × Il22BFP
A
WT mice
0h
(see B)
12h
(see C)
L/D
85.30
CD45
CD3
IL-22
0.05
0.20
0.29
B
γδ T
CD3
CD1d-Tetramer
CD4
9.42
16.2
33.20
41.2
γδ T cells
iNKT cells
CD4+ T cells
CD4- T cells
CD45 in vivo
CD45 in vitro
4.89
4.54
7.90
7.33
26.50
6.63
11.30
29.8
C
11.8
29.7
19.7
38.8
γδ T cells
iNKT cells
CD4+ T cells
CD4- T cells
3.97
7.87
10.80
18.90
12.70
7.07
18.30
20.5
D
12h
27.24±1.50% CD3+CD4+ cells
72.76±7.10% CD3+CD4- cells
Gated on iNKT+IL-22+ cells
E
CD45+ cells at 12h upon cancer cell injection
CD4 T cells
CD8 T cells
activated T cells
NKT cells
NK cells
B cells
Plasma cells
Macrophages
DCs
Neutrophils
undefined
Cd3e
Cd4
Cd8a
Mait1
Cd69
Zbtb16
Prf1
Ncr1
Cd19
Cd79a
Sdc1
Cd14
Csf1r
Bst2
Siglech
Ly6g
Normalized Expression
Tissue residency score
Rorc
Tmem176a
Tmem176b

Figure S7, related to Figure 7. IL-22 producing iNKT17 cells express tissue resident markers (A-C) Gating strategy used for Figure 7 C. (A) FACS plots showing the IL-22+ T cell populations in the livers of *Foxp3*^{RFP}*;Il17a*^{eGFP}*;Il22*^{BFP} mice 0h and 12h post MC38 cell injection compared to WT mice. (B,C) Representative FACS plots of the indicated fractions within the IL-22+ T cell population showing the percentage of infiltrating and circulating cells at 0h (B) and 12h (C). (D) The contribution of CD4+ and CD4- of iNKT+IL-22+ cells 12 hours upon intrasplenic cancer cell injection. (E) Cell clusters of identified CD45+ cells using single-cell sequencing in mouse livers 12 hours upon intrasplenic cancer cell injection, overlaid with tissue residency score and iNKT17 markers.

Supplementary table 1, related to the STAR method section: Taqman probes and primer sequences utilized for this study

gene	company	taqman probe/ primer name	sequence (5' → 3')
Il22-/-	Eurofins Genomics	IL22SU	TCA TCT GCT TGG TAC CAT GC
		IL22dRev	CAG AGA AAA TGG CAA GGC GG
		LacZ	GTC TGT CCT AGC TTC CTC ACT G
CD4Cre+	Eurofins Genomics	CD4Cre Mu	TTA GGG TGG GGC TCA GAA GG
		CD4Cre Co	AAC TTG CAC AGC TCA GAA TGC
		CD4Cre Wt	ACC TGA GAT TCC ACC AAA CTT GA
Il10GFP	Eurofins Genomics	GFP-3	AAG TCG TGC TGC TTC ATG TG
		GFP-5	ACG TAA ACG GCC ACA AGT TC
		IL10KOF	GTG TGT ATT GAG TCT GCT GGA C
		IL10KOR1	GTG TGG CCA GCC TTA GAA TAG
		IL10KOR2	GGT TGC CTT GAC CAT CGA TG
Foxp3RFP	Eurofins Genomics	FIR1	CAA AAC CAA GAA AAG GTG GGC
		FIR2	GGA ATG CTC GTC AAG AAG ACA GG
		FIR3	CAT CTT GGA GAG TCG GTG TG
Il22ra1-/-	Eurofins Genomics	CAS_R1_Term	TCG TGG TAT CGT TAT GCG CC
		IL22ra1_F	TCT GAT GCC CTC TTC TGC TG
		IL22ra1_R	TTG CTG GTC ACA GTC CAT CC
Il17Cre+	Eurofins Genomics	17AyfpF	CAA GTG CAC CCA GCA CCA GCT GAT C
		17AyfpRwt	CTT AGT GGG TTA GTT TCA TCA CAG C
		17AyfpCreR	GCA GCA GGG TGT AGG CAA TGC
Il22ra1flox/flox	Eurofins Genomics	IL22ra1_wt_R1	TGG GTC GGT TTG CAG ACT TG
		IL22ra1_wt_F1	GCC CTC TTC TGC TGT GTC TGA
Il22flox/flox	Eurofins Genomics	DNA460-40	CTC AGA CCT CTA CAG ACA ATC ATC
		DNA460-22	CAG CTG GCG GCC AAA GTC CC
AlbCre+	Eurofins Genomics	CreIA	GCA CTG ATT TCG ACC AGG TT
		CreIIB	CCC GGC AAA ACA GGT AGT TA
Cdh5Cre+	Eurofins Genomics	Cdh5-Cre Fw	GTC CAA TTT ACT GAC CGT ACA C
		Cdh5-Cre Rev	CTG TCA CTT GGT CGT GGC AGC
Rosa26YFP+	Eurofins Genomics	Rosa26 Seq1	AAA GTC GCT CTG AGT TGT TAT
		Rosa26 Seq2	GCG AAG AGT TTG TCC TCA ACC
		Rosa26 Seq3	GGA GCG GGA GAA ATG GAT ATG
Il17aeGFP	Eurofins Genomics	IL-17A KI sense	CAC CAG CGC TGT GTC AAT
		IL-17A KI anti sense	ACA AAC ACG AAG CAG TTT GG
		IL-17A KI IRES	ACC GGC CTT ATT CCA AGC
Il22BFP	Eurofins Genomics	TailWT22F	GTG CTC AGC AAG CAA ATG TC
		SiresFI	TAC GCT TGA GGA GAG CCA
		SHAGF	AAT GAT GGA CGT TAG CTT
		SHAGR	CCC GAC CAC ATG GGT TGA A
Apc15lox	Eurofins Genomics	int14loxF	AGG GTT ATT GAA TAT GAT CGG
		mInt14Apc-R4	AGC AGC AAA CTT ACT TTA CAG
		m14intApc-F3	AAC TTC TGA GTA TGA TGG AGG
	Eurofins Genomics	Kras22908	CTG CAT AGT ACG CTA TAC CCT GT

KrasG12D		Kras22907	TGT CTT TCC CCA GCA CAG T
		oIMR9592	GCA GGT CGA GGG ACC TAA TA
Il22tg8$^{(Tg)}$		Il22SV40_TG6/8	CCC ATT CAT CAG TTC CAT AG
		Il22CDNA_TG6/8	GAG TGG AGA GAG ATC AAG GCG ATT G
Il17aPe-Cy5	Eurofins Genomics	IL-17A KI sense	CAC CAG CGC TGT GTC AAT
		IL-17A KI anti sense	ACA AAC ACG AAG CAG TTT GG
		IL-17A KI IRES	ACC GGC CTT ATT CCA AGC
Rosa26 YFP	Eurofins Genomics	Rosa26 Seq1	AAA GTC GCT CTG AGT TGT TAT
		Rosa26 Seq2	GCG AAG AGT TTG TCC TCA ACC
		Rosa26 Seq3	GGA GCG GGA GAA ATG GAT ATG
Cd13-/-	Eurofins Genomics	CD13KO Forword	CAC CCC CAT CCC CCA TCC CTT AC
		CD13KO Reverse	GTG CCC ACG CCC TTG AAC CTT ACT T
		CD13KO IRESrev	ACAAACGCACACCGGCCTTATTCC
Rag1-/-	Eurofins Genomics	RagWF	GAG GTT CCG CTA CGA CTC TG
		RagR	CCG GAC AAG TTT TTC ATC GT
		RagMF	TGG ATG TGG AAT GTG TGC GAG
Ja18-/-	Eurofins Genomics	Ja18 Com	CTC AAA AGG CTG TGT AAT TGC T
		Ja18 Mut	CTT GGG GAT GTT TAC AGA GTA CC
		Ja18 WT	AGT CCC AGC TCC AAA ATG C
TcrdGDL/GDL	Eurofins Genomics	Delta FW	CTAGAAGAAAAGCAAAAGCCCTC
		Delta REV	CCTTCCTTTCGGTATTTTACTTTCA
		IRES REV	AAACGCACACCGGCCTTATT
Il22 cloning primer A	Eurofins Genomics	IL22 FW	ATG GCT GTC CTG CAG AAA TCT
		IL22 REV	TCA GAC GCA AGC ATT TCT CAG
Il22 cloning primer B	Eurofins Genomics	m_BglII_IL22	TCC GGA CTC AGA TCT ATG GCT GTC CTG CAG AAA TCT
		m_EcoRI _IL22	TCG ACT GCA GAA TTC TCA GAC GCA AGC ATT TCT CAG
Il22	Thermo Fisher Scientific	Mm01226722_g1	
Hprt	Thermo Fisher Scientific	Mm03024075_m1	
Anpep	Thermo Fisher Scientific	Mm00476227_m1	
Fgfr3	Thermo Fisher Scientific	Mm00433294_m1	
Epas1	Thermo Fisher Scientific	Mm00433294_m1	
Cdh5	Thermo Fisher Scientific	Mm00486938_m1	
Cxcl12	Thermo Fisher Scientific	Mm00445553_m1	
Nrp1	Thermo Fisher Scientific	Mm00435379_m1	
Angpt1	Thermo Fisher Scientific	Mm00456503_m1	
Plg	Thermo Fisher Scientific	Mm00447087_m1	
Cxcl16	Thermo Fisher Scientific	Mm00469712_m1	
Vegfa	Thermo Fisher Scientific	Mm00437306_m1	

Supplementary table 2, related to STAR method section: Cloning oligonucleotide sequences corresponding to shRNA and sgRNAs used in this study

Vector Backbone	Sigma mission #	Target of shRNA
pLKO.1-puro	SHC002	scrambled
pLKO.1-puro	TRCN0000050238	human *ANPEP* (CD13)
pLKO.1-puro	TRCN0000050239	human *ANPEP* (CD13)
pLKO.1-puro	TRCN0000050240	human *ANPEP* (CD13)
pLKO.1-puro	TRCN0000018482	human *ANPEP* (CD13)
pLKO.1-puro	TRCN0000025830	human *ANPEP* (CD13)
pLKO.1-puro	TRCN0000035991	human *ANPEP* (CD13)
pLKO.1-puro	TRCN0000065863	Mouse *Il22ra1*
pLKO.1-puro	TRCN0000065864	Mouse *Il22ra1*
pLKO.1-puro	TRCN0000065865	Mouse *Il22ra1*
pLKO.1-puro	TRCN0000065866	Mouse *Il22ra1*
pLKO.1-puro	TRCN0000065867	Mouse *Il22ra1*